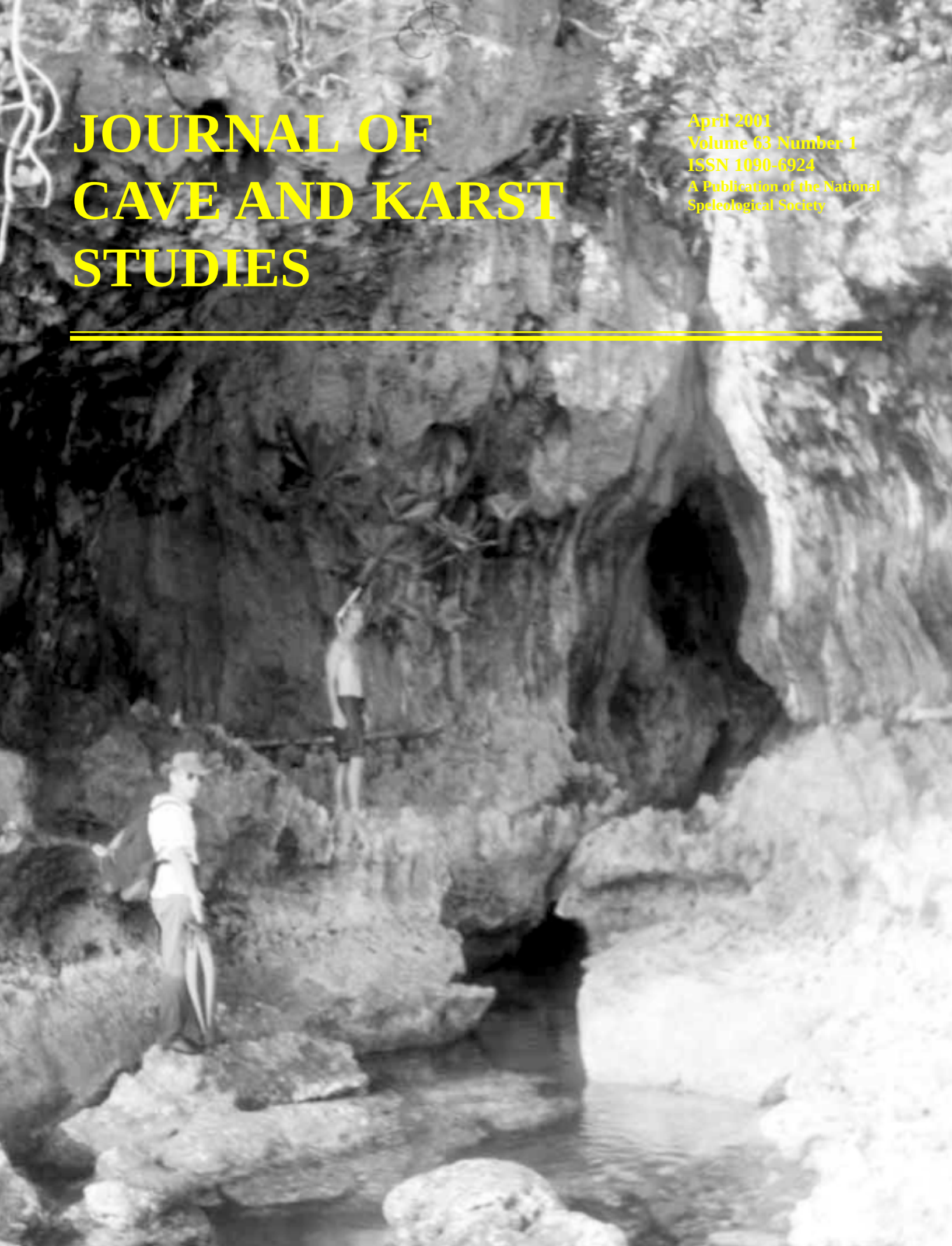

# JOURNAL OF CAVE AND KARST STUDIES

April 2001
Volume 63 Number 1
ISSN 1090-6924
A Publication of the National Speleological Society

# Journal of Cave and Karst Studies of the National Speleological Society

Volume 63 Number 1 April 2001


## CONTENTS




The *Journal of Cave and Karst Studies* (ISSN 1090-6924) is a multi-disciplinary, refereed journal published three times a year by the National Speleological Society, 2813 Cave Avenue, Huntsville, Alabama 35810-4431; (256) 852-1300; FAX (256) 851-9241, e-mail: nss@caves.org; World Wide Web: http://www.caves.org/~nss/. The annual subscription fee, worldwide, by surface mail, is $18 US. Airmail delivery outside the United States of both the *NSS News* and the *Journal of Cave and Karst Studies* is available for an additional fee of $40 (total $58); The *Journal of Cave and Karst Studies* is not available alone by airmail. Back issues and cumulative indices are available from the NSS office. POSTMASTER: send address changes to the *Journal of Cave and Karst Studies*, 2813 Cave Avenue, Huntsville, Alabama 35810-4431.




Cover: Large fracture cave along northwest coast of Guam. See Mylroie, Jenson, Taborosi, Jocson, Vann and Wexel pages 9-22.

# A MATHEMATICAL MODEL OF AIR TEMPERATURE IN MAMMOTH CAVE, KENTUCKY

JONATHAN W. JERNIGAN
*Department of Mathematics, Western Kentucky University, Bowling Green, KY 42101, USA Jonathan.Jernigan@wku.edu*
RANDALL J. SWIFT
*Department of Mathematics, Western Kentucky University, Bowling Green, KY 42101, USA*

*Alterations made to the Natural (Historic) Entrance into Mammoth Cave over the past two centuries have resulted in disrupted atmospheric conditions in the Historic Section of Mammoth Cave. In an effort to understand atmospheric phenomena in this section of the cave, Division of Science and Resources Management personnel at Mammoth Cave National Park collected atmospheric data from various sites throughout the Historic Section of Mammoth Cave.*

*These data are used to construct a mathematical model that predicts air temperature at various sites within the cave system. First, an approximate mathematical model is constructed that could apply to any cave system with characteristics (such as cave geometry and the natural force driving airflow) similar to those in Mammoth Cave. Then, the regression analysis of atmospheric data and the use of the derived model allow the construction of a mathematical model that is specific to the Historic Section of Mammoth Cave.*

Around 175 years ago, a sequence of structural changes to the Historic Section of Mammoth Cave, Mammoth Cave National Park, Kentucky, was initiated, the effects of which may still be seen today. The primary and most dramatic of these modifications was the clearance of large rockfall debris from the entrance passage known as Houchins Narrows. With a clearer entrance passage, air exchange between the Historic Section of the cave and the outdoors could readily occur. Historically, this air movement had been retarded by entrance structures that restricted airflow into the Historic Section of the cave; air movement, however, was not the only activity that these structures restricted. The movement of bats was also impeded (Olson 1995).

Historical and paleontological data indicate that the Historic Section of Mammoth Cave was once a major bat hibernation site. Several 19th century estimates reported that hibernating colonies totaled into the millions of bats (Olson 1996). Paleontological evidence includes bat bones and excrement found throughout the Historic Section of the cave (Toomey *et al.* 1998). Today, however, few bats are found in this same portion of the cave where they were once so abundant. In an effort to restore the bat hibernacula and atmospheric conditions, the existing gate structure was replaced in July 1990 with a bat gate. The removal of the preexisting structure opened the Historic Section of the cave to the effects of outdoor atmospheric conditions, and the atmospheric conditions within this portion of the cave fluctuated erratically (Olson 1995). The Park's Division of Science and Resources Management has attempted to control this behavior by partially covering the bat gates with Plexiglas panels (Fry 1996).

In order to understand atmospheric phenomena and quantify the effects of these entrance modifications, it is necessary to monitor atmospheric conditions within the Historic Section of Mammoth Cave. The Cave Atmospheric Monitoring program, initiated in 1994, is maintained by the Science and Resources Management division of the National Park Service at Mammoth Cave. The program began not in the Historic Section of Mammoth Cave, but in the ecotone of various artificial entrances to the Mammoth Cave system. The original goal of the monitoring program was to study the effects that airlock installations would have upon atmospheric conditions near each of these artificial entrances. The atmospheric monitoring stations installed a few months later in the Historic Section of Mammoth Cave were placed there in an effort to understand the ecotone in that area by providing baseline data that described atmospheric conditions in that section of the cave (Fry 1995).

The mathematical model created in this paper uses data from eight stations in the Historic Section of Mammoth Cave (Fig. 1). All of the Cave Atmospheric Monitoring (CAM) stations in the Historic Section of Mammoth Cave record air temperature data on fifteen-minute intervals.

The monitoring site that is central to this study is the Houchins Narrows site. Located 103 m from the Natural Entrance, the Houchins Narrows CAM station is the station closest to the Natural Entrance and the station where atmospheric conditions fluctuate most in response to weather patterns external to the cave system. Atmospheric parameters collected at this site include not only air temperature, but wind speed and direction measurements as well. Air flux, or the volume of air flowing past the station per unit time along with a directional indicator, is calculated using these wind speed and direction measurements. Denoted by $\mathbf{F}_H$ [$m^3/s$], air flux is assigned positive values when air is flowing into the cave and negative values when air is flowing out of the cave. Further, the cross-sectional area of the cave passage is 19.2 $m^2$ at the

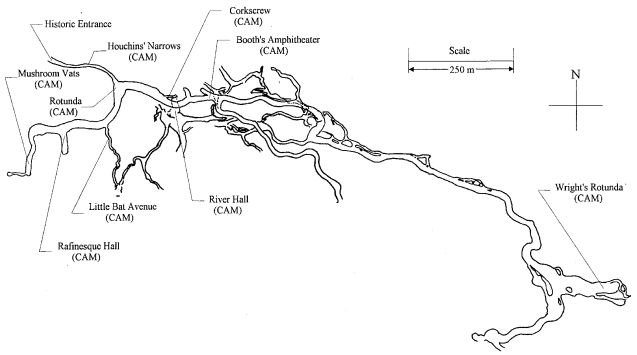


**Figure 1. Cave atmospheric monitoring (CAM) stations in the Historic Section of Mammoth Cave (modified after Kaemper 1908).**

Houchins Narrows CAM station so that air flux is given by

$$\mathbf{F}_{H} = \begin{cases} 19.2\,\mathrm{m}^2 \times \text{Wind Speed} & \text{If Incast} \\ -19.2\,\mathrm{m}^2 \times \text{Wind Speed} & \text{If Outcast} \end{cases} \quad (1)$$

The Natural Entrance is among the largest apertures that lead into the Historic Section of Mammoth Cave. Any disturbance to atmospheric conditions in the Historic Section of Mammoth Cave occurs in response to variations in atmospheric conditions outside the cave system. These variations are registered at the Houchins Narrows CAM station. It can be assumed that atmospheric conditions in Houchins Narrows are closely related to atmospheric conditions at other sites throughout the Historic Section's variable temperature zone. For this reason, the mathematical model derived in this paper uses data from the Houchins Narrows CAM site to predict air temperature data at sites that are deeper inside the Historic Section of Mammoth Cave but still within the variable temperature zone.

To formulate the desired mathematical model, the natural phenomenon that drives airflow in Mammoth Cave must be identified and understood. Empirical evidence indicates that airflow in Mammoth Cave is driven by the chimney effect (Jernigan 1997). The chimney effect is the natural *convection* process whereby air movement occurs due to density differentials between two neighboring air masses of differing temperatures (Wefer 1994). The baseline mathematical model derived in the following section considers a model that relates atmospheric conditions between two sites in the cave system.

## A BASELINE MODEL OF AIRFLOW IN MAMMOTH CAVE

As a first step in the mathematical modeling of a complex system, a model is derived that describes the behavior of the system in its simplest form. The physical model about to be presented cannot be applied directly to airflow in the Mammoth Cave system since many of the assumptions underlying the model are violated. However, the model is created not to be applied directly to airflow in Mammoth Cave, but to imply the set of basis functions that is used in the regression analysis of atmospheric data. Since the physical model is applied very loosely to airflow in the Mammoth Cave system, it is not rigorously constructed.

A cave system may be abstracted as a network of interconnecting pipes. So, when considering airflow in the Mammoth Cave system, the mathematical model may be one that depends upon the representation of the cave system as such a system of networked piping. To derive a model of airflow in this branching system, an undivided section of the network is considered.

The equation commonly used to relate conditions between two distinct locations in a straight, non-branching section of piping is Bernoulli's equation. If the fluid contained in the first location is labeled fluid element one, and the fluid contained in the second location is labeled fluid element two, then Bernoulli's equation relates conditions in fluid element one to those in fluid element two. Mott (1979) gives one form of Bernoulli's equation as

$$\frac{p_1}{\gamma} + z_1 + \frac{v_1^2}{2g} = \frac{p_2}{\gamma} + z_2 + \frac{v_2^2}{2g} \quad (2)$$

where $p_\alpha$ is atmospheric pressure [N/m$^2$], $\gamma$ is the specific weight of the fluid [N/m$^3$], $z_\alpha$ is the elevation of the element of fluid [m], $v_\alpha$ is the velocity of each element of fluid [m/s], and g is the acceleration due to gravity [m/s$^2$].

The system for which equation (2) applies has no lost work. In a cave system, lost work is a significant factor that dramatically affects the energy in a system, so it is necessary to modify equation (2) to introduce lost work into the model. Bernoulli's equation is a conservation of energy equation, and scaling the total energy at one location introduces the effects of lost work and gives the total energy at the second location. Jernigan (1997) derived

$$(1+\beta\Delta T)\left(\frac{p_1}{\gamma_1} + z_1 + \frac{v_1^2}{2g}\right) = \left(\frac{p_2}{\gamma_2} + z_2 + \frac{v_2^2}{2g}\right) \quad (3)$$

as a modified version of Bernoulli's equation. In equation (3), $\beta$ [C$^{-1}$] is an expansion coefficient dependent upon the substance and $\Delta T$ is the temperature differential $T_2$-$T_1$ [C]. Equation (3) implies that the work lost in the system is manifested by a temperature difference between locations one and two. Further, $\gamma$, the specific weight of the fluid, is temperature dependent and, therefore, different for each of the two elements of fluid. This difference is denoted by the subscripts on $\gamma$.

To use equation (3) as a model of airflow in the Historic Section of Mammoth Cave, the airflow must satisfy certain properties.

1. Air flows in the Historic Section as though it were incompressible.
2. With respect to energy exchange, the section of the cave considered is neither a source nor a sink for other sections of the cave.
3. The air in this section of the cave and the cave itself are thermodynamically isolated.
4. There is no energy loss due to friction between molecules within the fluid or between the fluid and its surroundings.

Assumption 1 is satisfied since air pressures and air velocities in Mammoth Cave are small enough in magnitude that there is no compression of the fluid occurring. Assumption 4 holds since the total energy of the system considered is very large, and, while there may be significant energy loss due to friction, it should be small when compared to the total energy of the system. Assumptions 2 and 3 do not hold for the Historic Section of Mammoth Cave. The model developed in this section is modified in the following section to include the effects described in assumptions 2 and 3.

The data from the CAM station in Booths Amphitheater is now predicted using data from Houchins Narrows. There are three temperature probes at the Booths Amphitheater CAM station, and the air temperature data considered are those obtained from the probe near the War of 1812 era saltpeter leaching vats. This probe is ~1 m above the floor and is referred to as the "vat probe."

To predict air temperatures at the vat probe using atmospheric data from Houchins Narrows, it is assumed that the velocity of the airflow at the vat probe is constant with time, so that $v_1 = c_1$, where $c_1$ is some constant. Further, Jernigan (1997) showed that airflow in Mammoth Cave fluctuates in response to variations in air temperature on the surface and not to changes in barometric pressure. Hence, it is assumed that airflow between two points in the cave system is driven by the temperature differential between those two points. Therefore, by existence of the term $\Delta T$ in equation (3), the resultant pressure gradient is indirectly measured, and the erroneous simplifying assumption that $p_1 \approx p_2 = c_2$, for $c_2$ a constant, is warranted. Last of all, the variation in the value of $\gamma$ is insignificant over the range of temperature values that are commonly realized in Mammoth Cave, so the value of $\gamma$ is taken to be constant over space and time. This means $\gamma_1 = \gamma_2 = c_3$ for some constant $c_3$.

Substitution of these values into equation (3) gives the following

$$(1 + \beta\Delta T)\left(\frac{c_2}{c_3} + z_1 + \frac{c_1^2}{2g}\right) = \left(\frac{c_2}{c_3} + z_2 + \frac{v_2^2}{2g}\right) \quad (4)$$

Since $\beta$, $z_\alpha$, and g are constants, by equation (1), equation (4) reduces to

$$T_B = aF_H^2 + c + T_H \quad (5)$$

where a and c are constants, and $T_B$ and $T_H$ are air temperatures at the vat probe and Houchins Narrows, respectively. Equation (5) is called the Phase 1 Bernoulli model since it is the first step in a sequence of refinements based upon Bernoulli's equation. The quantities that must now be determined are the values of a and c. This may be accomplished through regression analysis of Houchins Narrows and Booths Amphitheater CAM data using the set of basis functions $\{1, F_H^2\}$. Performance of this regression analysis for Julian days 1-20 of 1997 gives the set of results shown in table 1.

**Table 1. The phase 1 Bernoulli model applied to Houchins Narrows and Booths Amphitheater data.**

| Constant | Coefficient | P | R-squared | Normality | Constant Variance | Standard Error of Estimate |
|---|---|---|---|---|---|---|
| a | .010 | <.001 | .73 | Failed | Failed | 1.96 |
| c | 4.45 | <.001 | | | | |

The value of R-squared equaling only .73, together with the model's failure of the normality and constant variance tests, indicates that this model is not effective in predicting data at the vat probe. Further, the standard error of the estimate is large (1.96°C). This model is inaccurate, as expected, and is modified in the next section to include the effects of other natural phenomena that are influencing the interrelationship of data from Houchins Narrows and those at the vat probe.

## A REFINED MODEL OF AIRFLOW IN MAMMOTH CAVE

In this section, the Phase 1 Bernoulli model is modified to include the effects outlined in assumptions 2 and 3. These modifications will improve the values of R-squared realized by the Phase 1 Bernoulli model.

The assumption that no energy is lost to or gained from other passages when air moves from Houchins Narrows to Booths Amphitheater is incorrect since air may flow into or out of Audubon Avenue at the Rotunda. If $\mathbf{F}_H$, $\mathbf{F}_B$, and $\mathbf{F}_A$ represent air flux in Houchins Narrows, air flux near Booths Amphitheater, and air flux in Audubon Avenue, respectively, then the relationship between these variables is $\mathbf{F}_H = \mathbf{F}_A + \mathbf{F}_B$.

Since $\mathbf{F}_B$ is assumed to be approximately zero, then it is true that $\mathbf{F}_A \approx \mathbf{F}_H$. This approximation is transformed into equality by scaling the value of $\mathbf{F}_H$, so that

$$\mathbf{F}_A = (b+m)\mathbf{F}_H = b\mathbf{F}_H + m\mathbf{F}_H , \quad (6)$$

where b and m are constants so that b+m is also a constant. Introducing the rightmost representation of $\mathbf{F}_A$ into the Phase 1 Bernoulli model introduces the effects of energy exchange with adjoining passageways.

Further, since airflow in Mammoth Cave is driven by the

chimney effect, temperature differentials between air in the cave and air outside the cave influence airflow patterns throughout the cave. It will be assumed that air flux in Houchins Narrows is directly proportional to the temperature difference between the air in Houchins Narrows and the air outside the cave system. Hence, if $T_O$ represents the temperature of the air outside the cave system and n is a constant, then the following relationship may be established:
$\mathbf{F}_H = n (T_H - T_O)$.

Outdoor air temperature at Mammoth Cave National Park is collected on an hourly basis. This time scale does not correspond to the time scale of the CAM station measurements. As a convenience and as an assumption in the current model, the term $T_O$ will be discarded and the above equation reduces to:
$\mathbf{F}_H = n T_H$.

Substituting $\mathbf{F}_H$ into the rightmost representation of $\mathbf{F}_A$ in equation (6) yields

$$\mathbf{F}_A = b\mathbf{F}_H + (d-1)T_H , \quad (7)$$

where d = mn+1. This relationship replaces equation (6) as source for the basis functions being introduced into the Phase 1 Bernoulli model to account for energy lost or gained due to air exchange with Audubon Avenue.

Assumption 3 is that there is no energy exchange between the air in cave passages and the rock that defines the cave passages. Empirical evidence indicates that this is not the case. The amount of energy exchange between the air in Houchins Narrows and the rock in Houchins Narrows is assumed to be directly proportional to the temperature differential between these substances. Hence, if

$$\Delta T_{H\text{-}R} = T_H - T_R$$

represents the temperature differential obtained by subtracting the temperature of the rock in Houchins Narrows from the temperature of the air in Houchins Narrows, then a constant multiple of this quantity will represent this energy exchange. Further, the rate of energy exchange is assumed constant as air moves from Houchins Narrows to Booths Amphitheater, so that the total energy lost to, or gained from, the surrounding rock is approximately

$$TotE_{H,R} = k \cdot dist \cdot \Delta T_{H\text{-}R}$$

where "dist" is the distance from Houchins Narrows to Booths Amphitheater. The constant k is the scaling factor used to define the proportionality relationship between the temperature differential and energy exchange in Houchins Narrows. The term k×dist will be reduced to the constant term g. Hence, the term that describes energy exchange between the air and the rock as the air moves between Houchins Narrows and Booths Amphitheater is given by

$$TotE_{H,R} = g\Delta T_{H\text{-}R} \quad (8)$$

and this term is introduced into the Phase 1 Bernoulli model.

Adding the new basis functions given by equations (7) and (8) to the existing Phase 1 Bernoulli model, the revised model for predicting data at the vat probe is

$$T_B = a\mathbf{F}_H^2 + b\mathbf{F}_H + c + dT_H + g\Delta T_{H\text{-}R} \quad (9)$$

This model is used in the regression analysis performed in the following sections. It will be referred to as the Phase 4 Bernoulli model since its derivation required three refinements to the Phase 1 Bernoulli model.

## REGRESSION ANALYSIS AND THE PREDICTION OF AIR TEMPERATURE IN MAMMOTH CAVE

The Phase 4 Bernoulli model was constructed to predict air temperatures at the vat probe in Booths Amphitheater based upon atmospheric data that describe conditions in Houchins Narrows. However, the Phase 4 Bernoulli model contains constants a, b, c, d, and g that are unknown. These constants are obtained by regression analysis of Cave Atmospheric Monitoring data from Houchins Narrows and Booths Amphitheater. In performing this regression analysis, Cave Atmospheric Monitoring data are partitioned into time intervals ~20 days in length. Some results obtained by using the Phase 4 Bernoulli model along with these CAM data are shown in table 2.

In the table of results, the columns of data detail characteristics of the regression fits. The first column labels the data sets being used in the analysis. For example, the results for the data set "ba(hn)91-110,1996" present the results when Booths Amphitheater vat probe data are predicted using Houchins Narrows data for Julian days 91-110 of 1996. The next five columns of data are the values of the coefficients a, b, c, d, and g obtained through regression analysis. The seventh column contains the value of R-squared when regression analysis is performed on the indicated data set. The eighth and ninth columns describe whether the residuals obtained using the model passed (indicated by a 'P') or failed (indicated by an 'F') the normality and constant variance tests, respectively. The final column gives the standard error produced when the model is applied to the indicated data set.

Figure 2 shows the measured air temperature values at the vat probe for Julian days 1 through 20 of 1997 along with those predicted by the Phase 4 Bernoulli model and the coefficients listed in table 2. The model accurately predicts air temperature at the vat probe.

Values of R-squared are maximized during the winter months; in contrast, winter is also when standard errors are at a maximum. Cave geometry and the fact that airflow in Mammoth Cave is driven by the chimney effect explain this

**Table 2. Prediction of air temperature at the vat probe with the phase 4 Bernoulli model.**

| Data Set | a | b | c | d | g | R-squared | Normality | ConstVar | Std Error |
|---|---|---|---|---|---|---|---|---|---|
| ba(hn)91-110,1996 | 0.00022 | -0.029 | 4.94 | 0.46 | -0.42 | 0.96 | P | F | 0.15 |
| ba(hn)111-130,1996 | 0.00018 | -0.025 | 4.43 | 0.54 | -0.48 | 0.91 | P | F | 0.18 |
| ba(hn)131-150,1996 | -0.00032 | -0.025 | 4.24 | 0.58 | -0.58 | 0.91 | P | F | 0.15 |
| ba(hn)151-170,1996 | -0.00038 | -0.026 | 2.70 | 0.75 | -0.77 | 0.82 | P | F | 0.11 |
| ba(hn)195-210,1996 | -0.000032 | -0.018 | 7.47 | 0.28 | -0.20 | 0.49 | P | F | 0.1 |
| ba(hn)221-240,1996 | -0.00022 | -0.023 | -1.40 | 1.10 | -1.08 | 0.59 | P | F | 0.083 |
| ba(hn)245-265,1996 | -0.000036 | -0.013 | 5.79 | 0.45 | -0.46 | 0.83 | P | F | 0.074 |
| ba(hn)270-290,1996 | 0.000014 | -0.013 | 6.24 | 0.41 | -0.37 | 0.92 | P | P | 0.1 |
| ba(hn)321-346,1996 | 0.00009 | -0.026 | 6.94 | 0.31 | -0.25 | 0.95 | P | F | 0.12 |
| ba(hn)348-366,1996 | 0.00048 | -0.030 | 6.85 | 0.32 | -0.25 | 0.98 | P | F | 0.12 |
| ba(hn)1-20,1997 | 0.00035 | -0.020 | 6.04 | 0.42 | -0.37 | 0.99 | P | P | 0.19 |
| ba(hn)21-40,1997 | -0.00011 | -0.030 | 6.34 | 0.32 | -0.26 | 0.94 | P | F | 0.14 |
| ba(hn)41-60,1997 | -0.00065 | -0.018 | 5.99 | 0.41 | -0.37 | 0.98 | P | F | 0.12 |
| ba(hn)61-77,1997 | -0.00006 | -0.021 | 6.83 | 0.27 | -0.21 | 0.89 | P | F | 0.15 |

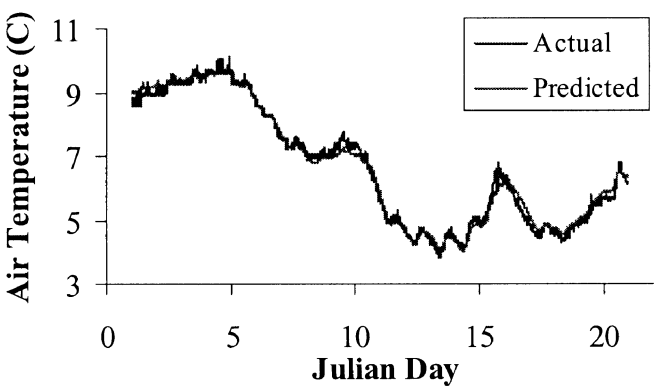


**Figure 2. Actual and predicted (using equation (9) and the coefficients in table 2) air temperatures at the vat probe (Julian days 1 through 20, 1997).**

anomaly. Since Houchins Narrows is adjacent to the Historic Entrance (a lower entrance into the cave system), air flows from the outdoors into Houchins Narrows in the winter. For the same reason, air flows out of the cave system through this passage during the summer. So, during the winter, fluctuations in the outdoor air temperature are immediately manifested in Houchins Narrows, as they also are in Booths Amphitheater. During the summer, however, the air flowing past these sites has been cooled and thermodynamically stabilized by the cave system. The small fluctuations in air temperature in Booths Amphitheater and Houchins Narrows do not reflect the large fluctuations in air temperature on the surface.

Although it was designed to model air temperatures at the vat probe in Booths Amphitheater, the Phase 4 Bernoulli model can be used to predict air temperatures at other points throughout the Historic Section of Mammoth Cave. Some sites where this is possible are Wrights Rotunda, River Hall, Rafinesque Hall, and the Corkscrew. Each of these sites (with the exception of Rafinesque Hall) has one air temperature probe on site. At Rafinesque Hall, there are two air temperature probes: one at the floor and one at the ceiling of the passage. The results for Rafinesque Hall presented in table 3 are those obtained when using the Phase 4 Bernoulli model to predict air temperature at the ceiling probe.

Some sample results are shown in table 3. The Phase 4 Bernoulli model does well when predicting air temperatures in Rafinesque Hall (abbreviated ra) and the Corkscrew (co), both sites that are close to Houchins Narrows. Also, the prediction of air temperature at the River Hall (ri) CAM station is good, with a value of R-squared equaling 0.84. Wrights Rotunda (wr), however, is a great distance from Houchins Narrows, and this may explain the low value of R-squared (0.32) shown in the table.

## SUMMARY AND CLOSING REMARKS

The authors have presented a mathematical model that predicts air temperature in the Historic Section of Mammoth Cave. Based upon basic laws of physics and Cave Atmospheric Monitoring data, this model accurately predicted air temperature at sites near Houchins Narrows during the winter. In the prediction of air temperature at the vat probe in Booths Amphitheater, values of R-squared obtained during the warmer, summer months were not as high as those obtained during the cooler, winter months. In contrast, standard errors are highest when the values of R-squared are highest. Air temperature could also be predicted at sites other than Booths Amphitheater, and the mathematical model that predicts these conditions also resulted in high values of R-squared.

In the development of the Phase 4 Bernoulli model, the effects of outdoor air temperature upon air temperature at the vat probe in Booths Amphitheater were disregarded. However, hourly air temperature measurements are available from a weather station located on the surface and near the boundary of Mammoth Cave National Park. One improvement to the model

**Table 3. Prediction of air temperature at sites in the Historic Section of Mammoth Cave.**

| Data Set | a | b | c | d | g | R-squared | Normality | ConstVar | Std Error |
|---|---|---|---|---|---|---|---|---|---|
| co(hn) 1-20, 1997 | -0.000013 | 0.0026 | 7.92 | 0.23 | -0.26 | 0.98 | P | P | 0.16 |
| ba(hn) 1-20, 1997 | 0.00035 | -0.02 | 6.04 | 0.42 | -0.37 | 0.99 | P | P | 0.19 |
| wr(hn) 1-20, 1997 | -0.00032 | 0.11 | 8.42 | 0.34 | -0.62 | 0.32 | F | F | 2.43 |
| ri(hn) 1-20, 1997 | -0.000021 | 0.0073 | 7.37 | 0.077 | -0.12 | 0.84 | F | F | 0.14 |
| ra(hn) 1-20, 1997 | -0.000013 | 0.0052 | 5.95 | 0.18 | -0.2 | 0.96 | P | F | 0.14 |

presented is the inclusion of outdoor air temperature as a new basis function. This inclusion should improve the regression results obtained using the Phase 4 Bernoulli model, particularly during the warmer months.

## ACKNOWLEDGMENTS

This work is the result of a masters thesis study completed within the Department of Mathematics at Western Kentucky University. The support provided by the university is greatly appreciated. The authors also gratefully acknowledge the support of the National Park Service, particularly the Division of Science and Resources Management at Mammoth Cave National Park. Without access to their Cave Atmospheric Monitoring data, this project would not have been possible. John Fry, Rick Olson, and Joe Meiman were especially helpful. Members of the first author's thesis committee were Dr. David Neal and Dr. Christopher Groves; their time and suggestions were greatly appreciated.

The regression analyses performed in this paper were executed using the statistical analysis software SigmaStat. Funding for the purchase of this software was provided by the National Speleological Society, the Department of Mathematics at Western Kentucky University, and in part with funds from a grant obtained by the second author. The authors would like to thank all of these parties for their financial assistance.

## REFERENCES

Fry, J.F., 1995, Cave atmospheric monitoring project in Mammoth Cave National Park, *in* Proceedings of Mammoth Cave National Park's Fourth Science Conference, Mammoth Cave National Park, p. 205-206.

Fry, J.F., 1996, Eighteen cave gates and airlocks: Conclusion of a three-year project to restore cave entrance dynamics at Mammoth Cave National Park, *in* Proceedings of the Fifth Annual Mammoth Cave National Park Science Conference, Mammoth Cave National Park, p. 69-83.

Jernigan, J.W., 1997, Mathematical Modeling of Convective Heat Transfer in Mammoth Cave [MA thesis]: Western Kentucky University, 109 p.

Kaemper, M., 1908, Map of the Mammoth Cave Kentucky: Cave Research Foundation with Cooperation of Mammoth Cave National Park.

Mott, R.L., 1979, Applied fluid mechanics, Charles E. Merrill Publishing Company, 405 p.

Olson, R., 1995, Ecological restoration in the Natural Entrance ecotone of Mammoth Cave with emphasis on endangered species habitat and mitigation of visitor impact., Division of Science and Resources Management: Mammoth Cave National Park, Mammoth Cave, Kentucky, 9 p.

Olson, R., 1996, This old cave: The ecological restoration of the Historic Entrance ecotone of Mammoth Cave, and mitigation of visitor impact, *in* Proceedings of the fifth annual Mammoth Cave National Park Science Conference, Mammoth Cave National Park, p. 87-95.

Toomey III, R.S., Colburn, M.L., Schubert, B.W. & Olson, R., 1998, Vertebrate paleontological projects at Mammoth Cave National Park, *in* Proceedings of Mammoth Cave National Park's Seventh Science Conference, Mammoth Cave National Park, p. 9-14.

Wefer, F.L., 1994, The meteorology of Harrison's Cave, Barbados, West Indies, *in* Hobbs, H.H., ed., A Study of Environmental Factors in Harrison's Cave, Barbados, West Indies: Huntsville, AL, National Speleological Society, p. 62-92.

John E. Mylroie, John W. Jenson, Danko Taborosi, John M.U. Jocson, David T. Vann and Curt Wexel - Karst features of Guam in terms of a general model of carbonate island karst. *Journal of Cave and Karst Studies 63*(1): 9-22.

# KARST FEATURES OF GUAM IN TERMS OF A GENERAL MODEL OF CARBONATE ISLAND KARST

JOHN E. MYLROIE
*Department of Geosciences, Mississippi State University, Mississippi State, MS 39762 USA*
JOHN W. JENSON, DANKO TABOROSI, JOHN M.U. JOCSON, DAVID T. VANN AND CURT WEXEL
*Water and Environmental Research Institute of the Western Pacific, University of Guam, Mangilao, Guam 96923 USA*

*This paper describes the karst of Guam in terms of the Carbonate Island Karst Model (CIKM), a general model for the unique karst carbonate islands. The CIKM recognizes several processes and conditions unique to carbonate islands: 1) enhanced dissolution at the surface, base, and margin of the fresh-water lens; 2) the history of both vertical migration and stable positioning of these zones according to glacioeustatic and tectonic changes in relative sea level; 3) the size of the island's catchment area relative to its perimeter, which can vary with sea level change; 4) the hydrologic implications of the unique eogenetic environment of their young limestones; and 5) the position of the island's carbonate-basement contact relative to sea level and the island surface over time.*

*Guam's complex depositional and tectonic histories have endowed it with a unique legacy of karst features. The northern half is a Pleistocene karst plateau in Plio-Pleistocene limestone units that exhibit all the characteristic karst features of carbonate islands, from the simplest to the most complex. The epikarst is similar to that on other carbonate islands. Most closed depressions are broad and shallow, probably reflecting original depositional morphology, although vertical-walled collapse and banana-hole type features are also present. Caves include a few pit caves, some of which are very deep. Traversable stream caves occur where the limestone-basement contact is exposed on the flanks of volcanic outcrops. The most abundant caves are flank margin caves, which can be found all along the modern coast, and which occupy distinct horizons in the faces of the cliff line surrounding the plateau. Discharge features have been documented for three types of coastline around the northern plateau: (1) deeply scalloped embayments with broad beaches; (2) linear beaches fronted by fringing reefs; and (3) sheer cliffs with narrow or no benches, and only occasional small reefs. In the embayments, karst groundwater discharges by diffuse flow from numerous seep fields and as concentrated flow from springs along the beach. Seeps are found along the linear beaches, but we have not noted significant flow from springs or coastal caves. Along the cliff-dominated coast, karst groundwaters discharge in spectacular flows from dissolution-widened fractures, coastal caves, and submarine vents, most notably along the northwest coast.*

*The southern half of Guam is an uplifted volcanic highland containing a karst terrain on Mio-Pliocene limestone remnants in the interior. Because these units lie above the influence of the fresh water lens, sea water mixing, and sea level change, the karst is a classic tropical continental karst, with features that include contact springs issuing from well-developed caves, sinking streams with resurgences, and conical cockpit karst. Along the southeast coast, which is flanked by a continuous uplifted Pleistocene limestone unit, antecedent streams draining the interior have incised deep canyons. Dry valleys and large closed depressions in this unit appear to be associated with allogenic waters originating in the interior.*

Guam is the largest and southernmost of the Mariana Islands (Fig. 1). It is 550 km$^2$ in area, 48 km long, and varies in width from 6-19 km (Fig. 2). The Mariana Islands are thought to have been first inhabited between 3000 and 2000 B.C. Spain colonized them subsequent to Magellan's landing in 1521 on either Guam or one of the islands to the north, his first landfall after crossing the Pacific Ocean. Spanish rule ended when the United States took possession during the Spanish-American War in 1898. The U.S. Navy administered the island until Japan captured it in 1941. Following liberation by U.S. forces in 1944, administration eventually shifted to the Department of Interior, but access was restricted for military security until 1962 (Rogers 1996). After the island was opened to commerce, the economy grew slowly but steadily until the Asian expansion of the 1980s brought an avalanche of capital investment and an economic boom. Guam's tourism-driven economy now supports 150,000 permanent residents plus over a million visitors a year.

Eighty percent of the island's drinking water is drawn from the karst aquifer in the limestone plateau of the northern half of the island (Jocson *et al.* 1999; Contractor & Jenson 2000). Mink & Vacher (1997) have summarized the results of previous hydrogeological studies of the northern aquifer. Such studies have been oriented, however, toward determining engineering parameters to support development rather than to gain more fundamental understanding of the karst geology. This paper is the first report from a two-year study aimed at inventorying and describing the karst on Guam in terms of a gener-

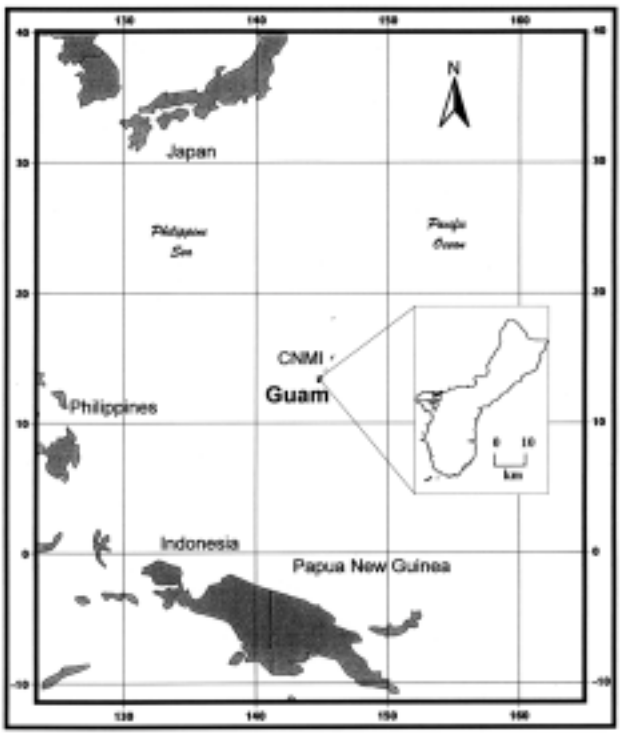


**Figure 1. Location of Guam, Mariana Islands, in the western Pacific Ocean. CNMI stands for "Commonwealth of the Northern Mariana Islands" and includes the islands of Rota, Tinian, and Saipan (after Tracey *et al.* 1964).**

al model of carbonate island karst (Mylroie *et al.* 1999; Mylroie & Jenson 2000).

## THE CARBONATE ISLAND KARST MODEL

Small carbonate islands are a unique genetic environment, which produce a distinct karst (Mylroie & Vacher 1999). First, the carbonate units on islands have all spent some time in the island's fresh-water lens, where they have been exposed to the vadose-to-phreatic groundwater transition zone at the top of the lens (as in karst in general), and to the brackish transition zone between the fresh-water lens and the underlying marine groundwater (which is peculiar to coastal/island karst aquifers). Each is an especially aggressive dissolutional environment (Mylroie & Carew 1995). Second, carbonate islands worldwide have experienced Quaternary glacioeustatic sea-level changes. The fresh water lens, along with its upper and lower zones of aggressive dissolution, has similarly migrated, with the longest exposure durations associated with stratigraphic levels coinciding with eustatic sea-level maxima, minima, and stadial intervals. On tectonically active islands such as Guam, episodes of uplift and subsidence overprint glacioeustatic sea level migration, introducing further complexity. Third, the small catchment-to-perimeter ratio (for which catchment area is proportional to the square of the island radius, while the perimeter is only directly proportional)

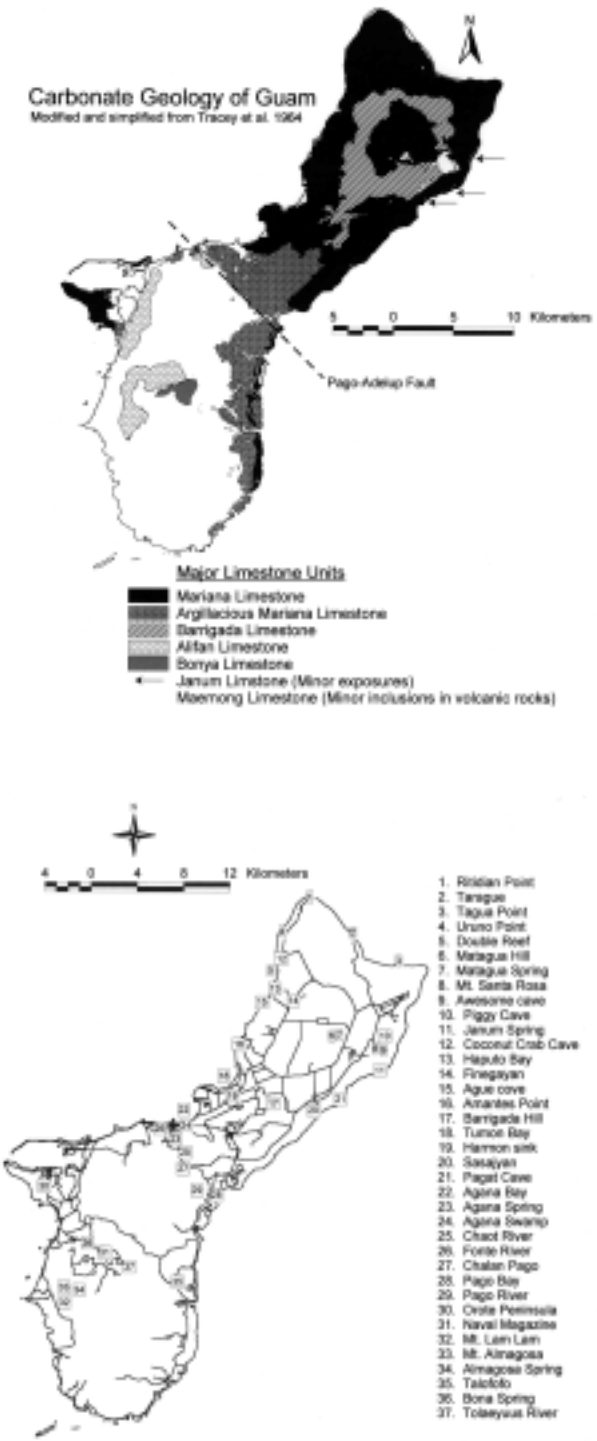


**Figure 2. (a-top) Simplified geologic map of Guam (volcanic rocks in white). The Marianas units are Plio-Pleistocene; the Alifan, Bonya, Janum, and Maemong limestones are Miocene. The Holocene Merizo Limestone occurs as small, isolated patches primarily along the southeast coast. (b-bottom) Locations of features described in the text and figures. Major roads are shown for reference.**

on small islands is hypothesized to facilitate diffuse discharge at any given rate of recharge, obviating—but not necessarily eliminating—the development of conduits to promote more efficient discharge (Mylroie & Vacher 1999). On large islands, on the other hand, the larger catchment-to-perimeter ratio favors the development of conduits. Moreover, the karst in the interior of islands such as Jamaica or Puerto Rico is likely to have been out of the influence of fresh/salt water mixing and glacio-eustasy for much of its history. Islands with interior carbonates thus exhibit forms similar to continental karst. Finally, the karst in most island environments, whether large or small, is *eogenetic, i.e.*, it has developed in young carbonate rocks that have never undergone deep burial, and thus have never been out of the reach of meteoric diagenesis (Mylroie & Vacher 1999). This situation implies that the rock began with and can retain high porosity, and that development of secondary porosity takes place concurrently with the ongoing occlusion of primary porosity. This has important implications for interception, storage, and transmission of groundwater, and the consequent evolution of karst landforms and aquifer properties.

Mylroie & Jenson (2000, in press) have integrated these observations with Mylroie & Carew's (1995, 1997) systematic geomorphic description of small carbonate islands studied in the Atlantic-Caribbean to propose the Carbonate Island Karst Model (CIKM) as a descriptive model for the unique karst of small carbonate islands. Initial research to develop a general model for carbonate island karst began in the Bahamas and Bermuda, which are relatively uncomplicated islands that have developed in tectonically stable settings (e.g. Mylroie *et al.* 1995). Subsequent observations from Isla de Mona, Puerto Rico (see Wicks 1998), a simple carbonate island that has been tectonically uplifted, extended the model to include the effects of relative sea-level change. Current work to extend the CIKM is focused on Guam (Jenson 1999; Taborosi 1999, 2000), which has not only been uplifted but has had complicated tectonic and depositional histories, with important consequences for the evolution of its karst features. Extending the CIKM to accommodate the unique characteristics of the karst on Guam takes it an important step closer to a fully general model of karst for small carbonate islands. Such a model is prerequisite to successful development and management of groundwater resources on small carbonate islands, especially in the face of their rapidly growing populations and economies (Falkland 1991).

Besides recognizing the unique attributes of island karst, the CIKM divides carbonate islands into three broad geomorphic types (Fig. 3) in terms of the position of the carbonate-basement contact with respect to sea level and the island surface. *Simple carbonate islands* contain only carbonate rocks on the surface and at a depth deep enough to interact with the fresh water lens. The Bahama Islands are an excellent example. *Carbonate cover islands* are defined by non-carbonate basement rocks that extend above sea level beneath the carbonate bedrock (but are not exposed at the surface), deflecting descending vadose water to the flank of the fresh water lens.

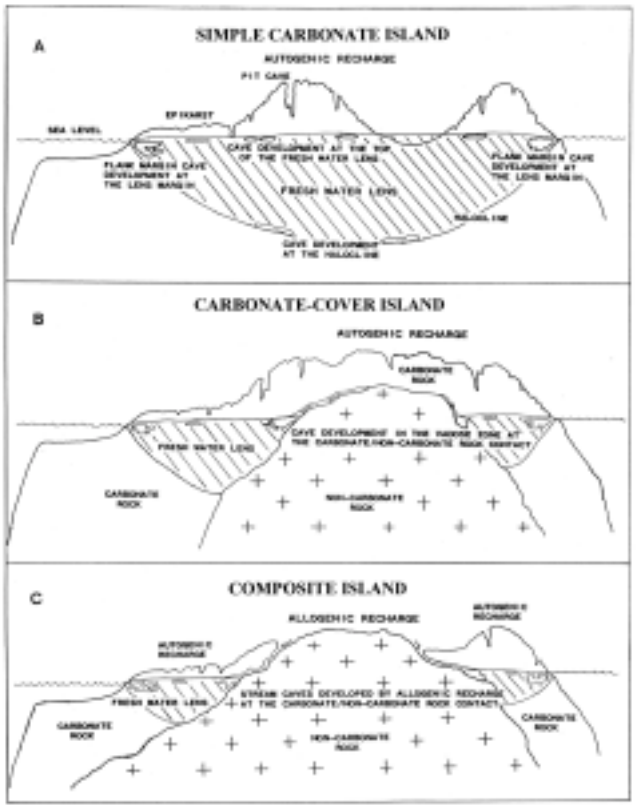


**Figure 3. Geomorphic classification of carbonate islands, based on the position of the carbonate-noncarbonate contact with respect to sea level and the surface of the island (from Mylroie *et al*. 1999).**

Islands can shift between simple and carbonate cover conditions with changes in relative sea level. Bermuda, for example, is a simple carbonate island during glacioeustatic sea-level highstands, but a carbonate cover island during lowstands (Mylroie *et al.* 1995). *Composite islands* contain carbonate and non-carbonate rocks exposed on the surface, in varying relationships and amounts. Barbados is a well-studied example. Islands in which volcanic rocks form the vast majority of the surface outcrop, with only limited carbonate exposures, as on some Hawaiian islands, are considered to be volcanic islands (Vacher 1997), outside of the CIKM classification scheme. The full range of differences in carbonate island aquifer characteristics occurs in the transition from a small, simple carbonate island to a large composite island. For a given island, sea level change may control the transition of island type. When sea level falls, an island will become larger as lagoons and forereef slopes become exposed. The fresh-water lens may also drop into the area of influence of basement rocks, forcing a simple carbonate island transition to a carbonate cover island. If a carbonate island has a minor basement rock inlier at a high elevation, a rise in relative sea level can decrease overall island size and carbonate outcrop area, making the basement outcrop a consequently more important component of the island's hydrology.

## CLIMATIC AND GEOLOGIC CONDITIONS

### CLIMATE AND HYDROLOGY

Guam is located at 13º28' north latitude, and has an equable mean annual temperature of 27º C. Rainfall averages 220-250 cm/yr, 70-80% of which arrives during the wet season from July to December. Trade winds bring dry conditions from January to May. During El Niño events, drought can be severe. Daily rainfall is highly variable, with important hydrological consequences. Some 20% of the mean annual rainfall arrives on days seeing less than 0.6 cm; it is thus unlikely to infiltrate past the root zone. At least another 20% arrives on days receiving 5 cm or more. Rapid rise and recovery of aquifer water levels immediately following such events, especially during the wet season, suggests that recharge from such heavy rainfall is transient. The proportion of rainfall contributing to the long-term equilibrium thickness of the fresh water lens thus seems likely to be no more than about 60% of the mean annual rainfall (Jocson *et al.* 1999; Contractor & Jenson 2000). Tropical cyclones, with an average recurrence of about one in three years, can bring up to 50 cm of rain in a single event. Although the hydrologic responses to these heavy storms are transient, cumulative effects on cave and karst evolution over geologic time could be significant. The nature of Guam's paleoclimate is unknown, including the degree to which Quaternary climate fluctuation affected rainfall and evapotranspiration. It should, therefore, be kept in mind that while the island's fresh-water lens is now equilibrated to current climatic conditions, the carbonate rock and the terrain formed on it might have gained their current characteristics under different (and varying) climatic conditions.

### LIMESTONE GEOLOGY OF GUAM AND ITS RELATION TO THE CIKM

The seminal study on the geology of Guam is the work of Tracey *et al.* (1964). Reagan and Meijer (1984) made some revisions to the volcanic stratigraphy, but Tracey *et al.*'s report, with its 1:50,000 scale map, remains the primary reference (Fig. 2a). Early stage island-arc volcanism is recorded by Late Middle Eocene pillow lavas, breccias, and dikes. Subsequent volcanism in the Late Eocene to Middle Oligocene produced an overlying unit of breccias, tuffaceous sandstones, flows, and sills. These two units are unconformably overlain by a Late Miocene volcaniclastic unit containing occasional limestone fragments named the Maemong Limestone Member, indicating that a shallow carbonate depositional environment existed nearby. Overlying the Miocene volcanic unit are the Miocene Bonya and Alifan Limestones. These limestones now appear primarily as outliers on the high points of the underlying volcanic terrain of southern Guam, although small outcrops are mapped in northeastern Guam, near Mt. Santa Rosa, where the contemporaneous Janum Limestone, a rhythmically bedded argillaceous limestone deposited on its flank, is also exposed in the sea cliffs nearby.

On northern Guam, the most extensive limestone unit is the detrital Mio-Pliocene Barrigada Limestone, which lies atop the volcanic basement and comprises most of the bedrock. In much of the interior of northern Guam, the Barrigada Limestone extends to the plateau surface. Elsewhere, it grades laterally and upward into the Plio-Pleistocene Mariana Limestone, a reef and lagoonal deposit that occupies the largest surface area of any carbonate unit on Guam and dominates the perimeter of the northern plateau as well as the eastern edge of southern Guam. The Barrigada and Mariana Limestones are the major aquifers of northern Guam.

Guam has evolved in a tectonically active area. Episodes of uplift and subsidence, with associated normal faulting, have been ongoing prior to, during, and subsequent to carbonate deposition. Earthquakes are common, including a magnitude 8.1 event in August 1993. Recent uplift can be seen in the raised terraces of the Holocene Merizo Limestone, which is the final unit of the limestone succession on Guam. The predominant structural feature of the island is the NW-SE trending Pago-Adelup Fault, which separates the limestone plateau in the north from the primarily volcanic terrane in the south. (See Fig. 2 for the location of this and the rest of the features referred to in this report.) The northern plateau rises from near sea level adjacent to the fault to 190 m at the northernmost tip of the island. Volcanic outcrops form the summits of Mt. Santa Rosa and Mataguac Hill, rising to 252 m and 189 m, respectively, above the limestone plateau. The volcanic terrane in the south is deeply dissected hilly to mountainous uplands, with scattered limestone remnants. Mount Lamlam, the highest point on Guam at 405 meters (1,334 ft) a.s.l., is formed in the remnant of Alifan Limestone comprising much of the crest of the cuesta fronting the western coast of southern Guam.

The complex geologic history of Guam has produced an especially wide variety of karst landforms and caves. Guam combines, on a single island, features ranging from those characteristic of the simplest islands to those resembling continental landforms. At modern sea level, the volcanic basement lies well below the base of the fresh-water lens beneath about 80% of the northern limestone plateau. This portion of the plateau, thus, fits the simple carbonate island model (Fig. 3). Beneath the other 20% of the surface, however, the volcanic basement rises above sea level, thus fitting the carbonate cover model. Emery (1962) concluded that there were four submerged terrace levels around Guam, presumably marking prolonged relative sea level stillstands. Figure 4 shows the relative proportions of the plateau occupying simple vs. carbonate cover conditions for sea levels inferred to correspond with each of the terrace levels reported by Emery (neglecting any errors due to differential displacements of separate fault blocks). Finally, at Mt. Santa Rosa and Mataguac Hill in the northeastern corner of the plateau, about 1% of the basement is exposed at the surface, fitting the composite island model. Uplifted terraces are also common (Fig. 5).

The southern half of Guam is uplifted volcanic terrane upon which lies carbonate remnants, outliers, and occasional fragments of shallow-water carbonate deposits embedded in


**Figure 4. Contours (in feet) on volcanic basement rock corresponding to modern sea level and the four submerged terrace levels as mapped by Emery (1962).**

**Figure 5. Karrenfeld on marine terrace, with further uplifted terraces in the background, on the east side of Guam, south of Sasajavan.**

the upper volcanic units. With the exception of the Mariana Limestone on the Orote Peninsula and the eastern coast of southern Guam, the base of the carbonate units in the south is now elevated above modern sea level, so that the units are removed from the direct influence of glacioeustasy and from the dissolution effects of fresh and marine water mixing. The karst of southern Guam is, thus, more analogous to that in larger islands such as Puerto Rico and Jamaica; as in these larger islands, the inland limestone units of southern Guam exhibit caves and karst landforms similar to those found in tropical continental settings.

## KARST FEATURES ON GUAM

The karst landforms of Guam can be placed into two broad physiographic groups: those exemplary of carbonate island karst, which dominate the north, and those that imitate the karst of continental settings at similar latitude, which are found in the upland areas of the south. From the hydrologic and karst genetic perspectives, there are three logical subdivisions for karst features on carbonate islands regardless of physiographic provenance: surficial features, which are associated with catchment, infiltration, and surface dissolution from meteoric waters; subsurface features, which are involved in vadose and phreatic groundwater transport and dissolution; and coastal features, which are associated with groundwater discharge. We now describe the major types of karst features found on both northern and southern Guam in terms of these three groupings. For a complete and thorough description of caves and karst on Guam, with numerous maps and figures, the reader is referred to Taborosi (2000), a masters thesis written as the foundation for the karst inventory of Guam.

### SURFACE FEATURES: EPIKARST & CLOSED DEPRESSIONS

The epikarst is the zone of dissolutional sculpturing (karren), weathered bedrock and soil products that develops from the surface downward for a few meters. Karren is a general term for dissolutional sculpturing in the millimeter to meter scale. Carbonate island karren is similar to that in interior continental settings, except that the salt spray of island and coastal environments produces the phytokarst of Folk *et al*. (1973) or the biokarst of Viles (1988) (Fig. 5). Below the salients of the karren, soil and weathered bedrock debris overlie solution fissures, holes and other shallow, small cavities in the bedrock to make up the epikarst. The most striking difference between island and continental epikarsts follows from the eogenetic character of the island rocks, which commonly produces an extensive chaotic surface of porous, dissolutionally modified rock fragments. The epikarst on Guam appears identical to that found on any number of carbonate islands in the Atlantic and Caribbean region (e.g., Bermuda, the Bahamas, Isla de Mona).

Closed depressions on carbonate islands can result from any combination of dissolution, natural construction, and human modification. Dissolution on young islands generally produces closed depressions of small to modest size, meters to tens of meters (Mylroie & Carew 1995; Wilson *et al.* 1995). Areas with autogenic recharge are unlikely to develop large, deep depressions because dissolution tends to be dispersed rather than focussed. Most large depressions on simple carbonate islands appear to be constructional, i.e., they are the result of depositional topography, or subsequent tectonic deformation (Mylroie & Carew 1997). In Bermuda and the Bahamas, for example, swales between eolianite ridges produce extremely large and deep closed depressions. Human activities such as quarrying and construction of stormwater ponding basins tend to accentuate pre-existing closed depressions because closed depressions are typically selected for

such activities. On the other hand, depressions are also frequently filled to support construction or dispose of waste.

In the Barrigada and Mariana Limestones of northern Guam, closed depressions tend to be broad and shallow, suggesting origin by deposition and secondary structural modification. Streams are completely absent, except in the vicinity of Mt. Santa Rosa, Mataguac Hill, and Harmon Sink. Small ephemeral streams head on the volcanic outcrops at Mt. Santa Rosa and Mataguac Hill, where allogenic water sinking at the limestone contact has produced blind valleys that have evolved into locally significant dissolutional depressions. Harmon Sink, a deep elongate depression in a westward-trending valley terminating just inland of Tumon Bay (Fig. 2), is fed by autogenic water carried by an ephemeral sinking stream. The Harmon Sink stream system appears to be the single, though significant, exception to the otherwise general absence of deep closed depressions and stream courses on the limestone terrain of the northern plateau. Collapsed sinkholes can also be found on Guam, although they do not appear to be common. The few collapsed sinkholes that we have documented include some small cenotes 3-10 m deep in the Tarague area, a 25-m deep, vertical-walled sink in Chalan Pago (Carinos Pit), a 10-m deep sink in Barrigada (Appealing Cave), and a 3-m deep banana hole-type depression at Finegayan. The Chalan Pago and Barrigada pits are each associated with about 100 m of lateral passage development.

Immediately north of the Pago-Adelup Fault, the limestone area mapped (by Tracey *et al.* 1964) as the Argillaceous Member of the Mariana Limestone exhibits karst topography and hydrologic characteristics that set it apart from the rest of the northern plateau. Terrain is characterized by relatively large and deep, steep-walled, closed depressions and deeply incised rectilinear dry valleys following trends consistent with local fracture orientations. These valleys support ephemeral sinking streams that disappear into the valley floor before emptying into the Agana Swamp to the west, or Pago Bay to the east. The terrain is, thus, reminiscent of classic karst terrain in continental settings, in contrast to the rest of the limestone plateau. The reason for this contrast is not yet clear, but seems likely to be related to differences in the lithology (as suggested by Tracey *et al.* 1964) and/or stratigraphy arising from the area's juxtaposition against the nearby higher volcanic terrain, which provided a source of non-carbonate terrigenous sediment during and following carbonate deposition. The armoring of the carbonate surface by volcaniclastic debris from the highlands to the south may also be responsible for the large number of sinking streams. This question is under active study (Mylroie *et al.* 1999).

The Bonya Limestone in southern Guam is entirely surrounded by volcanic rocks, and several streams flow through the area. These streams provide local base level and underdrain the limestone. As a result, large, deep closed depressions (50 m across, 20 m deep) have developed so close to one another that they are now separated by very narrow (down to less than a meter wide) ridges reflecting the original surface, to form terrain reminiscent of the cockpit karst of Jamaica. At least one of the base-level streams flows through the subsurface in large conduit passages. To the west, in the Mt. Almagosa area, some large closed depressions are found in the Alifan Limestone, probably associated with major internal conduits. Contact springs at the base of the Alifan Limestone augment stream flow that develops on the volcanic terrain of the mountain flanks. Large closed depressions are also located in southern Guam within the broad band of limestone mapped as Agana Argillaceous Member on the southeastern flank of the island (Fig. 2a). Such depressions in the vicinity of Talofofo include dry valleys. We propose that the observed large closed depressions could not have formed without the adjacent insoluble volcanic surfaces, and the colluvium derived from them, to perch surface water and isolate it from active contact with the limestone prior to the stream sink point.

### CAVES

Systematic attempts to document the caves on Guam have begun only in recent years. Historically, indigenous people used sea-level caves containing fresh water as water sources, but not as dwellings. During the Second World War, Japanese garrisons modified caves for fortification, and stragglers took refuge in caves following the liberation. Live ordinance remains in many (Fig 6). Subsequent to the war, U.S. military personnel and other visitors made maps and sketches of caves, but none were published, and most maps left the island with their authors. The single best published source of information about caves on Guam is the comprehensive compendium by Rogers & Legge (1992), who list 74 caves based on systematic work that they did as part of the Pacific Basin Speleological Survey. In recent years, a local NSS-affiliated group, the

**Figure 6. Live munitions from World War II exposed in a cave. Care must be taken to avoid these and other relics when working in caves on Guam.**

**Figure 7. Deep vadose shaft (45 m) behind Amantes Point, west coast of Guam.**

Micronesian Cavers, has been making systematic efforts to locate and explore caves on Guam and elsewhere in the region. Currently, a scientific karst and cave inventory of Guam is being led by the Water and Environmental Research Institute of the Western Pacific, University of Guam (Taborosi 1999, 2000), as part of the work reported in this paper.

We discuss the caves of Guam here in terms of three field categories that are germane to carbonate islands: pit caves, stream caves, and flank margin caves. Pit caves (Mylroie & Carew 1995; Mylroie *et al.* 1995) carry vadose water from the epikarst into the subsurface, and can be very abundant locally on carbonate islands in general. A broad gradation of sizes can exist, from shallow and narrow pipes that barely penetrate the epikarst, to enlarged fissures, to classic vadose shafts. The deeper ones are effective vadose bypass routes for infiltrating water. Pit caves may intersect other voids at depth, including stream caves or flank margin caves (Mylroie & Carew 1995; Mylroie *et al.* 1995). In contrast to their occurrence on Caribbean islands (Harris *et al.* 1995), pit caves on Guam do not occur in clusters and are relatively rare. Tracey *et al.* (1964) noted the presence of cavernous development in the Mariana Limestone. This unit features well-developed pits along the cliffs at Amantes Point (45 m deep, Fig. 7) and Tanguisson (10 m deep) on the west coast, and at Talafofo Caves (35 m deep) on the east coast.

Traversable stream caves have developed on Guam along the contacts between limestone and the underlying volcanic units (Jenson *et al.* 1997) in both the north and the south. In northern Guam, several can be found on the flank of Mt. Santa Rosa. These are active caves fed by allogenic water from the volcanic slopes above the contacts. The primary discharge point for the water carried by the caves on the eastern flank of Mt. Santa Rosa is probably Janum Spring (discussed in "Discharge features" below). The upper levels of Awesome Cave, one of the more spectacular of the several Mt. Santa Rosa caves, exhibits a series of wide chambers, now undercut by a vadose streamway (Fig. 8). We propose that these are dissolutional features marking relative sea-level stillstands, during which vadose stream water mixed with the top of the fresh-water lens to create a broad dissolutional horizon. Alternatively, the broad chambers may represent collapse features formed as a result of vadose streamways meandering and undercutting the volcanic-limestone contact, as has been proposed for large chambers in Bermuda (Mylroie *et al.* 1995). In Awesome Cave, the well-developed phreatic dissolution features on the cave walls (cusps, rock pillars, etc.) argue for an *in situ* dissolutional origin in the fresh-water lens. Nearby Piggy Cave, however, has large collapse chambers that might follow the Bermuda model or merely be large phreatic dissolution chambers now undergoing collapse. In the Agana Argillaceous Member of the Mariana Limestone, at the opposite end of the plateau, we have identified no stream caves in the dry valleys we have explored so far. Relief is low, however, so whatever conduits may have developed during Pleistocene sea-level lowerings might now be below base level and inaccessible, perhaps clogged with sediment in the low gradient conditions currently present.

In southern Guam, stream caves occur in the Bonya Limestone and in the Alifan Limestone at Mt. Almagosa (Fig. 9). These caves have also formed at the contact with underlying volcanic rock, but are in limestone remnants positioned well above sea level, and thus unaffected by dissolution associated with fresh-water lens positions. These caves are, therefore, similar in origin and morphology, if not size, to similarly situated continental or large-island caves. In the Bonya Limestone, the perennial Tolaeyuus River (a.k.a. "Lost River") is fed by allogenic water from streams heading on the volcanic terrain above, plus discharge from Bona Spring, which rises on the contact between the Alifan Limestone and the underlying volcanic rock. In the basin, it disappears into a flooded cave and reemerges some 500 meters downstream. Almagosa Spring, one of the contact springs at the base of the Alifan Limestone, issues from a cave that is traversable for some 250 m. Flow is seasonally variable, but sufficient to have justified

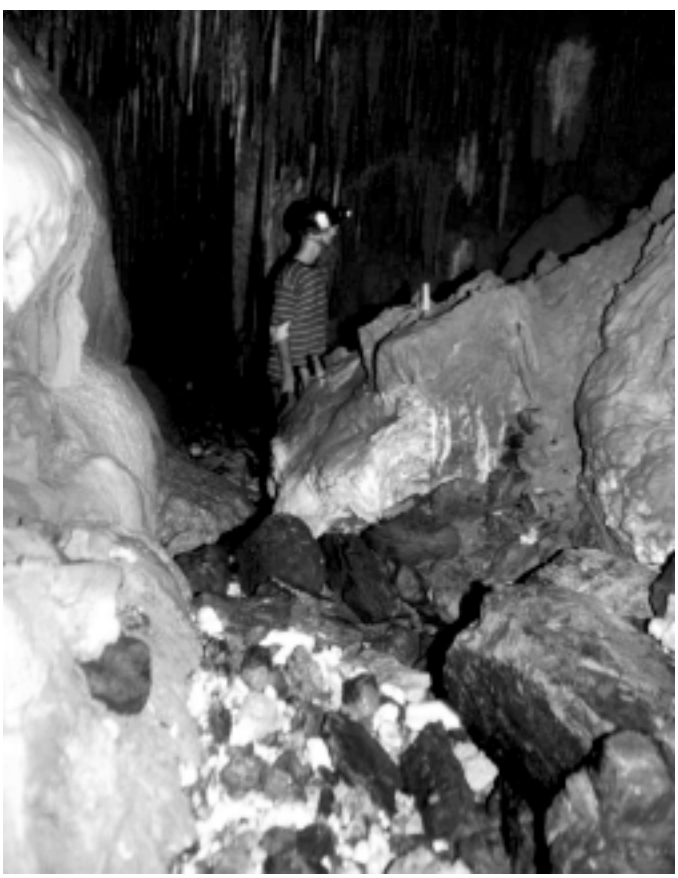

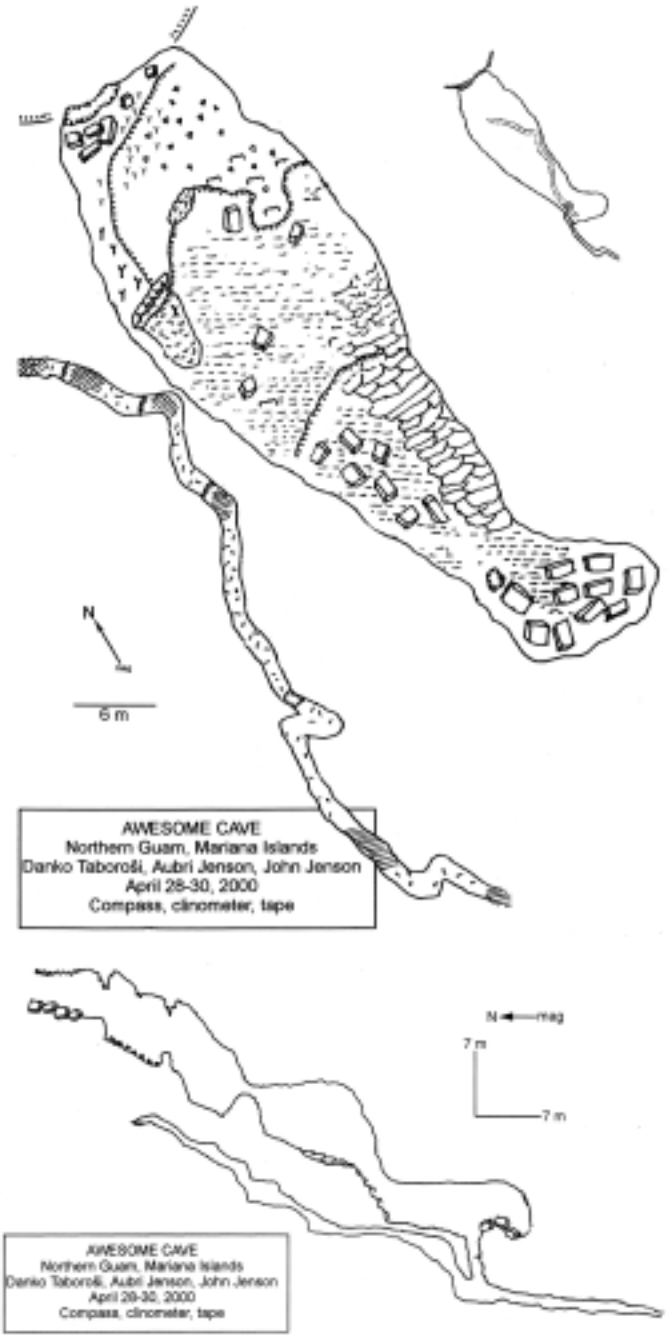


**Figure 8. a-left top) Upper phreatic chamber of Awesome Cave, on the flank of Mt. Santa Rosa, northeast Guam. Note the dissolutional surfaces. b-left bottom) Typical vadose passage found at Mt. Santa Rosa, formed at the contact of the white limestone and the black volcanics, with incision into the volcanics. c-right) Map of Awesome Cave (Taborosi 2000) showing stacked phreatic chambers underdrained by vadose flow. The phreatic chambers formed within a fresh-water lens, fed by allogenic vadose flow, and were sequentially abandoned by tectonic uplift of the island.**

development of the spring as a water source by the U.S. Navy.

Flank margin caves are characteristic carbonate island features that form at sea level in the distal margin of the fresh-water lens. They have been well documented in the Caribbean (Mylroie & Carew 1995; Mylroie *et al.* 1995 and references therein). Because they are fed by diffuse groundwater flow, they reflect mixing chambers rather than conduits. Their presence indicates, in fact, that conduit flow was not operating in their immediate vicinity—or it would have captured the diffuse flow that helped develop the caves. Low, wide chambers oriented parallel to past shorelines are abundant on Guam. We have interpreted these as flank margin caves. Pagat Cave (Fig.

**Figure 9. Cave in southern Guam, developed in the Bonya Limestone, which carries a base level stream at the limestone/volcanic contact and connects to deep cockpits.**

10) at sea level on the northeastern coast of Guam, for example, is typical of flank margin caves, and shows overprinting by subsequent sea level events. It is currently half-filled with fresh water, yet the walls show evidence of vadose calcite deposition with later dissolution under phreatic conditions; stalagmites are found beneath the fresh water currently filling the lower regions of the cave. Given glacio-eustasy, and the uplift of the island, such a complex history is expected. During aerial reconnaissance of the island, we saw numerous cave openings on the cliffs along the periphery of the northern half of the island, as well as in the Talofofo area on the southeast coast (Fig. 11). Most of these voids were clearly at preferred horizons, indicating paleo-horizons of the fresh-water lens associated with a glacio-eustatic sea level stillstand, a period of tectonic quiescence, or both.

DISCHARGE FEATURES

In the karst region in the interior basin of southern Guam, water discharges from karst springs and resurgences into streams that determine the local base level, as in classical continental karst. The streams from the interior converge on trunks that flow east out of the basin across volcanic terrane until they intercept the limestone apron flanking the southeast coast. Because they are antecedent to the limestone, they have incised sheer canyon walls where they pass through. Between the trunk streams, small amounts of locally captured water discharge from the limestone.

In the northern plateau, fresh water discharges entirely from ubiquitous coastal springs and seeps, except at the southern end near the Pago-Adelup Fault. Here, the Fonte and Pago Rivers head on the volcanic terrain opposite the fault, then turn to run parallel or along it, discharging, respectively, into Agana Bay on the northwest and Pago Bay on the southeast. Immediately south of the Agana Swamp, the perennial Chaot

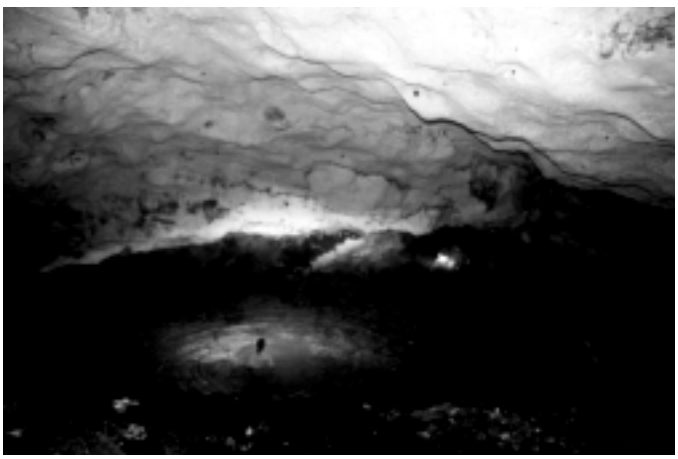

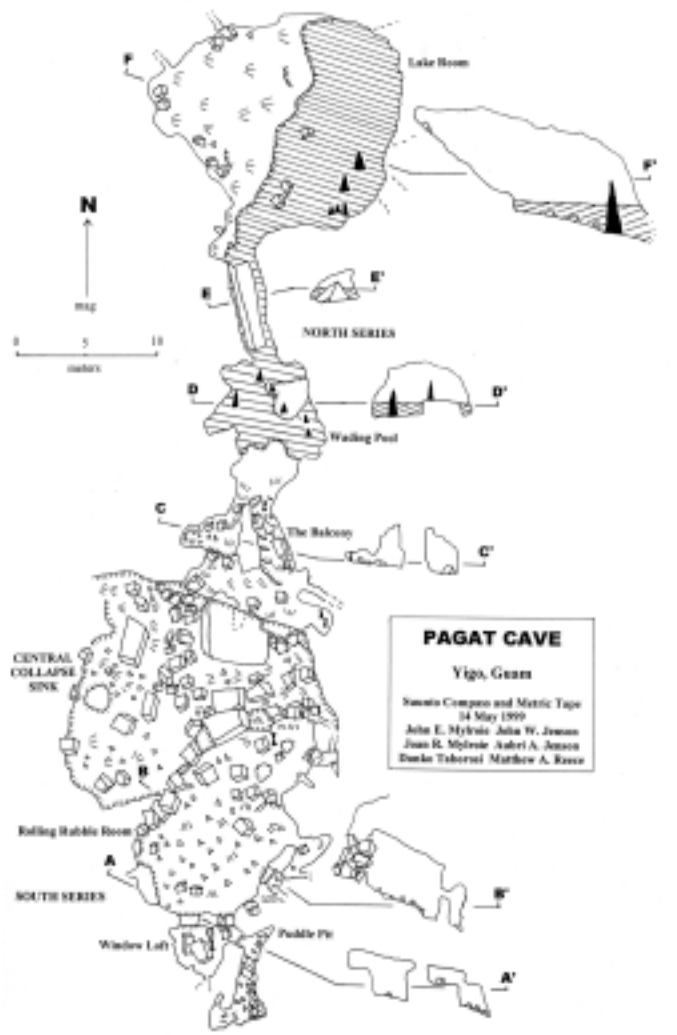


**Figure 10. (a-top) Fresh water pool at sea level in the Lake Room of Pagat Cave, a typical flank margin cave located on the northeast coast of Guam. (b-bottom) Map of Pagat Cave showing development north-south, parallel to the coast line and the distal margin of a past fresh-water lens.**

**Figure 11. (a-top) Air photo of the Talafofo area, showing cave entrances in a cliff developed in Mariana Limestone; it is uncertain if these are flank margin caves or remnants of stream caves draining the volcanic uplands to the west. (b-bottom) Tarague cliffs on the north coast of Guam, showing breached flank margin caves containing abundant speleothems. The caves, while at a constant horizon, show the "beads-on-a-string" morphology produced by cliff intersection of adjacent cave chambers.**

River heads and runs through a deeply incised valley in the Agana Argillaceous Member, first running inland, then turning back to discharge into the swamp. Agana Spring, which rises in the Agana Argillaceous Member and discharges at the south end of the Agana Swamp, is reported to have been a long-used local drinking water source, but from reports by local residents, flow fell to insignificance when pumping wells were installed on the terrain above. The only other inland spring on northern Guam is Mataguac Spring, in the northeast, on the flank of Mataguac Hill. It disappears into a small cave that is traversable for only some 30 meters.

**Figure 12. Vista of Tumon Bay, looking southeast. Note the extensive beach, with the recessed cliff line trending from the foreground inland to the east and trending back west in the background.**

Coastal groundwater discharge around the northern plateau is highly variable from one location to another, both in volume and style, as reported by earlier workers (Emery 1962; Matson 1993). We have examined the entire coastline on various occasions by foot or from boat or airplane. Our efforts have focused, however, on the 16-km sector along the northwest coast from Tumon Bay to Double Reef, which we have examined in detail on foot and by diving along the near-shore to locate sources of fresh-water discharge. This sector is accessible and representative of the coast as a whole in that it exhibits each discharge style found along the 80-km coastline of northern Guam. Significantly, it drains about 40% of the plateau while constituting only 20% of the coastline.

Jenson *et al.* (1997) described the coastline of northern Guam in terms of three distinct coastal morphologies. About 16% of the coastline is occupied by deeply scalloped embayments with broad interior beaches fronted by shallow platform reefs extending to the mouth of the bay (Fig. 12.). These include Agana Bay and Tumon Bay on the southwest coast, Pago Bay at the southeast corner of the plateau, and Haputo Bay, much smaller than the other three, on the northwest coast. In each of these embayments the cliffline is typically recessed 10s to 100s of meters behind the beachfront, and groundwater discharge is characterized by permanent seeps (Fig. 13 ) and springs (Fig. 14) distributed along the perimeter of the bay, with rarely more than about 100 meters between significant seeps or springs. Effluent is well exposed by the lowest tides, with the larger springs typically reworking the beach sand into meter-scale channels and deltas, as seen in figure 13. Jocson (1998) estimated low tide discharge for the largest Agana Bay and Tumon Bay springs to be about 0.2 $m^3s^{-1}$. On the east side of the island, nearly opposite Tumon Bay, is Sasajyan, a scalloped area where the cliff line lies about 1.5 km inland and is fronted by a sloping surface (4-5% grade) rising from a few

**Figure 13. Large seep field behind Pacific Island Club complex in Tumon Bay. Estimated flow is about 30 L/sec (Jocson 1998). Sand channels and small deltas are built and destroyed with each tidal cycle.**

**Figure 14. Wet Willies Spring. Estimated flow is about 50 L/sec (Jocson 1998).**

meters at the shoreline to 50-60 meters near the base of the cliff line. Its size and shape are reminiscent of Tumon Bay, suggesting it could be an uplifted embayment of similar origin, although this question has yet to be investigated.

The second type of coastal morphology is sandy beaches following linear coastline with fringing reefs, which provide the sand and protect the beach from the surf (Fig. 15). These occupy about 24% of the total coastline, mostly in a continuous stretch from Uruno Point clockwise around Ritidian Point to Tagua Point at the northwestern corner of the island. The cliffline is generally recessed 10s to 100s of meters behind the shoreline. We have observed numerous seeps along the beaches but, with one exception partway between Ritidian and Tarague Points, we have not found significant concentrated flow from either caves or sea-level coastal springs in this environment.

About 60% of the total coastline is sheer cliffs with narrow

**Figure 15. Linear beach along north coast of Guam, between Tarague Beach and Ritidian Point; lowest cliff near beach in center of the photograph contains the cave entrances shown in figure 11b.**

to no benches, which support no beaches and only occasional small reefs (Fig. 16). Rock along the coast is typically strongly indurated, and we have found no evidence of distributed, diffuse seepage in this zone. Discharge appears rather to be associated with dissolution-widened fractures, flowing caves, and submarine vents. The largest of the dissolution-widened fractures are up to about 2 or more meters wide, are traversable a few 10s of meters into the cliff face, and discharge an estimated 0.1 $m^3s^{-1}$ (Fig. 17-19). The largest single discharge observed on the coast of the plateau so far is at Coconut Crab Cave, which Jocson (1998) estimated to be at least 0.25 $m^3s^{-1}$. Finally, we have observed a few small submarine discharges at ~4-6 m depth along this zone, and three larger vents at ~10 m depth. Flux is difficult to measure from these, but our initial impression of discharge from the large vents, based on visual observation while diving to observe the cold plume issuing

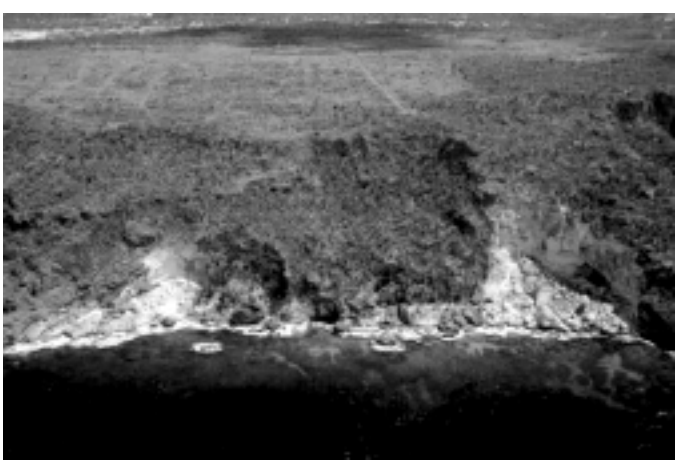

**Figure 16. Rocky coastline with no beach along northeast Guam, near Janum.**

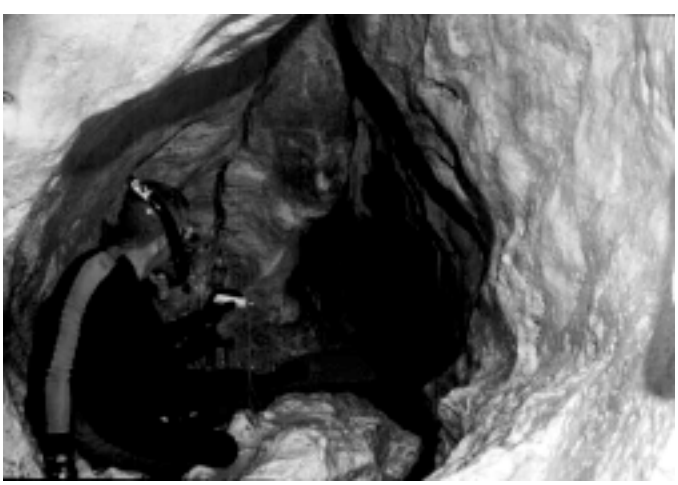

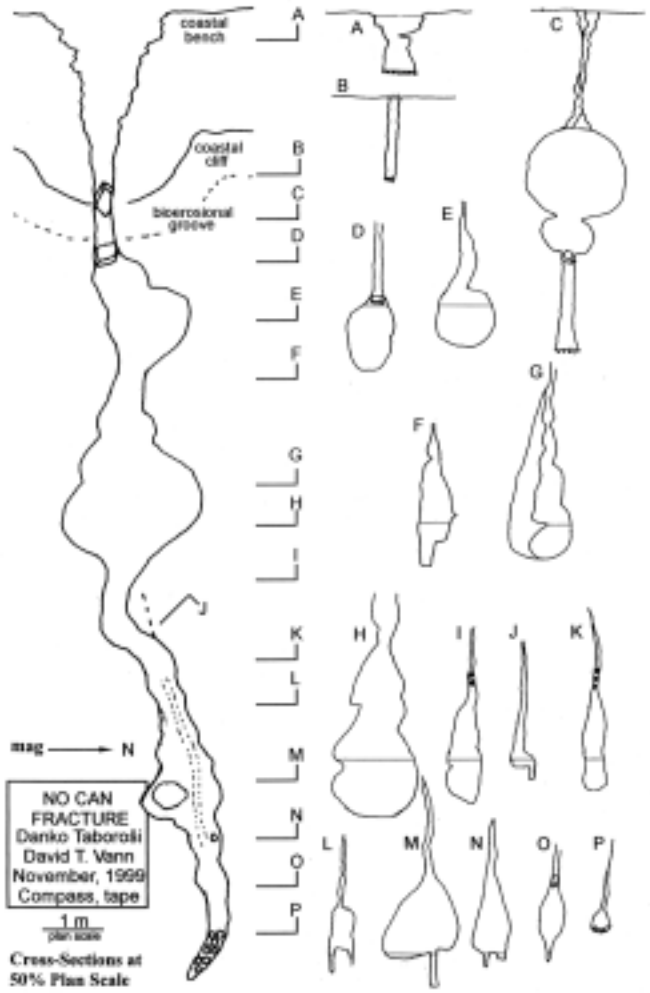


**Figure 17. a-left top) Entrance to No Can Fracture. b-left bottom) Phreatic tube, back end of No Can Fracture. c-right above) Map of No Can Fracture (Taborosi 2000).**

from the vents, is that flux from each may be comparable to the discharge from Coconut Crab Cave (the term "cold" is relative, as the springs discharge water at a temperature of 26-27ºC, while the shallow lagoon can easily exceed 30ºC as a result of solar heating).

The Pacific (eastern) coastline of the northern plateau is notably devoid of beaches and reefs, and the total discharge is limited by the restricted size of the groundwater catchment area bounded by the basement ridge (Figs. 2 and 4) running from the Barrigada Hill area to Mt. Santa Rosa. Here, some 35% of the coastline drains only about 10% of the plateau. Discharge is difficult to observe because of the usually heavy surf from the easterly Trade Winds and lack of footing beneath the cliffs, but observations so far suggest that discharge is sparse and relatively small over most of this stretch of coastline. The important exception is Janum Spring, which is well known locally and supported an ancient settlement on the adjacent terrace. The cavern at the mouth of the spring collapsed during the 1993 earthquake, so that the discharge point is now covered with rubble and is unobservable. Authors Jenson and Wexel, however, observed an extensive plume of reddish discharge from Janum Spring during a local heavy rainfall while working in the Mt. Santa Rosa area, suggesting that Janum Spring is the mouth of a trunk by which water discharges from a cave system descending the eastern flank of Mt. Santa Rosa.

## CONCLUSIONS

Guam represents as complete a site for the investigation of island karst as exists anywhere in the world. In the south, it has

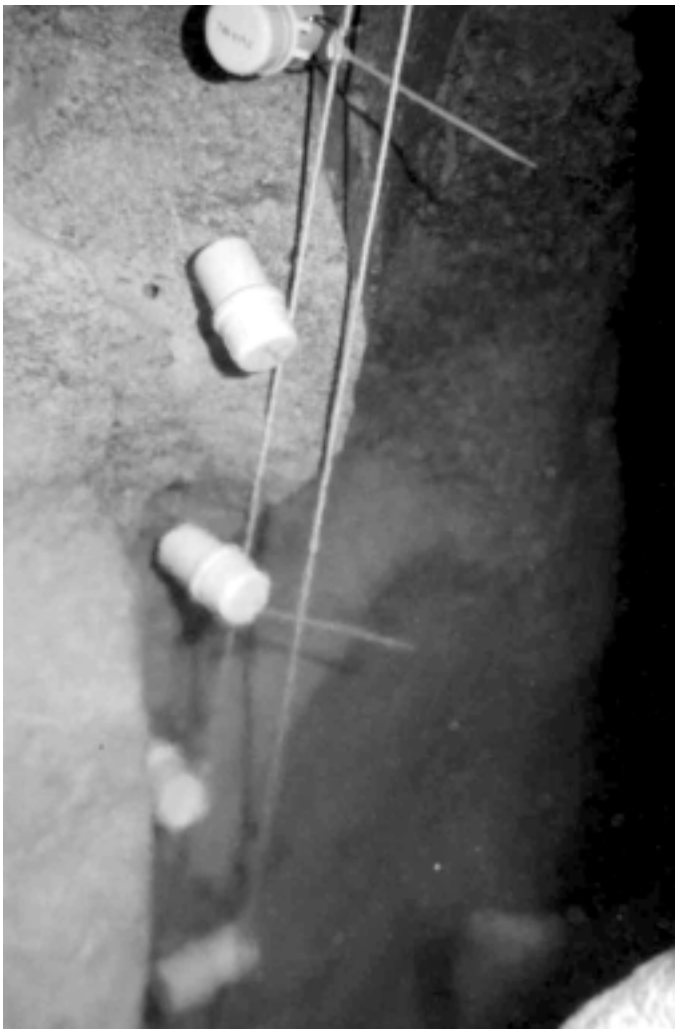

**Figure 18. Halocline in No Can Fracture. White objects are waterproof casings holding temperature probes, note that lower ones appear fuzzy as they are below the halocline. The entire view is under water. Photo by J. Carew.**

**Figure 19. Large fracture cave on the coast, a few hundred meters south of No Can Fracture. These features are common along the northwest coast of Guam.**

interior elevated limestones that contain karst identical to that of inland, tropical continental situations. In the north, it contains the karst characteristic of simple carbonate islands, carbonate cover islands, and composite islands (Fig. 19). The southern half of Guam therefore can be characterized in terms of established karst ideas derived from continental settings. However, the northern half of the island, which contains the vast majority of the island's water reserves, must be viewed in terms of the unique characteristics of the Carbonate Island Karst Model (CIKM) in order for those water resources to be successfully conserved and utilized.

## ACKNOWLEDGEMENTS

The research reported here was funded by the U.S. Geological Survey, Water Resources Division, through the Water Resources Research Institute, Regional Competitive Award Program, award no. 1434-HQ-96-GR-02665. Initial work was also supported by the Guam Hydrologic Survey Program of the Water & Environmental Research Institute of the Western Pacific, University of Guam, which was initiated by the 24th Guam Legislature. We wish to express our appreciation to the commanders of the local Navy and Air Force installations for allowing access to military property on Guam. Dirk Ballendorf, Micronesian Area Research Center, University of Guam, took the time to check our historical references. Bruce Rogers has been an active source of information regarding previous exploration of caves on Guam. Mike Brown is thanked for assisting JEM with image manipulation. Reviews by Walt Ebaugh and Fiona Whitaker were extremely useful.

**Figure 19. Cliff at Amantes Point, showing stacked cave levels, now breached with speleothems exposed. A modern bioerosion notch is visible at sea level. As uplift occurs, cliff erosion first removes evidence of older bioerosion notches, then further erosion exposes the flank margin caves within the cliff.**

## REFERENCES


Contractor, D.N. & Jenson, J.W., 2000, Simulated effect of vadose infiltration on water levels in the Northern Guam Lens Aquifer: Journal of Hydrology, v. 229, p. 232-254.

Emery, K.O., 1962, Marine Geology of Guam, U.S. Geological Survey Professional Paper 403-B: US Government Printing Office, Washington, D.C., p. B1-B76.

Falkland, A., 1991, Hydrology and water resources of small islands: A practical guide: UNESCO, Paris, 435 p.

Folk, R.L., Roberts H.H. & Moore, C.C., 1973, Black phytokarst from Hell, Cayman Islands, British West Indies: Geological Society of America Bulletin, v. 84, p. 2351-2360.

Harris, J.G., Mylroie, J. E. & Carew, J. L., 1995, Banana holes: Unique karst features of the Bahamas: Carbonates and Evaporites, v. 10, no. 2, p. 215-224.

Jenson, J.W., Jocson, J.M.U. & Siegrist, H.G., 1997, Groundwater discharge styles from an uplifted Pleistocene island karst aquifer, Guam, Mariana Islands, *in* Beck, B.F. & Stephenson, J.B., ed., The Engineering Geology and Hydrology of Karst Terranes: Springfield, Missouri, Balkema, p. 15-19.

Jenson, J.W., 1999, Toward a suitable conceptual model of the Northern Guam Lens Aquifer, *in* Palmer, A.N., Palmer, M.V. & Sasowsky, I.D., ed., Karst Modeling, Karst Waters Institute Special Publication 5, p. 58.

Jocson, J.M.U., 1998, Hydrologic model for the Yigo-Tumon and Finegayan subbasins of the Northern Guam Lens Aquifer, Guam [MS thesis]: University of Guam, Mangilao, 95 p.

Jocson, J.M.U., Jenson, J.W. & Contractor, D.N., 1999, Numerical Modeling and Field Investigation of infiltration, recharge, and discharge in the Northern Guam Lens Aquifer, Water and Environmental Research Institute of the Western Pacific, Technical Report #88, University of Guam, Mangilao, 22 p.

Matson, E.A., 1993, Nutrient flux through soils and aquifers to the coastal zone of Guam (Mariana Islands): Limnology and Oceanography, v. 38, no. 2, p. 361-371.

Mink, J.F. & Vacher, H.L., 1997, Hydrogeology of northern Guam, *in* Vacher, H.L. & Quinn, T., ed., Geology and Hydrogeology of Carbonate Islands: Developments in Sedimentology 54: Amsterdam, Elsevier Science, p. 743-761.

Mylroie, J.E. & Carew, J.L., 1995, Karst development on carbonate islands, *in* Budd, D.A., Harris, P.M. & Saller, A., ed., Unconformities and Porosity in Carbonate Strata, American Association of Petroleum Geologists, p. 55-76.

Mylroie, J.E., Carew, J.L. & Vacher, H.L., 1995, Karst development in the Bahamas and Bermuda, *in* Curran, H.A. & White, B., ed., Terrestrial and Shallow Marine Geology of the Bahamas and Bermuda, Geological Society of America Special Paper 300, p. 251-267.

Mylroie, J.E. & Carew, J.L., 1997, Land use and carbonate island karst, *in* Beck, B.F. & Stephenson, J.B., ed., The Engineering Geology and Hydrology of Karst Terranes: Springfield, Missouri, Balkema, p. 3-12.

Mylroie, J.E., Jenson, J.W., Jocson, J.M.U. & Lander, M., 1999, Karst Geology and Hydrology of Guam: A Preliminary Report, Technical Report #89, Water & Environmental Research Institute of the Western Pacific, University of Guam, Mangilao, 32 p.

Mylroie, J.E. & Vacher, H.L., 1999, A conceptual view of carbonate island karst, *in* Palmer, A.N., Palmer, M.V. & Sasowsky, I.D., ed., Karst Modeling, Karst Waters Institute Special Publication 5, p. 48-58.

Mylroie, J.M. & Jenson, J.W., 2000, CIKM, the carbonate island karst model, *in* Geological Society of America Abstracts with Programs, p. A-355.

Mylroie, J.M. & Jenson, J.W., in press, Guam and the Carbonate Island Karst Model: Theoretical and Applied Karstology, v. 11.

Reagan, M.K. & Meijer, A., 1984, Geology and geochemistry of early arc-volcanic rocks from Guam: Geological Society of America Bulletin, v. 95, p. 701-713.

Rogers, B.W. & Legge, C.J., 1992, Karst features of the territory of Guam: Pacific Basin Speleological Survey, Bulletin 5, p. 1-33.

Rogers, R.F., 1996, Destiny's Landfall: A History of Guam, University of Hawaii, 380 p.

Taborosi, D.S., 1999, Karst inventory of the northern Guam lens aquifer, *in* Palmer, A.N., Palmer, M.V. & Sasowsky, I.D., ed., Karst Modeling, Karst Waters Institute Special Publication 5, p. 244.

Taborosi, D.S., 2000, Karst Features of Guam [MS thesis]: University of Guam, Mangilao, 196 p.

Tracey, J.I., Jr., Schlanger, S.O., Stark, J.T., Doan, D.B. & May, H.G., 1964, General Geology of Guam, U.S. Geological Survey Professional Paper 403-A, US Government Printing Office: Washington, D.C., p. 104.

Vacher, H.L., 1997, Introduction: Varieties of carbonate islands and a historical perspective, *in* Vacher, H.L. & Quin, T.M., ed., Geology and hydrogeology of carbonate islands, Elsevier Science Publishers, p. 1-33.

Viles, H.A., 1988, Organisms and karst geomorphology, *in* Viles, H.A., ed. Biogeomorphology: New York, NY, Basil Blackwell, Ltd., p. 319-350.

Wicks, C.C., 1998, Isla de Mona Special Issue: Journal of Cave and Karst Studies, v. 60, no. 2, p. 68-125.

Wilson, W.L., J.E. Mylroie, J.E. & Carew, J.L., 1995, Quantitative analysis of caves as a geologic hazard on San Salvador Island, Bahamas, *in* Proceedings of the 7th Symposium on the Geology of the Bahamas, San Salvador Island, Bahamian Field Station, p. 103-121.

Victor J. Polyak and Paula Provencio - By-product materials relatied to $H_2S$-$H_2SO_4$-influenced speleogenesis of Carlsbad, Lechuguilla, and other caves of the Guadalupe Mountains, New Mexico. *Journal of Cave and Karst Studies 63*(1): 23-32.

# BY-PRODUCT MATERIALS RELATED TO $H_2S$-$H_2SO_4$ INFLUENCED SPELEOGENESIS OF CARLSBAD, LECHUGUILLA, AND OTHER CAVES OF THE GUADALUPE MOUNTAINS, NEW MEXICO

VICTOR J. POLYAK
*Department of Earth and Planetary Sciences, University of New Mexico, Albuquerque, New Mexico 87131, U.S.A.*
PAULA PROVENCIO
*Sandia National Laboratories, Albuquerque, New Mexico 87185, U.S.A.*

*Carlsbad Cavern, Lechuguilla Cave, and other large caves of the Guadalupe Mountains, New Mexico, contain minerals and amorphous materials derived as by-products from $H_2SO_4$ speleogenesis (process of cave formation influenced by sulfuric acid). These materials, referred to as "speleogenetic by-products," are categorized as primary or secondary. Primary speleogenetic by-products are formed directly from $H_2SO_4$ speleogenesis by $H_2S$-$H_2SO_4$ reaction with carbonate bedrock and internal sediments. They are found in cave areas protected from flood or drip waters. Secondary speleogenetic by-products are minerals and amorphous materials that formed by the alteration of the primary speleogenetic by-products, or by the late-stage remobilization of elements concentrated during speleogenesis. Primary speleogenetic by-products in these caves are gypsum, elemental sulfur, hydrated halloysite, alunite, natroalunite, jarosite, hydrobasaluminite, quartz, todorokite, rancieite, and amorphous silica and aluminum sulfates. Gypsum is the most abundant by-product, whereas alunite is the most significant because it can reveal the timing of speleogenesis. Aluminite, tyuyamunite, quartz, opal, and gypsum are secondary speleogenetic by-products. Other possible speleogenetic by-products are celestite, hydrous iron sulfates, gibbsite, nordstrandite, goethite and dolomite. The carbonate bedrocks in which the caves have formed are predominantly dolostone and limestone; mineral assemblages of these host rocks include calcite, dolomite, quartz, illite, dickite, kaolinite, interstratified illite/smectite, montmorillonite, and mica. The process of $H_2SO_4$ speleogenesis for Carlsbad Cavern and Lechuguilla Cave, and its by-products provide a general model for similar cave and non-cave systems worldwide.*

Caves formed solely by the most widely known process of cave formation, carbonic acid dissolution of limestone, are not known to contain obvious remnant by-product materials of speleogenesis. In contrast, speleogenesis influenced by $H_2SO_4$ ($H_2SO_4$ speleogenesis) produces by-product materials (speleogenetic by-products) by: (1) the alteration of insoluble sediments, (2) replacement or alteration of the carbonate rocks, or (3) precipitation of dissolved species. This is of importance to the subject of speleogenesis, because there is "left-over" material directly related to speleogenesis. Carlsbad Cavern, Lechuguilla Cave, and other caves of the Guadalupe Mountains, New Mexico, formed partly if not predominantly by $H_2SO_4$ speleogenesis. We do not imply that $H_2SO_4$ speleogenesis is influenced solely by $H_2SO_4$; carbonic acid generated from significant amounts of $CO_2$ must also play a role. These caves of the Guadalupe Mountains formed by $H_2SO_4$ speleogenesis, herein referred to as the "Carlsbad caves," contain an exceptional assemblage of materials generated by speleogenesis that will serve as a template for future studies. Figure 1 shows the study area with locations of caves most pertinent to this study.

The idea of $H_2SO_4$ speleogenesis was introduced by Morehouse (1968), Egemeier (1973, 1981), Jagnow (1977), Davis (1980), Hill (1981, 1987), and van Everdingen *et al*. (1985). More recently, White (1988), Hill (1990, 1996), Palmer (1991), Ford and Williams (1992), Buck *et al*. (1994), Pisarowicz (1994), Polyak and Güven (1996), Polyak *et al*. (1998), Polyak and Provencio (1998), and Palmer and Palmer (2000) made contributions to strengthen the theories that caves form by the influence of $H_2SO_4$. Studies of $H_2SO_4$ caves thus far have been focussed on four cave systems: (1) the Kane caves in Wyoming, (2) the Carlsbad caves in New Mexico, (3) Cueva de Villa Luz in Tabasco, Mexico, and (4) caves of the

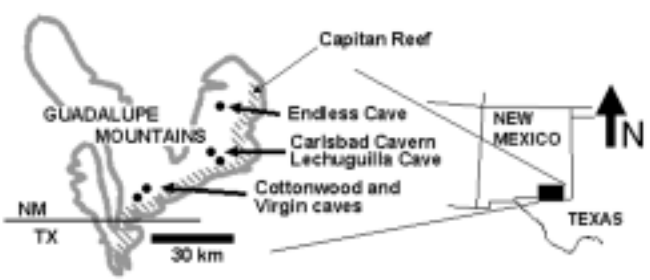


**Figure 1. Map showing location of the study area. The approximate locations of the five most pertinent $H_2SO_4$ caves are also given. The stippled pattern shows the extent of the exposed section of the Capitan reef in the study area.**

Umbria and Marche regions, Italy. Cueva de Villa Luz is an active $H_2SO_4$ cave, whereas the Carlsbad caves are relict $H_2SO_4$ caves. Lower Kane Cave is still actively forming, whereas Upper Kane Cave is relict. The Italian caves are also both relict and active (Galdenzi & Menichetti 1995). The lower passages of Movile Cave, Romania, are probably being formed in an active $H_2SO_4$ cave environment (Sarbu & Kane 1995). Mbobo Mkulu Cave in South Africa contains minerals that are characteristic of $H_2SO_4$ speleogenesis (Martini *et al*. 1997), and may be a relict $H_2SO_4$ cave. The Carlsbad caves are represented by at least 15 of the 300+ caves in the Guadalupe Mountains, five of which contain significant quantities of speleogenetic by-products.

### ORIGIN OF THE CARLSBAD CAVES

Five Carlsbad caves important to this study are Carlsbad, Lechuguilla, Cottonwood, Endless, and Virgin (Fig. 1), which are located in the Permian Capitan Limestone, Goat Seep Dolomite, and associated backreef carbonate rocks in the Guadalupe Mountains of southeastern New Mexico and West Texas (Hill 1987, 1996). These caves formed when $H_2S$ was oxidized to $H_2SO_4$ as it migrated upward and mixed with fresh waters in the thick Capitan reef and forereef limestones and dolostones (Hill 1987). The ascending $H_2S$-rich water exchanged its sulfur with many of the by-product minerals of speleogenesis. Light isotopic values of sulfur from speleogenetic by-products [$\delta^{34}S$ = -30 to 0 per mil (‰); relative to the Cañon Diablo troilite] reported by Hill (1987), Pisarowicz (1994), and Polyak & Güven (1996) indicated that the $H_2S$-$H_2SO_4$ associated with speleogenesis was derived from biogenic alteration of hydrocarbons. The dissolved $H_2S$ gas was most likely produced at the base of the highly impermeable Permian Castile (anhydrite) Formation in the Delaware Basin immediately south of the Guadalupe Mountains (Hill 1987).

The gross morphology of the Carlsbad caves suggests large horizontal passages were formed at the water table, and vertical pits and fissures were formed below the water table along the paths of rising $H_2S$ (Hill 1987; Palmer 1991). Formation of these caves followed an apparent decline of the water table, which created the multi-levels of Carlsbad Cavern and Lechuguilla Cave (Jagnow & Jagnow 1992; Polyak *et al*. 1998). Large quantities of carbonate rocks were dissolved or replaced with gypsum by $H_2SO_4$-bearing waters during this process. Recently published ages of formation for the Carlsbad caves, using the $^{40}Ar/^{39}Ar$ dating of alunite, indicated that $H_2SO_4$ speleogenesis took place in the late Miocene and Pliocene (Polyak *et al*. 1998). A simple schematic of this type of speleogenesis is presented in figure 2.

### ENVIRONMENT OF $H_2SO_4$ SPELEOGENESIS

The environment of $H_2SO_4$ speleogenesis in the Carlsbad area during the late Miocene was probably similar to the low temperature cave environment reported for the active $H_2SO_4$ caves today. Studies of Lower Kane Cave and Cueva de Villa Luz are providing significant insight into the environment of

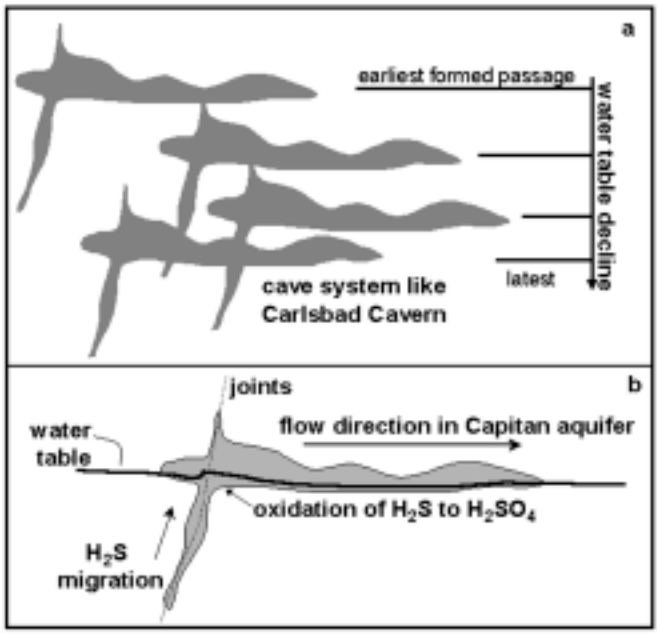


**Figure 2. (a) Proposed progression of speleogenesis that formed the large complex multi-level caves such as Carlsbad Cavern and Lechuguilla Cave. Major speleogenesis occurred mainly along the water table as the water table declined relative to the strata during the Miocene. Deeper phreatic development occurred along paths of $H_2S$ input. The younger caves or cave sections comprise the passages at the lowest elevation intervals. (b) Simple model of $H_2SO_4$-influenced speleogenesis for a single level in the Carlsbad caves. This simplified model comes from ideas of Hill (1987), Jagnow & Jagnow (1992), Polyak *et al*. (1998), and Palmer & Palmer (2000).**

$H_2SO_4$ speleogenesis, especially at and above the water table. This is an environment conducive to the production of speleogenetic by-products. For example, Lower Kane Cave and Cueva de Villa Luz have microbe-bearing, bubbling, sulfurous springs, and gypsum-encrusted cave walls. Some bacteria and other organisms seemingly thrive in the $H_2SO_4$-bearing cave environment (Kane *et al*. 1994, Sarbu & Kane 1995, Lavoie *et al*. 1998, Taylor 1999, Engel *et al.* 2000, Hose *et al*. 2000). In Cueva de Villa Luz, Pisarowicz (1994) reported acid burns to clothing worn by investigators. Skin burns were experienced by investigators, and values of pH <1 were measured on some drip water and microbial substances in this cave (Hose 1998; Lavoie *et al*. 1998; Palmer & Palmer 1998; Hose & Pisarowicz 1999; Taylor 1999). Maslyn and Pisarowicz (1994) described seepage of $H_2S$ and small globules of hydrocarbons from springs in Lower Kane Cave. Palmer and Palmer (2000) provide important constraints on the hydrologic and chemical conditions for the $H_2SO_4$ speleogenesis of the Carlsbad caves based on cave patterns and speleogenetic by-products.

The speleogenetic by-products from $H_2SO_4$ speleogenesis are important indicators of the cave-forming environment, and

probably equally important for some non-cave environments. We present the mineral assemblage associated with relict $H_2SO_4$ caves of the Guadalupe Mountains, New Mexico and briefly discuss the significance of this assemblage to geology and speleology.

## SAMPLE COLLECTION AND IDENTIFICATION

Samples were collected with the permission of the National Park Service, Lincoln National Forest, and Bureau of Land Management. Mineral assemblages were established using X-ray diffraction (XRD), energy dispersive X-ray (EDX) microanalysis, transmission electron microscopy (TEM), and optical microscopy. Table 1 lists all the speleogenetic by-products identified, states chemical composition, and establishes the by-products as primary, secondary, and not-yet-classified. All of the materials listed in table 1, with the exception of sulfur and celestite, were examined by this study.

## SPELEOGENETIC BY-PRODUCTS AND THEIR GENETIC CLASSIFICATION

We refer to speleogenetic by-products that formed as a direct result of $H_2SO_4$ speleogenesis as "primary speleogenetic by-products." Speleogenetic by-products that have formed from the alteration of primary speleogenetic by-products or by late-stage remobilization of elements associated with speleogenesis are referred to as "secondary speleogenetic by-products." Primary speleogenetic by-products of $H_2SO_4$ speleogenesis are gypsum, elemental sulfur, hydrated halloysite, alunite, natroalunite, jarosite, hydrobasaluminite, quartz, todorokite, and rancieite. Amorphous materials produced by this process are opal and aluminum sulfates. Secondary speleogenetic by-products are aluminite, tyuyamunite, gypsum, opal, and quartz. Less-understood, and therefore not-yet-classified, speleogenetic by-products are celestite, hydrated Fe-sulfates, gibbsite, nordstrandite, goethite, dolomite, and perhaps crandallite-beudantite group minerals such as goyazite and svanbergite. Speleogenetic by-products are preserved in the Carlsbad caves only in areas that have been protected from post-speleogenesis drip and flood water. For this reason, many other $H_2SO_4$ caves in the Guadalupe Mountains that were subjected to extensive drip and floodwaters are devoid of these materials.

### PRIMARY SPELEOGENETIC BY-PRODUCTS

*Gypsum*. Gypsum is the most abundant primary speleogenetic by-product in the Carlsbad caves. Gypsum may also occur as a secondary precipitate (speleothem) unrelated to speleogenesis (Hill 1987). In the Carlsbad caves, speleogenetic gypsum is observed as thick floor blocks and wall/ceiling rinds. Floor blocks in Lechuguilla Cave exceed 6 m in thickness, and 3 m in Carlsbad Cavern. Egemeier (1973, 1981) and Jagnow (1977) first recognized the exceptional quantities of gypsum floor blocks and wall rinds as evidence of speleogenesis related to $H_2SO_4$. Later, Hill (1981, 1987) showed that negative sulfur isotope values measured for the gypsum blocks and rinds linked the source of sulfur to hydrocarbons in the adjacent Permian Delaware Basin. Queen *et al*. (1977) and Egemeier (1981) described some of these wall rinds as replacement of dolostone by gypsum. Hill (1987) showed that gypsum could either replace bedrock during speleogenesis, or be precipitated during and soon after speleogenesis as thick floor blocks. Buck *et al*. (1994) provided a genetic classification for $H_2S$-$H_2SO_4$–derived gypsum, which includes: (1) subaqueous replacement crust; (2) subaqueous sediment; (3) subaerial replacement crust; (4) subaerial replacement-crust breccia; and (5) evaporitic crust. This genetic classification is particularly significant as it shows a spatial relationship to the water table, thus adding information about the cave-forming environment. Figure 3 shows primary speleogenetic gypsum in a passage in Endless Cave.

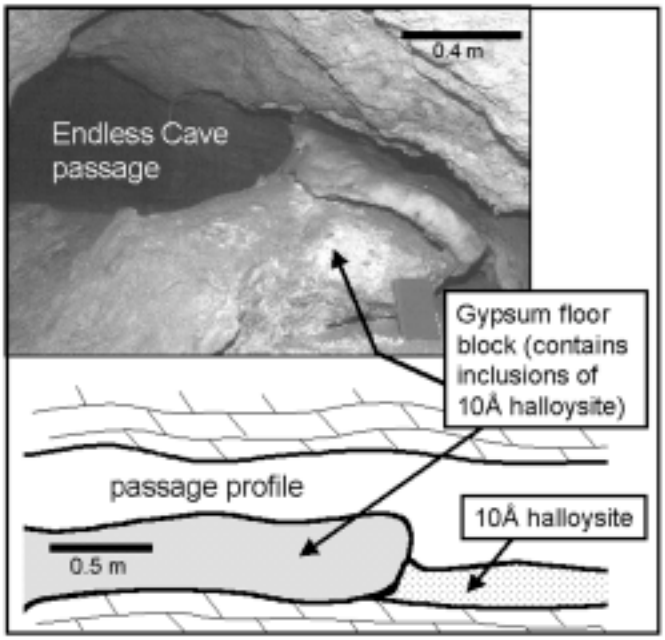


**Figure 3. Photograph and sketch of speleogenetic gypsum in a passage in Endless Cave. The gypsum floor block is a replacement of the dolomitic bedrock. The bedrock contains a moderate amount of quartz, illite, and dickite, and these minerals have apparently been altered to hydrated halloysite, which is found as small pods in the gypsum. The hydrated halloysite fell out onto the passage floor as the gypsum is removed by condensation-induced weathering.**

Although the morphology of these gypsum deposits has been moderately well described, the purity of the gypsum remains relatively unknown. For example, gypsum in Endless Cave contains pods of hydrated halloysite in replacement floor blocks. Removal of the gypsum by later condensation-induced weathering has left remnant floor deposits of the halloysite (Fig. 3). Minerals and amorphous materials incorporated within primary speleogenetic gypsum have potential to reveal fur-

**Table 1: List of known speleogenetic byproducts in the Carlsbad caves.**

| Mineral | Formula | Cave |
|---|---|---|
| *Primary speleogenetic byproducts* | | |
| alunite | $KAl_3(SO_4)_2(OH)_6$ | Ca,C,E,H,Le,V |
| amorphous silica | $SiO_2 \cdot nH_2O$ | C |
| gypsum | $CaSO_4 \cdot 2H_2O$ | B,Ca,C,D,E,H,K,Le,S,V |
| hydrated halloysite | $Al_2Si_2O_5(OH)_4 \cdot 2H_2O$ | Ca,C,E,H,Le,V |
| hydrobasaluminite | $Al_4(SO_4)(OH)_{10} \cdot 12\text{-}36H_2O$ | C |
| jarosite | $KFe_3(SO_4)_2(OH)_6$ | C,Le |
| natroalunite | $NaAl_3(SO_4)_2(OH)_6$ | Ca,Le |
| quartz | $SiO_2$ | Ca,C,E, |
| rancieite | $(Ca,Mn)Mn_4O_9 \cdot 3H_2O$ | Le,Sp |
| sulfur (elemental) | S | C,Ca,Le |
| todorokite | $(Mn,Ca)Mn_5O_{11} \cdot 4H_2O$ | Ca,Le |
| *Secondary speleogenetic byproducts* | | |
| aluminite | $Al_2(SO_4)(OH)_4 \cdot 7H_2O$ | C |
| amorphous silica | $SiO_2 \cdot nH_2O$ | Ca,C,E,H,Le,V |
| gypsum | $CaSO_4 \cdot 2H_2O$ | Sp |
| metatyuyamunite | $Ca(UO_2)_2(VO_4)_2 \cdot 3H_2O$ | Ca,Le,Sp |
| quartz | $SiO_2$ | Ca,Le |
| tyuyamunite | $Ca(UO_2)_2V_2O_8 \cdot 5\text{-}8H_2O$ | Ca,Le |
| *Other possible or less-understood speleogenetic byproducts* | | |
| celestite | $SrSO_4$ | Ca,Le |
| copiapite | $(Fe,Mg)Fe_4(SO_4)_6(OH)_2 \cdot 20H_2O$ | Ca |
| coquimbite | $Fe_2(SO_4)_3 \cdot 9H_2O$ | Ca |
| dolomite | $CaMg(CO_3)_2$ | Le |
| gibbsite | $Al(OH)_3$ | C,V |
| nordstrandite | $Al(OH)_3$ | Le |
| römerite | $Fe_3(SO_4)_4 \cdot 14H_2O$ | Ca |
| *Bedrock minerals* | | |
| calcite | $CaCO_3$ | |
| crandallite-beudanite group | $AB_3(XO_4)_2(OH)_6$, where A=Ca, Ce, Sr, Th; B=Al, Fe; X=P, S, As | |
| dickite | $Al_2Si_2O_5(OH)_4$ | |
| dolomite | $CaMg(CO_3)_2$ | |
| illite | $K(Al,Mg,Fe)_2(Si,Al)_4O_{10}(OH)_2$ | |
| illite-smectite mixed-layers | $KAl_4(Si,Al)_8O_{10}(OH)_4 \cdot 4H_2O$ | |
| kaolinite | $Al_2Si_2O_5(OH)_4$ | |
| montmorillonite | $(Na,Ca,K)_{0.3}(Al,Mg)_2Si_4O_{10}(OH)_2 \cdot nH_2O$ | |

B=Black Cave, Ca=Carlsbad Cavern, C=Cottonwood Cave, D=Dry Cave, E=Endless Cave, H=Hell Below Cave, K=KFFC Cave, Le=Lechuguilla Cave, S=Slaughter Canyon Cave, Sp=Spider Cave, V=Virgin Cave

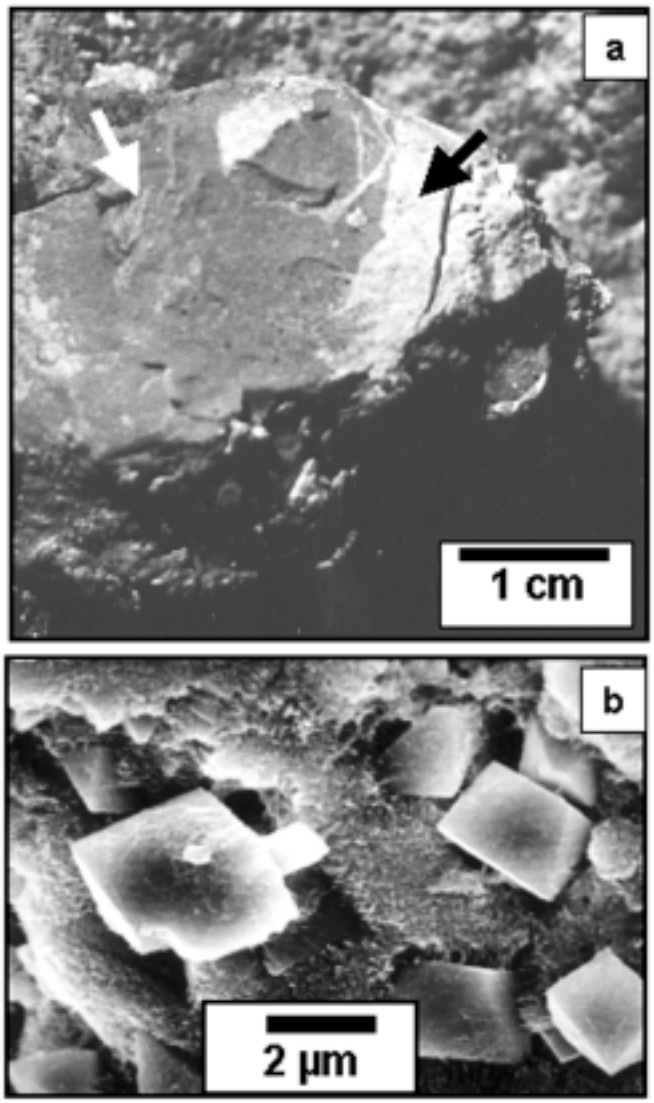


**Figure 4. (a) Photograph of green montmorillonite-rich clay pod with white alteration rims of hydrated halloysite and alunite. (b) Scanning electron micrograph of alunite rhombs in a matrix of hydrated halloysite tubes. These two minerals are usually found together as white pasty to chalky material in the alteration zones.**

ther information about the environment of speleogenesis.

*Elemental sulfur*. Davis (1973) reported elemental sulfur in Cottonwood Cave. Later, Davis (1980) and Hill (1981) suggested that such elemental sulfur might be a by-product of $H_2SO_4$ speleogenesis. Hill (1981, 1987) and Pisarowicz (1994) measured negative stable isotope values for the elemental sulfur, which linked the source of sulfur to microbial activity and hydrocarbons (Hill 1987). Some deposits of elemental sulfur are so large in Lechuguilla Cave (>1000 kg, Cunningham *et al.* 1994) that open flame lights are no longer allowed in this cave.

*Hydrated halloysite*. Davies and Moore (1957) first reported hydrated halloysite (endellite) from Carlsbad Cavern. Hill (1981, 1987, 1990) and Polyak and Güven (1996) later reported it as a primary by-product of $H_2SO_4$ speleogenesis by the alteration of smectite (montmorillonite) and other clays. In the Carlsbad caves, hydrated halloysite is most discernable as waxy, white or blue nodules in pockets of altered bedrock, disseminated in speleogenetic wall residues, and less commonly as floor deposits. Hydrated halloysite is generally associated with alunite, and the blue variety is relatively pure. The Green Clay Room of Carlsbad Cavern exhibits the most convincing evidence of green smectitic clay-filled solution cavities that were truncated and altered by the $H_2SO_4$ speleogenesis. The hydrated halloysite with alunite makes up a white reaction rind around the green montmorillonite clay (Polyak *et al*. 1998) (Fig. 4). In Endless Cave**,** hydrated halloysite in pockets of altered bedrock and floor deposits is probably the by-product of alteration of illite, interstratified illite-smectite, and dickite, which are the most common clay minerals in the surrounding Permian carbonate rocks (Polyak 1998).

*Alunite group minerals*. Alunite, natroalunite, and jarosite are primary speleogenetic by-products found in pockets of altered bedrock, some floor deposits, and in wall residues in the Carlsbad caves. Alunite and natroalunite are associated with hydrated halloysite in nearly all occurrences (Polyak & Güven 1996). The alunite occurs as white to pale-white chalky nodules of <1 to 30 µm diameter cube-like rhombs. Hydrated halloysite and alunite are the result of clay alteration by $H_2SO_4$ speleogenesis. Clay minerals such as illite and montmorillonite, in internal sediments and in the bedrock, provide the source of the potassium for alunite. Natroalunite instead of alunite may form if sufficient sodium is available (Polyak & Güven 2000). The alunite group minerals are probably the most significant speleogenetic by-products because they can be dated using the K-Ar or $^{40}Ar/^{39}Ar$ method. Their stable isotope geochemistry can also reveal important information about the environment of speleogenesis. Jarosite has been noted only in trace amounts. This iron-bearing, yellow mineral was found in association with opal near an occurrence of hydrobasaluminite in Cottonwood Cave (Polyak & Provencio 1998).

*Hydrobasaluminite*. Hydrobasaluminite occurs as white pods in pockets of altered bedrock. It results from the interaction of the $H_2SO_4$-bearing waters with kaolinite rather than with potassium-bearing clays such as illite and smectite. Crystals are micrometer-sized platelets, which dehydrate to basaluminite in <2 hours exposure to a relative humidity <70% at 25°C. In Cottonwood Cave, a kaolinite-rich seam in dolostone has been altered to hydrobasaluminite, amorphous silica, amorphous aluminum sulfate, and minor amounts of alunite and hydrated halloysite (Polyak & Provencio 1998) (Fig. 5).

*Quartz*. Chert was reported by Hill (1987) as a speleogenetic by-product of the alteration of montmorillonite (Big Room, Carlsbad Cavern). In other occurrences, quartz is found in the Carlsbad caves as chert and chalky unconsolidated powder in association with primary speleogenetic gypsum. A well-exposed gypsum block in Endless Cave, which replaced dolostone, contains a line of white chalky pods of micrometer- to

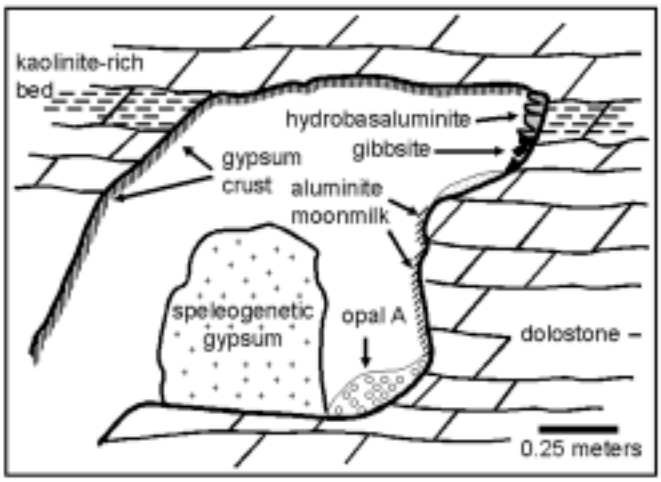


**Figure 5. Sketch of a small room in Cottonwood Cave containing by-product materials such as hydrobasaluminite. In this case, kaolinite-bearing dolostone was altered to hydrobasaluminite during speleogenesis. Hydrobasaluminite was the primary speleogenetic by-product mineral because potassium and sodium were lacking in the bedrock. Figure modified after Polyak and Provencio (1988). Note that aluminite moonmilk (secondary by-product) formed along the cave walls below, and from the alteration of, the hydrobasaluminite.**

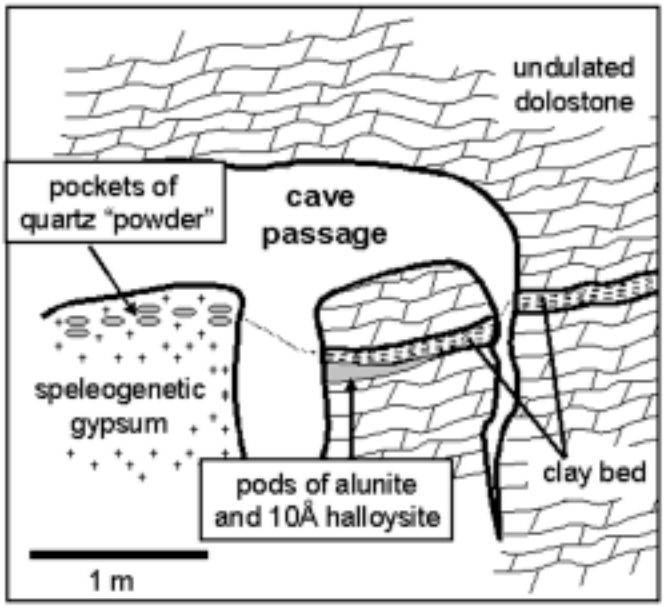


**Figure 6. Setting in Endless Cave showing the relationship between speleogenetic gypsum, quartz, alunite, hydrated halloysite, and a thin Permian clay bed. The clay bed containing kaolinite and interstratified illite-smectite was altered to alunite and hydrated halloysite at the gypsum-bedrock interface, and to quartz in the replacement gypsum. Note that the quartz pods are stratigraphically equivalent to the clay bed.**

deci-micrometer-sized, double-terminated euhedral quartz crystals. These pods form a stratum that is in line with a Permian clay bed in the nearby unaltered cave wall (Fig. 6). It appears that during $H_2SO_4$ speleogenesis, the surrounding dolostone was replaced by gypsum and the clay was altered to quartz within the gypsum. The unaltered clay bed consists of kaolinite and interstratified illite/smectite. Between the gypsum block and the unaltered bedrock, the clay bed was partly altered to hydrated halloysite and alunite during $H_2SO_4$ speleogenesis (Fig. 6). A chert bed with the same thickness as the Permian clay bed (10 cm) is remnant along the same stratum in other areas of this cave. A similarly thick chert bed occurs in gypsum blocks in Cottonwood Cave. Near the Bottomless Pit in Carlsbad Cavern, a chalky layer of quartz has formed directly under a thick (3 m) gypsum block. Crystals in this deposit are clay-sized (0.2 – 0.5 μm) euhedral quartz. Clay and silt were altered to quartz, probably at low temperature during final stages of $H_2SO_4$ speleogenesis. Study of the stable isotope geochemistry of this quartz may yield important information about the environment of speleogenesis. Chafetz and Zhang (1998) reported a similar low-temperature occurrence of quartz in Quaternary evaporite-associated carbonate rocks.

*Hydrous manganese oxides*. Todorokite and other hydrous manganese oxides occur around the perimeter of many pockets of altered bedrock closely associated with alunite and hydrated halloysite (Polyak & Güven 1996, 2000). Todorokite and rancieite are also constituents of the black wall residues in Lechuguilla Cave. In silvery black wall residues, rancieite is most abundant on the surface of truncated schalenohedral calcite spar (Modreski 1989). The todorokite associated with alunite, natroalunite, hydrated halloysite, and hydrobasaluminite probably formed along sharp high-low pH or Eh boundaries produced by $H_2SO_4$ speleogenesis (Polyak 1998). TEM of todorokite, rancieite, and other hydrous manganese oxides show three-dimensional, box-like or dendritic crystal-fiber structures, platelets that consist of packed fibers, or individual fibers. Some occurrences of hydrous manganese oxides are probably secondary speleogenetic by-products, or unrelated to speleogenesis.

### SECONDARY SPELEOGENETIC BY-PRODUCTS

*Aluminite*. In Cottonwood Cave, aluminite moonmilk drapes the walls below hydrobasaluminite (a primary speleogenetic by-product). It formed as a secondary speleogenetic by-product by the alteration of the overlying hydrobasaluminite (Polyak & Provencio 1998). Gypsum moonmilk, another secondary speleogenetic by-product, is associated with the aluminite moonmilk. Pods of dark gray gibbsite also occur in the hydrobasaluminite/aluminite setting.

*Gypsum*. Speleothemic gypsum derived from speleogenetic gypsum is common in the Carlsbad caves, but may have little significance as a speleogenetic indicator mineral because speleothemic gypsum is common in all types of caves.

*Uranyl vanadates*. Tyuyamunite and metatyuyamunite have been found in association with quartz and opal coatings on dolomite and gypsum crusts and floor clay in three Carlsbad caves (Polyak & Mosch 1995; Polyak 1998). The uranyl vanadates precipitated long after speleogenesis as a result of excess silica from clay alteration and concentration of uranium and vanadium along oxidation/reduction zones created by $H_2SO_4$ speleogenesis. The quartz and opal coatings associated with the uranyl vanadates are also secondary speleogenetic by-products.

### OTHER POSSIBLE SPELEOGENETIC BY-PRODUCTS

*Celestite*. Celestite occurs in Carlsbad Cavern (Hill 1987) and Lechuguilla Cave (DuChene 1997) as crusts and crystals on cave walls. The moderately light sulfur isotope compositions of -14.5 to +7.4‰ 9Hill 1996, DuChene 1997) suggest that celestite may also be a speleogenetic by-product. However, Hill (1987) reported celestite as probably speleothemic and unrelated to speleogenesis.

*Hydrous iron-sulfate minerals*. Hydrous iron-sulfate minerals (copiapite, coquimbite, römerite) are associated with some occurrences of celestite in Carlsbad Cavern, and were suggested to be speleogenetic by-products by Mosch and Polyak (1996).

*Gibbsite*. Gibbsite occurs in two Carlsbad caves in pockets of altered bedrock that were partly covered with calcite coatings. The pockets contain speleogenetic by-products that were subjected to alteration by the carbonate-bearing seepage water that deposited the calcite during post-speleogenesis weathering. The gibbsite may be a secondary speleogenetic by-product from the alteration of alunite. Gibbsite can be obtained from alunite by the Bayer Process (Ruvalcaba *et al*. 1995), by which alunite is dissolved slowly in alkaline solutions (i.e., containing $CO_3^{2-}$), and gibbsite is consequently precipitated.

*Nordstrandite*. Nordstrandite occurs in Lechuguilla Cave as a floor deposit below what appears to be leached speleogenetic wall residues, and may be the result of the alteration of hydrated halloysite and alunite in the black wall residues at this location.

*Crandallite-beudantite group minerals*. Goyazite-svanbergite and other crandallite-beudantite group minerals occur with the nordstrandite in this floor deposit. EDX microanalysis of some of the goyazite-svanbergite rhombs indicates the presence of rare earth elements. The crandallite-beudantite group minerals were noted in trace amounts in residues of dolomite bedrock dissolved in the laboratory (Polyak 1998). It is therefore possible that these minerals may be inherited from dissolved bedrock as insoluble residues.

*Goethite*. Goethite is the most abundant crystalline iron oxide phase in the Carlsbad caves. It is common in brown wall residues, which are probably products of condensation-induced weathering rather than speleogenesis. It is also commonly associated with pockets of altered bedrock. Provencio & Polyak (2001) suggested that goethite in the "Rusticles" is associated with speleogenesis. It is likely a speleogenetic by-product, but may be difficult to show in many cases because of its widespread occurrences in these caves.

*Dolomite*. Dolomite occurs in Lechuguilla Cave as white clasts of a breccia with primary speleogenetic gypsum as the matrix between the clasts. The altered (dolomite) clasts contain *in situ* Permian fossils, which indicate they were fragments of altered bedrock. The stable isotope values of these dolomite clasts (two samples) are $\delta^{13}C$ = -5.49 to -4.95 and $\delta^{18}O$ = -6.02 to -4.40‰ V-PDB, which are in contrast with values for Permian dolostone samples ($\delta^{13}C$ = 6.4 to 7.1‰ and $\delta^{18}O$ = 0.6 to 2.8‰, Polyak *et al*., 2001). This at least suggests that the dolomite clasts inherited their lighter isotopes from meteoric waters. Palmer and Palmer (1992) reported similar replacement dolomite as crusts in Lechuguilla Cave, and Hill (1996) speculated the possible origin of speleogenetic dolomite. The dolomite clasts in the gypsum matrix are fragments of bedrock (originally limestone) that appear to have been altered by $H_2SO_4$ speleogenesis.

### $H_2SO_4$ SPELEOGENETIC FEATURES

*Pockets of altered bedrock*. Polyak and Güven (1996) described centimeter-sized pockets of altered bedrock, which contain nodules of hydrated halloysite and alunite bounded by hydrous manganese- and iron-oxides. Pockets of altered bedrock are important features because they contain abundant amounts of primary speleogenetic by-products.

*Cusp features*. Buck *et al*. (1994) described gypsum-carbonate rock replacement boundaries as rounded and oblong bulges extending into the bedrock. They suggested that these oblong bulges were due to differential solubility of individual beds or varying rates of diffusion of ions through the developing gypsum-replacement crusts. Given this scenario, removal of the replacement gypsum bulges by post-speleogenesis weathering would expose cusp features in the cave walls. Such meter-sized scallop-like features appear to be exhibited throughout much of Carlsbad Cavern. In the New Mexico Room of Carlsbad Cavern, pockets of altered bedrock that contain alunite, hydrated halloysite, and hydrous manganese oxides are associated with these features possibly indicating that the pockets formed at the gypsum/bedrock interface (Fig. 7).

*Black wall residues*. Wall residues in the Carlsbad caves are complex. These have been referred to as condensation-corrosion residues (Hill 1987; Cunningham *et al*. 1995). Northup *et al*. (2000) favored a condensation-corrosion method of origin related to microbial-assisted dissolution of the bedrock. Our mention of condensation-induced weathering or speleogenesis-related weathering does not discriminate between inorganic or microbial-related origin for the wall residues. We suggest that at least two types of wall residues exist: (1) brown goethite- and clay-rich wall residues, and (2) black manganiferous wall residues. The brown wall residues appear to be related to weathering of dolostone bedrock by condensation water (condensation-corrosion). These contain abundant amounts of illite and dickite inherited from the bedrock

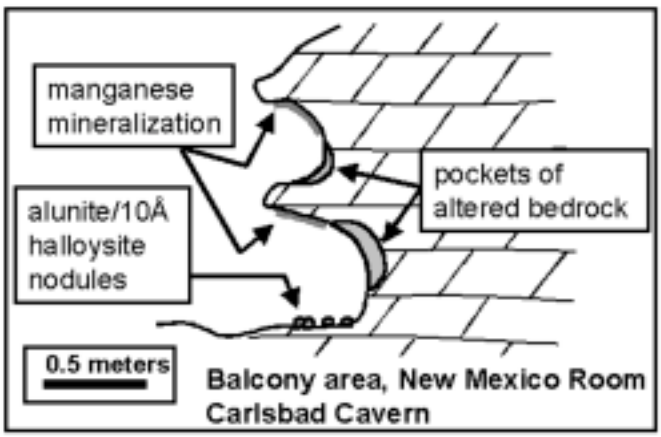


**Figure 7. Sketch of cusp features in the New Mexico Room of Carlsbad Cavern. The cusp features are found throughout Carlsbad caves, and they probably result from differential replacement of the bedrock gypsum during speleogenesis as described by Buck *et al.* (1994).**

(Polyak & Güven 2000), and formed during post-speleogenesis weathering. Samples of black residues from Lechuguilla Cave contain todorokite, alunite, and hydrated halloysite, and are probably indicative of differing pH and Eh boundaries related to $H_2SO_4$ speleogenesis (Polyak 1998). We therefore suggest that the black wall residues formed primarily during $H_2SO_4$ speleogenesis. These may have initially developed behind the speleogenetic gypsum blocks/rinds at the gypsum-bedrock contact. Condensation-induced weathering (after speleogenesis) probably removed the gypsum and later modified the wall residues. The black wall residues contain significant microbial communities (Northup *et al.* 2000), and may contain minor goethite, dickite, illite, and nordstrandite (Polyak 1998).

## IMPLICATIONS

The material assemblages presented in this study have a potentially far-reaching impact, even beyond the study of caves. Hill (1981, 1987, 1990), Polyak and Güven (1996), Polyak and Provencio (1998), and Palmer and Palmer (2000) reported that the $H_2S$- $H_2SO_4$–bearing waters that formed these caves also altered the carbonate rocks as well as the insoluble residues from their dissolution to produce various speleogenetic by-products. Carbonic acid generated from significant amounts of $CO_2$ that migrated with $H_2S$ must have also played a role in the dissolution of the carbonate rocks to form these caves (Hill 1987). However, it was the $H_2S$-oxidation-process that produced $H_2SO_4$ and other sulfur species that resulted in the formation of speleogenetic by-products. We suspect, because of the abundant microbial communities associated with active $H_2SO_4$ caves today (Engel *et al.* 2000, Hose *et al.* 2000), that microorganisms and their excretions also played a role in the alteration of clays and other insoluble minerals during speleogenesis. Studies of the material assemblages associated with speleogenesis are important because they enable advanced interpretations of cave-forming environment, in this case, during and subsequent to the late Miocene.

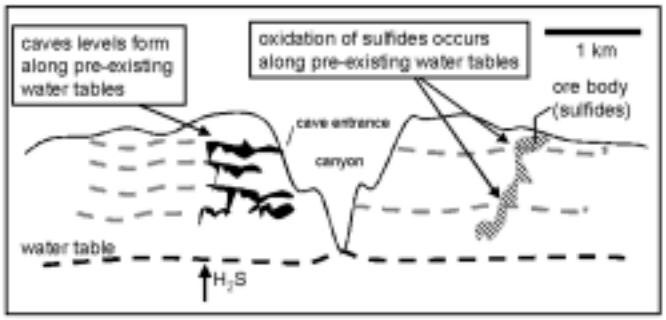


**Figure 8. Idealized model of sulfide oxidation along a declining water table. The model of speleogenesis presented for the Carlsbad caves may apply in non-cave areas as well. For instance, water table decline through sulfide ore zones could also result in the same acid-sulfate by-product materials as found in the Carlsbad caves.**

The ages of formation of the Carlsbad caves, and the timing of an apparent regional water table decline during the late Miocene and Pliocene were derived from the study of speleogenetic by-products (Polyak *et al.* 1998). This has offered insight into the development of the Guadalupe Mountains, which took place concurrently with $H_2SO_4$ speleogenesis. This illustrates how understanding the origin of the by-products of $H_2SO_4$ speleogenesis offers a potentially powerful tool for the study of Cenozoic geologic history.

Furthermore, the substance of this study is not restricted to the cave environment. For instance, we predict that sulfide ore deposits, or clays above hydrocarbon reservoirs, can undergo alteration to similar mineral associations (where regional water table movement has been active, Fig. 8). A potential example of this is the Grand Canyon, Arizona, where similar minerals are found in association with a possible water table decline that may be related to the canyon's origin (Hill *et al.* 1999). Study of speleogenetic by-products has advanced our understanding of the Carlsbad caves and the Guadalupe Mountains, and will provide information that can be applied elsewhere.

## ACKNOWLEDGEMENTS

We are very grateful to Necip Güven at Texas Tech University for the use of his laboratory and for his expertise in clay mineralogy and to Carol A. Hill for her very constructive review of this manuscript. We thank Ransom Turner and the Lincoln National Forest, Dale Pate and Jason Richards of the Carlsbad Caverns National Park, and Jim Goodbar and the Carlsbad District, Bureau of Land Management for field assistance and permission to collect samples. We thank Cyndi Mosch for information regarding the hydrous iron sulfates. An anonymous reviewer provided critical comments that improved the focus of our paper.

## REFERENCES


Buck, M.J., Ford, D.C. & Schwarcz, H.P., 1994, Classification of cave gypsum deposits derived from oxidation of $H_2S$, *in* Sasowsky, I.D. & Palmer, M.V. eds., Breakthroughs in Karst Geomicrobiology, Colorado Springs, Colorado, p. 5-9.

Chafetz, H.S. & Zhang, J., 1998, Authigenic euhedral megaquartz crystals in a Quaternary dolomite: Journal of Sedimentary Research, v. 68, p. 994-1000.

Cunningham, K.I., DuChene, H.R., Spirakis, C.S. & McLean, J. S., 1994, Elemental sulfur in caves of the Guadalupe Mountains, New Mexico, *in* Sasowsky, I.D. & Palmer, M.V. eds., Breakthroughs in Karst Geomicrobiology, Colorado Springs, Colorado, p. 11-12.

Cunningham, K.I., Northup, D.E., Pollastro, R.M., Wright, W.G. & LaRock, E.J., 1995, Bacteria, fungi and biokarst in Lechuguilla Cave, Carlsbad Caverns National Park, New Mexico: Environmental Geology, v. 25, p. 2-8.

Davies, W.E. & Moore, G.W., 1957, Endellite and hydromagnesite from Carlsbad Caverns: National Speleological Society Bulletin, v. 19, p. 24-27.

Davis, D.G., 1973, Sulfur in Cottonwood Cave, Eddy County, New Mexico: National Speleological Society Bulletin, v. 35, p. 89-95.

Davis, D.G., 1980, Cavern development in the Guadalupe Mountains: A critical review of recent hypotheses: National Speleological Society Bulletin, v. 42, p. 42-48.

DuChene, H.R., 1997, Lechuguilla Cave, New Mexico, U.S.A, *in* Hill, C.A. & Forti, P., ed., Cave Minerals of the World: Huntsville, Alabama, National Speleological Society, p. 343-350.

Egemeier, S.J., 1973, Cavern development by thermal waters with a possible bearing on ore deposition [PhD thesis]: Stanford University, 88 p.

Egemeier, S.J., 1981, Cavern development by thermal waters: National Speleological Society Bulletin, v. 43, p. 31-51.

Engel, A.S., Bennett, P.C. & Stern L.A., 2000, Mineralogic and geochemical consequences of microbial habitat modification in sulfidic karst systems: Examples from the Kane Caves, Wyoming: Eos, Transactions, American Geophysical Union, v. 81, p. F215.

Ford, D.C. & Williams, P.W., 1992, Karst geomorphology and hydrology: New York, Chapman and Hall, 601 p.

Galdenzi, S. & Manichetti, M., 1995, Occurrence of hypogenic caves in a karst region: Examples from central Italy: Environmental Geology, v. 26, p. 39-47.

Hill, C.A., 1981, Speleogenesis of Carlsbad Cavern and other caves in the Guadalupe Mountains, *in* Proceedings of the 8th International Congress of Speleology, Bowling Green, Kentucky, p. 143-144.

Hill, C.A., 1987, Geology of Carlsbad Cavern and other caves in the Guadalupe Mountains, New Mexico and Texas, New Mexico Bureau of Mines and Mineral Resources, Bulletin, 150 p.

Hill, C.A., 1990, Sulfuric acid speleogenesis of Carlsbad Cavern and its relationship to hydrocarbons. Delaware Basin, New Mexico and Texas: American Association of Petroleum Geologists Bulletin, v. 74, p. 1685-1694.

Hill, C.A., 1996, Geology of the Delaware Basin, Guadalupe, Apache, and Glass mountains, New Mexico and West Texas, Permian Basin Section-SEPM Publication 96-39, 480 p.

Hill, C., Polyak, V., Buecher, B., Buecher, D., Provencio, P. & Hill, A., 1999, Tsean-Bida Cave and Riverview Mine, March 19-21, 1999, and Kaibab Trail Barite Locality, November 18, 1998: Grand Canyon National Park.

Hose, L.D., 1998, Impact of microbial processes on karst development: A modern example in southern Mexico, *in* Geological Society of America Annual Meeting, Toronto, Ontario, p. A155-A156.

Hose, L.D. & Pisarowicz, J.A., 1999, Cueva de Villa Luz, Tabasco, Mexico: Reconnaissance study of an active sulfur spring cave and ecosystem: Journal of Cave and Karst Studies, v. 61, no. 1, p. 13-21.

Hose L.D., Northup, D.E., Boston P.J., DuChene H.R., Palmer A.N. & Palmer M.V., 2000, Microbiology and geochemistry in a hydrogen-sulphide-rich karst environment: Chemical Geology, v. 169, p. 399-423.

Jagnow, D.H., 1977, Geologic factors influencing speleogenesis in the Capitan reef complex, New Mexico and Texas [MS thesis]: University of New Mexico, 203 p.

Jagnow, D.H. & Jagnow, R.R., 1992, Stories from stones - The geology of the Guadalupe Mountains: Carlsbad, New Mexico, Carlsbad Caverns-Guadalupe Mountains Association, 40 p.

Kane, T.C., Sarbu, S. & Kinkle, B. K., 1994, Chemoautotrophy: Methodological approaches, geological implications, and a case study from southern Romania, *in* Sasowsky, I.D. & Palmer, M.V. eds., Breakthroughs in Karst Geomicrobiology, Colorado Springs, Colorado, p. 38.

Lavoie, K., Northup, D., Boston, P. & Blanco-Montero, C., 1998, Preliminary report on the biology of Cueva de Villa Luz, Tabasco, Mexico: Journal of Cave and Karst Studies, v. 60, no. 3, p. 180.

Martini, J.E.J., Wipplinger, P.E. & Moen, F.G., 1997, Mbobo Mkulu Cave, South Africa, *in* Hill, C.A. & Forti, P., ed., Cave Minerals of the World: Huntsville, Alabama, National Speleological Society, p. 336-339.

Maslyn, R.M. & Pisarowicz, J.A., 1994, Microbiology of Lower Kane Cave, Wyoming, *in* Sasowsky, I.D. & Palmer, M.V. eds., Breakthroughs in Karst Geomicrobiology, Colorado Springs, Colorado, p. 52.

Modreski, P.J., 1989, Mineralogical studies of some caves in Colorado and New Mexico: New Mexico Geology, v. 11, p. 50.

Morehouse, D.F., 1968, Cave development via the sulfuric acid reaction: National Speleological Society Bulletin, v. 30, p. 1-10.

Mosch, C.J. & Polyak, V.J., 1996, Canary-yellow cave precipitates: Late-stage hydrated uranyl vanadate, uranyl silicate, and iron sulfate cave minerals: Journal of Cave and Karst Studies, v. 58, no. 3, p. 209.

Northup D.E., Dahm, C.N., Melim L.A., Spilde M.N., Crossey L.J., Lavoie K.H., Mallory L.M., Boston P.J., Cunningham K.I. & Barns S.M., 2000, Evidence for geomicrobiological interactions in Guadalupe caves: Journal of Cave and Karst Studies, v. 62, no. 2, p. 80-90.

Palmer, A.N., 1991, Origin and morphology of limestone caves: Geological Society of America Bulletin, v. 103, p. 1-21.

Palmer, M.V. & Palmer, A.N., 1992, Geochemical and petrologic observations in Lechuguilla Cave, New Mexico, *in* Ogden, A.E., ed., Friends of Karst Meeting, Tennessee Technical University, Cookesville, TN, p. 25-26.

Palmer, M.V. & Palmer, A.N., 1994, Sulfate-induced diagenesis in the Madison aquifer of South Dakota, *in* Sasowsky, I.D. & Palmer, M.V. eds., Breakthroughs in Karst Geomicrobiology, Colorado Springs, Colorado, p. 57-58.

Palmer, A.N. & Palmer, M.V., 1998, Geochemistry of Cueva de Villa Luz, Mexico, an active $H_2S$ cave: Journal of Cave and Karst Studies, v. 60, no. 3, p. 188.

Palmer, A.N. & Palmer, M.V., 2000, Hydrochemical interpretation of cave patterns in the Guadalupe Mountains, New Mexico: Journal of Cave and Karst Studies, v. 62, no. 2, p. 91-108.

Pisarowicz, J.A., 1994, Cueva de Villa Luz - an active case of $H_2S$ speleogenesis, *in* Sasowsky, I.D. & Palmer, M.V. eds., Breakthroughs in Karst Geomicrobiology, Colorado Springs, Colorado, p. 60-62.

Polyak, V.J. & Mosch, C.J., 1995, Metatyuyamunite from Spider Cave, Carlsbad Caverns National Park: National Speleological Society Bulletin, v. 57, no. 2, p. 85-90.

Polyak, V.J. & Güven, N., 1996, Mineralization of alunite, natroalunite, and hydrated halloysite in Carlsbad Cavern and Lechuguilla Cave, New Mexico: Clays and Clay Minerals, v. 44, p. 843-850.

Polyak, V.J., 1998, Clays and associated minerals in caves of the Guadalupe Mountains, New Mexico [PhD thesis]: Texas Tech University, 190 p.

Polyak, V.J., McIntosh, W.C., Güven, N. & Provencio, P., 1998, Age and origin of Carlsbad Cavern and related caves from $^{40}Ar/^{39}Ar$ of alunite: Science, v. 279, p. 1919-1922.

Polyak, V.J. & Provencio, P., 1998, Hydrobasaluminite and aluminite in caves of the Guadalupe Mountains, New Mexico: Journal of Cave and Karst Studies, v. 60, no. 1, p. 51-57.

Polyak, V.J. & Güven, N., 2000, Clays in caves of the Guadalupe Mountains, New Mexico: Journal of Cave and Karst Studies, v. 62, no. 2, p. 120-126.

Polyak, V.J., Karlsson, H.R. & Provencio, P., 2001, Cave-authigenic dolomite in the Guadalupe Mountains, New Mexico [unpublished manuscript]: Carlsbad Caverns National Park files.

Provencio, P.P. & Polyak, V.J., in press, Iron oxide filaments: Possible fossil bacteria in Lechuguilla Cave, New Mexico: Geomicrobiology Journal.

Queen, J.M., Palmer, A.N., & Palmer, M.V., 1977. Speleogenesis in the Guadalupe Mountains, New Mexico: Gypsum replacement of carbonates by brine mixing: Cave Research Foundation Annual Report v, 19, p. 22-23.

Ruvalcaba, J.M., Vargas, O.A., Cuesta, J.R. & Juarez, H., 1995, Adjustment of the Bayer Process to obtain gibbsite from Mexican alunite: Boletin de la Sociedad Chilena de Quimica, v. 40, p. 421.

Rye, R.O., Bethke, P.M. & Wasserman, M.D., 1992, The stable isotope geochemistry of acid sulfate alteration: Economic Geology, v. 87, p. 225-262.

Sarbu, S.M. & Kane, T.C., 1995, A subterranean chemoautotrophically based ecosystem: National Speleological Society Bulletin, v. 57, no. 2, p. 91-98.

Taylor, M.R., 1999, A trip to lighted house: National Speleological Society News, v. 57, p. 36-41.

van Everdingen, R.O., Shakur, M.A. & Krouse, H.R., 1985, Role of corrosion by $H_2SO_4$ fallout in cave development in a travertine deposit - Evidence from sulfur and oxygen isotopes: Economic Geology, v. 49, p. 205-211.

White, W.B., 1988, Geomorphology and hydrology of karst terrains: New York, Oxford University Press, 464 p.

# RESPONSE OF KARST AQUIFERS TO RAINFALL AND EVAPORATION, MAHARLU BASIN, IRAN

NOZAR SAMANI
*Department of Geology, Shiraz University, Shiraz 71454, IRAN samani@geology.susc.ac.ir*

*Maharlu basin, with an approximate surface area of 4000 km², is located in the central part of Fars Province, Iran. The basin is the first candidate site for karst hydrogeology research in the country. The karstified Asmari-Jahrum Formation covers ~37% of the total surface area of the basin with huge reservoirs of karst water. To establish the relationship between rainfall and evaporation with groundwater level and spring discharge, the fluctuations of groundwater level at nine piezometric and exploration wells, discharge of two springs, rainfall records, and pan evaporation are analyzed by employing time-series techniques both in time and frequency domains. Results are presented as correlograms, variance spectra, phase diagrams, coherency diagrams and cross correlograms. A time lag of 1-3 months was found between rainfall occurrence and the response of groundwater levels and spring discharges. There is no clear relation between evaporation and groundwater level and spring discharge. Different response in different wells is due to the different path lengths of percolated water from sinking point to the water table. The time response of groundwater level and spring discharge suggests that springs are fed through a diffuse karstic flow system that is in accordance with the physical characteristics of the springs. The lag times of Pirbanow and Pol-Brengi springs are equal in response to rainfall, but zero and 1-2 months respectively, in response to groundwater level at exploration well E-17. This point, together with the high value of specific conductivity of Pol-Brengi spring, suggests that the two springs have no hydrogeologic connection. The Ghasrodasht Fault may be the cause of this separation. It is finally concluded that a combination of time series analysis/physical properties of springs and geologic evidence can provide useful information about the hydrogeology of a region prior to large-scale and expensive tests.*

A groundwater level indicates the elevation at which the water is at atmospheric pressure within the aquifer. Any phenomenon that produces a change in pressure on groundwater will cause the groundwater level to vary. Differences between supply and withdrawal of groundwater cause levels to fluctuate. Rainfall, evapotranspiration, pumpage, stream flow, and spring discharge variations are closely related to groundwater levels. The mechanism of groundwater level variations by these factors and other diverse phenomena, urbanization, earthquakes, and external loads, is given by Todd (1980). Groundwater level variations in some karst aquifers are analyzed in this work.

Karst aquifers are, in general, heterogeneous in character. As a result, quantitative data obtained from selected points in the system either by pumping or by using tracer dyes can be rarely extrapolated to evaluate the average function of the system as a whole. In contrast, analysis of groundwater level and spring discharge variations and related hydrologic controls (e.g., precipitation, evaporation) can reflect overall response of the aquifer and help in evaluating its storage, drainage potential, degree of karstification, hydrogeologic boundaries, etc., without imposing any external stresses on the system. Spring hydrograph recession curves may also be used to define the degree of karstification and conduit/diffuse flow regimes in karst aquifers (Padilla *et al.* 1994; Samani & Ebrahimi 1996). In this paper, an attempt has been made to determine whether the existing record of natural groundwater level variation could yield information on the hydrogeology of the Maharlu karst basin situated in Fars Province of Iran prior to large-scale tests. For this purpose, time-series techniques are used and the following thirteen sets of data (Sahraie 1995; Tamab 1993) are analyzed (Fig. 1):

a) monthly rainfall (cumulative rainfall depth of all rainfall events during each month) monitored at Shiraz Airport and Doboneh stations;
b) monthly pan evaporation (cumulative evaporation during a month) at the above stations;
c) monthly groundwater level at three piezometers and four exploration wells;
d) instantaneous monthly discharge of Pirbanow and Pol-Brengi springs.

All data sets extend for 7 years from October 1987 to September 1994. Figure 2 is the geological map of the Maharlu basin and shows the location of meteorological stations, piezometers, exploration wells and springs. Note from table 3 that piezometers are wells of small diameter (101 mm) with high depth (>400m) and exploration wells are shallower, large diameter wells (300-360 mm). Methods of investigation began with the application of various time-series techniques and geologic evidence and physical properties of springs are used to test the inference drawn from the time series analysis.

## GEOLOGY AND HYDROGEOLOGY OF THE BASIN

Maharlu karst basin has an approximate surface area of 4000 km² and is located in the central part of Fars Province,

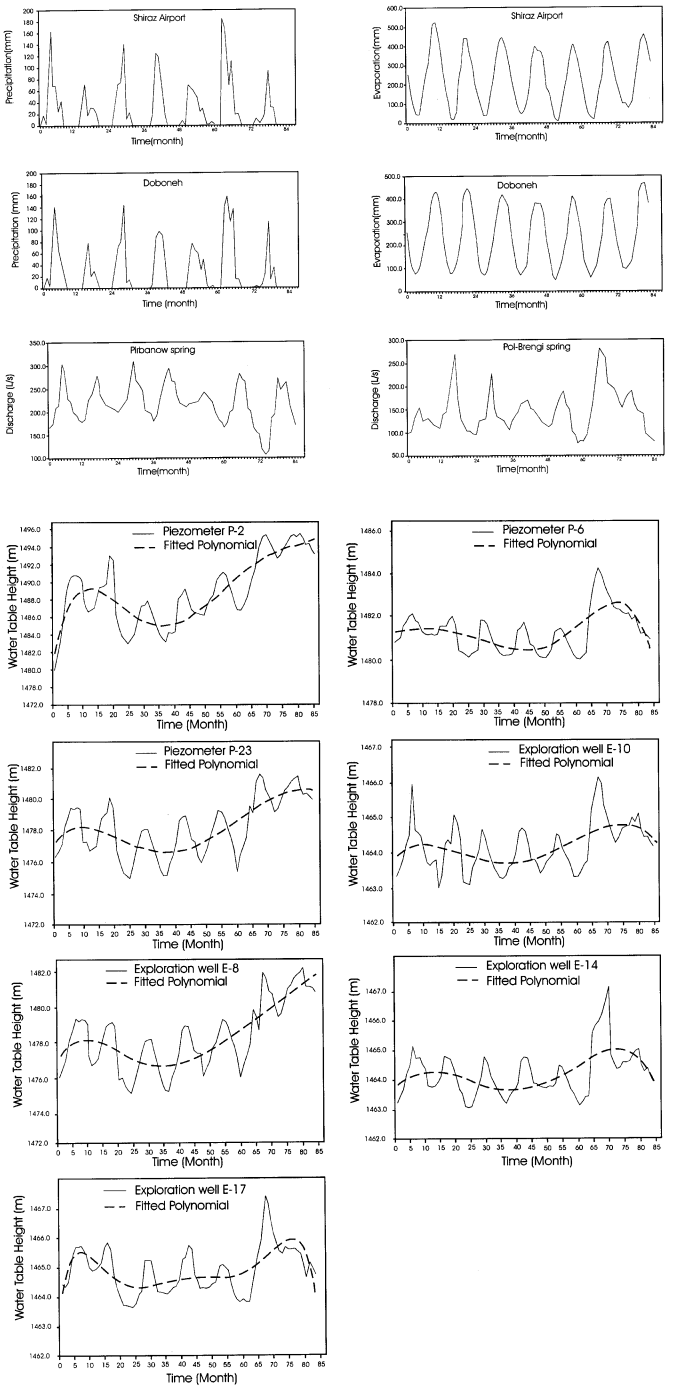


**Figure 1. Raw data.**

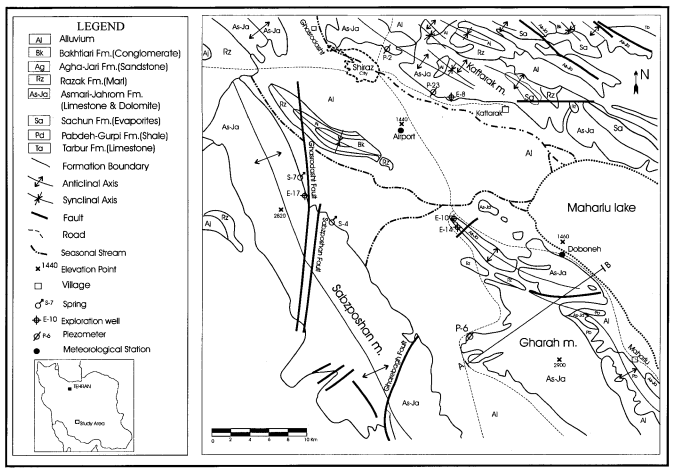


**Figure 2. Geological map of Maharlu basin, location of springs, piezometers and exploration wells and meteorological stations.**

Iran (29°1'30"N, 52°12'28"E). The basin falls in zone three (simple folded belt) of the Zagros Orogenic Belt. The exposed geologic formations in decreasing order of age consist of Pabdeh-Gurpi shales and gypsiferous marls (Santonian-Oligocene), Sachun gypsum (Paleocene-L.Eocene), Asmari-Jahrum limestones and dolomites (Paleocene-Oligocene), Razak evaporites (Oligocene-Miocene), Aghajari sandstone (Miocene-Pliocene), and Bakhtiari conglomerates (Pliocene) (Fig. 2). James and Wynd (1965) give the detailed lithology of these formations. The karstified Asmari-Jahrum Formation is exposed over 37% of the total surface area of the basin (Tamab 1993), forming three huge reservoirs of karst water in the Gharah, Kaftarak, and Sabzposhan anticlines. The overall trend of these anticlines follows the general NW-SE trend of the Zagros Orogeny.

Sabzposhan anticline, in the south of the basin, is crossed by three major faults and many minor ones. The major faults are the Ghasrodasht, Sabzposhan, and Gharebagh faults (Fig. 2). Pirbanow (S-4) and Pol-brengi (S-7) springs drain the Sabzposhan aquifer. The exploration well E-17 penetrates this aquifer. Tables 1 and 2 summarize the statistics for some of the physical parameters of Pirbanow and Pol-Brengi springs (Sahraei 1995).

The Kaftarak anticline, in the north of the basin, is crossed by a major fault whose hydrogeologic role is not known. The exploration well E-8 and the piezometric wells P-2 and P-23 penetrate the karst aquifer in the south flank of this anticline. Gharah anticline forms the third karst aquifer studied in this paper. The exploration wells E-14 and E-10 and the piezometric well P-6 are located in the Gharah aquifer. Some specifications of all the wells are presented in table 3.

The climate is semi-arid, with an average annual precipitation over the basin of about 350 mm. Rainfall infiltrates through karst formations to the impermeable cores (Gurpi Formation) of the anticlines. The Razak Formation behaves as an aquitard and segregates the groundwater of the karst aquifers from that of the alluvial aquifers in the basin.

## METHODOLOGY

The statistical methods for analyzing time series are well established (Jenkins & Watts 1968; Chow 1978; Yevjeich 1982; Chatfield 1982; Salas *et al*. 1988). This paper focuses on

**Table 1. Physical parameters of Pirbanow spring (S-7).**

| Parameter | Minimum | Maximum | Mean | Standard deviation | Coefficient of variation% |
|---|---|---|---|---|---|
| Discharge (L/s) | 107.00 | 311.00 | 216.76 | 39.59 | 18.35 |
| EC (µS/cm) | 647.00 | 762.00 | 708.86 | 39.76 | 5.61 |
| Water temperature (°C) | 18.00 | 22.00 | 19.80 | 1.04 | 5.24 |
| Air temperature (°C) | 4.89 | 28.98 | 16.88 | 7.93 | 47.00 |

**Table 2. Physical parameters of Pol-Brengi spring (S-4).**

| Parameter | Minimum | Maximum | Mean | Standard deviation | Coefficient of variation% |
|---|---|---|---|---|---|
| Discharge (L/s) | 75.00 | 282.00 | 144.55 | 44.92 | 31.08 |
| EC (µS/cm) | 1190.00 | 1693.00 | 1437.00 | 126.21 | 8.78 |
| Water temperature (°C) | 19.00 | 23.00 | 20.83 | 1.10 | 5.29 |
| Air temperature (°C) | 4.89 | 28.98 | 16.88 | 7.93 | 47.00 |

**Table 3. Some specifications of wells, elevations are from m.s.l (Tamab 1993).**

| Well no. | Elevation of of well site (m) | Mean elevation of GWL* (m) | Mean depth to GWL (m) | Depth of well (m) | Diameter (mm) | Casing depth |
|---|---|---|---|---|---|---|
| E-8 | 1509.2 | 1478.5 | 30.70 | 177 | 300 | 105 |
| E-10 | 1474.43 | 1464.24 | 10.19 | 186 | 360 | 12 |
| E-14 | 1513.32 | 1464.25 | 49.07 | 187 | 360 | 135 |
| E-17 | 1527.87 | 1484.55 | 43.32 | 174 | 300 | 50 |
| P-2 | 1562.49 | 1489.77 | 72.72 | 500 | 101 | 99 |
| P-6 | 1489.04 | 1481.43 | 7.61 | 400 | 101 | 70 |
| P-23 | 1512.62 | 1478.54 | 34.08 | 400 | 101 | 48 |

*Groundwater level

the methods of analyzing a single time series (univariate) as well as a double time series (bivariate). The traditional method for analyzing a univariate time series involves isolating the deterministic (trend and periodic) components and stochastic components. The stochastic components may then be explained in terms of stochastic models such as moving-average or autoregressive models. It is often the case in hydrology that a variable proceeds the other variable in time, like peak rainfall intensity proceeding the peak runoff discharge. In such cases bivariate time series techniques may be used to examine the relationship between two time series. A brief summary of the methods used to screen the components of a single time series is first discussed and then the methods for examining the relationship between two time series are followed.

### TREND

The presence of trend or long-term fluctuations can be easily distinguished by inspection of annual mean against the sample mean. Other procedures, such as weighted moving average, differencing, and curve fitting may also be used. Figure 1 illustrates the polynomials fitted to the water level in wells and discharge at springs and table 4 shows the values of coefficients in the polynomials. In this table and in table 5, symbols E, P, and S denote exploration well, piezometer, and spring, respectively. Of thirteen time series considered, coefficients of polynomials fitted to the rainfall and evaporation time series (in both stations) were not statistically significant and, therefore, not included in table 4.

### PERIODICITY

To inspect the presence of periodic components, among which seasonality is the most important, two diagnostic tools are the correlogram and power spectrum in time and frequency domains.

The correlogram is a graphical representation of serial-correlation coefficient r(k) as a function of lag k, where the values of r(k) are plotted as ordinates against their respective values of k. The serial correlation coefficients of lag k are calculated by (Chatfield 1982):

$$r(k) = \frac{C(k)}{C(0)} \tag{1}$$

Where C(k) is the auto covariance of a sample of N values of X with an estimated mean $\overline{X}$ at lag k, that is:

$$C(k) = \frac{1}{N}\sum_{t=1}^{N-k}(X_t - \overline{X})(X_{t+1} - \overline{X})$$

and C(0) is the estimation of the variance of the process as follows:

$$C(0) = \frac{1}{N}\sum_{t=1}^{N}(X_t - \overline{X})^2$$

As an example correlograms of rainfall and evaporation in Doboneh station are shown in figure 3a, and those of water level at piezometer P-6 and Pirbanow spring discharge (S-4) are shown in figure 3b.

Correlograms for all the time series analyzed show oscillations with negligible damping, thus revealing the presence of a periodic component in the total data set.

The spectrum can help determine the periods of the harmonic components in a time series. It is a plot of the spectral density S(f) against frequency f. In the case of an infinite series, Jenkins and Watts (1968) show that the spectral density is:

**Table 4. Coefficients of polynomials fitted to time series.**

| well or spring | order of polynomial | $a_0$ | $a_1$ | $a_2$ | $a_3$ | $a_4$ | $a_5$ | $a_6$ | $r^2$ |
|---|---|---|---|---|---|---|---|---|---|
| E-8 | 5 | 1476.93 | 0.295 | -0.023 | 6.15 E-04 | -6.4 E-06 | 2.37 E-08 | | 0.679 |
| E-10 | 4 | 1463.82 | 0.088 | -.006 | 1.00 E-04 | -7.7 E-07 | | | 0.411 |
| E-14 | 5 | 1463.76 | 0.095 | -0.0051 | 5.59 E-05 | 5.7E-07 | 8.12 E-09 | | 0.436 |
| E-17 | 6 | 1483.81 | 0.311 | -0.034 | 1.50 E-03 | -3.1-E-05 | 3.21 E-07 | -1.25 E-09 | 0.548 |
| P-2 | 5 | 1480.10 | 1.822 | -0.121 | 3.05 E-03 | -3.2 E-05 | 1.25 E-07 | | 0.742 |
| P-6 | 5 | 1481.35 | -0.007 | -0.004 | -2.74 E-04 | 5.6 E-06 | -3.52 E-08 | | 0.755 |
| P-23 | 5 | 1477.08 | 0.2732 | -0.021 | 4.90 E-04 | -4.3 E-06 | 1.25 E-08 | | 0.594 |
| S-4* | 5 | 117.84 | 0.3225 | 0.291 | -1.68 E-02 | 3.1 E-04 | -1.83 E-06 | | 0.381 |
| S-7** | 4 | 219.53 | -2.224 | 0.219 | -5.24 E-03 | 3.5 E-05 | | | 0.695 |

* Pol-Brengi spring, $r^2$ is coefficient of correlation
** Pirbanow spring

$$S(f) = \int_{-\infty}^{+\infty} C(i) \cos 2\pi fi\,\delta \tag{2}$$

and for a finite series:

$$S(f) = \frac{1}{n}\left[C(0) + 2\sum_{i=1}^{n-1} C(i).\cos\frac{\pi ki}{n} + C(n).\cos\pi k\right] \tag{3}$$

Where frequency $f = k/2n\delta_i$, n=maximum number of lags investigated, and $\delta_i$ is the time interval of one month. If the time series contains distinct periodic terms, the spectral density of these terms will appear as high and sharp peaks in the estimated spectrum. Figure 3 illustrates the raw or detrended data, correlograms, and spectra of four sample time series. The spectrum of all series exhibits highest peaks at 0.083 cycle per month, The sharp peak indicates a significant amount of the variance having a 12-month periodicity (annual cycle). A smaller peak with a 6-month periodicity is also observed in the rainfall series. This apparently reflects the influence of the regular annual variations implied in the climatic condition of the region. Rainfall records show an obvious division of rainfall occurrence throughout the year, with the bulk of rainfall occurring from mid-fall to mid-spring, while the rest of the year is almost rainless.

The methods for examining the relationship between two time series are cross correlation and cross-spectrum functions in time and in frequency domain, as follows:

CROSS-CORRELATION FUNCTION

The cross-correlation function $r_{xy}(k)$ is defined as (Chatfield 1982):

$$r_{xy}(k) = \frac{C_{xy}(k)}{\sqrt{C_{xx}(0) \times C_{yy}(0)}} \tag{4}$$

**Table 5. Cross-correlation coefficient and lag-time response of groundwater level and spring discharge to rainfall.**

| Rainfall | A | D | D | A | A | D | A | A | A |
|---|---|---|---|---|---|---|---|---|---|
| Spring or well | E-8 | E-10 | E-14 | E-17 | P-2 | P-6 | P-23 | S-4 | S-7 |
| Cross corr. coeff. | 0.62 | 0.72 | 0.70 | 0.82 | 0.60 | 0.70 | 0.60 | 0.60 | 0.70 |
| Lag time (month) | 1-2 | 1-2 | 1-2 | 2-3 | 2-3 | 2 | 1-2 | 1 | 1 |

A: Airport, D: Doboneh

where

$$C_{xy}(k) = \frac{1}{N-k}\sum_{i=1}^{N-k} X_i Y_{i+k} - \frac{1}{N^2}\sum_{i=1}^{N} X_i \sum_{i=1}^{N} Y_i$$

is coefficient of cross covariance at lag k for time series $X_t$ and $Y_t$, and

$$C_{xx}(0) = \frac{1}{N}\sum_{i=1}^{N} (X_i - \bar{X})^2$$

and

$$C_{yy}(0) = \frac{1}{N}\sum_{i=1}^{N} (Y_i - \bar{Y})^2$$

are variance at lag zero for the two series. The plot of $r_{xy}(k)$ against k is the cross correlogram. The maximum values of $r_{xy}(k)$ observed at a lag d indicates that one series is related to the other when delayed by time d. Figure 4 illustrates the cross correlogram of four pairs namely a) rainfall-spring discharge, b) pan evaporation-water table, c) rainfall-water table, and d) pan evaporation-spring discharge. From these figures it can be

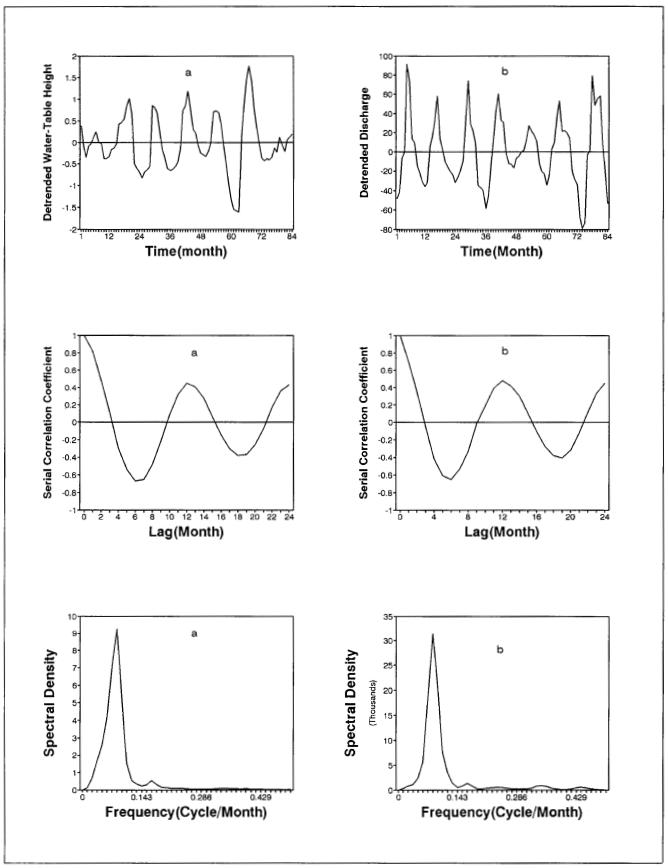


**Figure 3a. Raw (or detrended) data, correlogram and spectrum. a) Groundwater level (P-6) b) Spring discharge (S-4).**

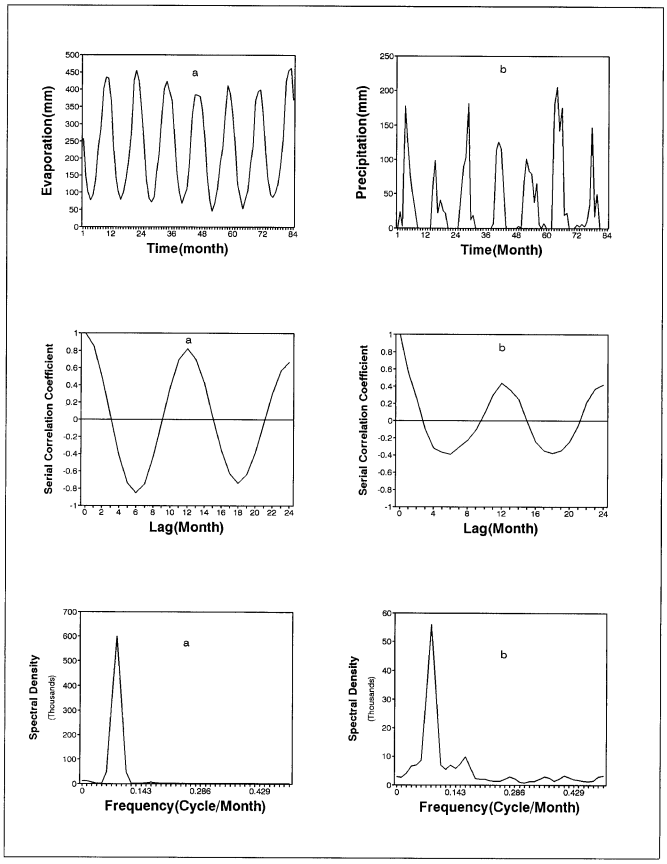


**Figure 3b. Raw data, correlogram and spectrum of a) Evaporation and b) Rainfall at Doboneh station.**

observed that there is no relation (i.e. no clear peak observed) between *pan evaporation-water table* and *pan evaporation-spring discharge* pair series, however there is a month lag between *rainfall-spring discharge* and a two-month lag between *rainfall-water table*. Table 5 summarizes the maximum value of $r_{xy}(k)$ and corresponding lag time for the related series.

CROSS- SPECTRUM FUNCTION

The cross spectrum function is the Fourier transform of the cross covariance. Various functions may be derived from the cross spectrum among which the coherence and phase spectra are used in this paper. The coherence spectrum is defined as:

$$Ch_{xy}(f) = \frac{C_{xy}^2(f) + q_{xy}^2(f)}{S_x(f) \times S_y(f)} \qquad (5)$$

in which $Ch_{xy}(f)$ is the coherence spectrum in frequency domain,

$$q_{xy}(f) = \frac{1}{\pi}\left[\sum_{k=1}^{\infty}\left[C_{xy}(k) - C_{yx}(k)\right]\right]\sin fk$$

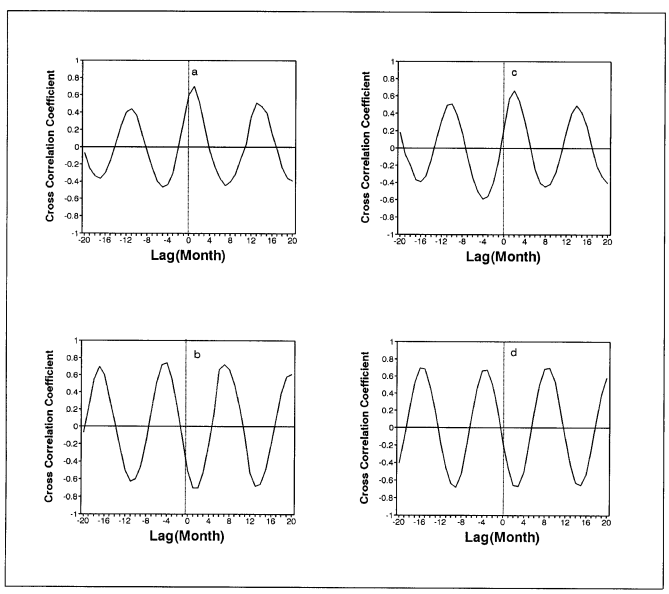


**Figure 4. Cross correlograms: a) Rainfall (Airport)-spring discharge (Pirbanow), b) Evaporation (Airport)-spring discharge (Pirbanow), c) Rainfall (Doboneh)-groundwater level (P-6), and d) Evaporation (Doboneh)-groundwater level (P-6).**

is the quadrature spectrum, and

$$C_{xy}(f) = \frac{1}{\pi}\left[C_{xy}(0) + \sum_{k=1}^{\infty}\left[C_{xy}(k) + C_{yx}(k)\right]\right]\cos fk$$

is the co-spectrum, and $S_x(f)$ and $S_y(f)$ are spectral densities of time series $X_t$ and $Y_t$, respectively (Eq. 3). The plot of coherence spectrum against frequency is the coherency diagram. The values of $Ch_{xy}$ vary between unity and zero, where unity indicates that the two series are fully dependent and zero shows two independent series (Chow 1978; Granger & Hatanaka 1964).

The phase spectrum determines the time lag between the two series and defined as:

$$P_{xy}(f) = \arctan\left[\frac{q_{xy}(f)}{C_{xy}(f)}\right] \qquad (6)$$

Where

$$q_{xy}(f) = \frac{1}{\pi}\left[\sum_{k=1}^{\infty}\left[C_{xy}(k) - C_{yx}(k)\right]\right]\sin fk$$

The plot of $P_{xy}(f)$ against $f$ is the phase diagram. On the phase diagram, the frequency at which coherence is maximum gives the phase between the two series. In turn, division of phase by angular frequency gives the lag between the two series. This time lag may be compared with that found from the cross correlogram, table 5. As an example, coherence and phase diagrams for the four pair series of rainfall-water table, rainfall-spring discharge, evaporation-water table and evaporation-spring discharge are shown in figure 5. Maximum coherency and phase between these series are noted on these figures and listed in table 6. The values in the sixth column are calculated from $k = \theta T/2\pi$, where k is the time lag, θ angular frequency, and T is period.

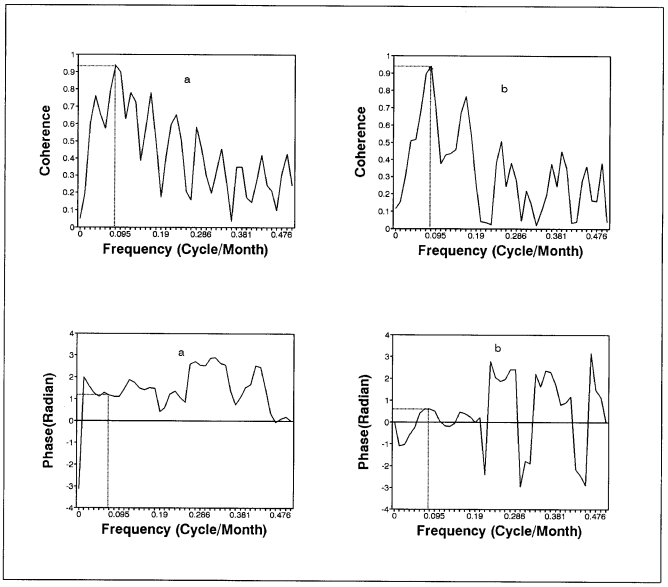


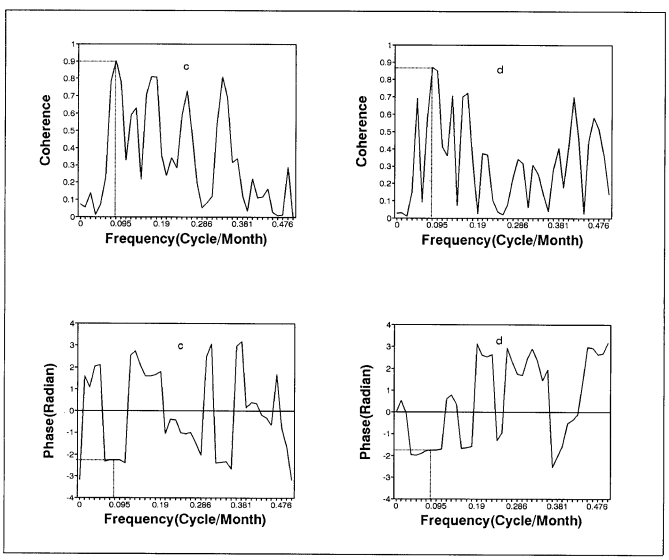


**Figure 5. Coherency and phase diagrams:**
**a) Rainfall(Airport)-groundwater level(P-6)**
**b) Rainfall(Airport)-spring discharge(S-4).**
**c) Evaporation(Airport)-spring discharge(S-4), and**
**d) Evaporation(Doboneh)-groundwater level(P-6).**

## DISCUSSION

The time series analyses conducted in this study show that a time lag of one to three months exists between rainfall occurrence and both the groundwater level response and spring discharge, whereas there is no significant relation between evaporation and groundwater level or spring discharge (see Figs. 3b and 3d). To draw some conclusions about the hydrogeology of the karst basin from these analyses the following discussion is pertinent.

The response time of the groundwater level and spring discharge to rainfall gives some indication of the degree of karstification, type of flow regime, and the drainage/transmission and storage potential of a karst aquifer. A short time response of less than 10-15 days, or a long time response of more than 2 months, corresponds to high and low degree of karstification, respectively (Obarti *et al.* 1988). A high degree of karstification reflects development of speleological features, like sinkholes, interconnected caves, and solution channels. As a result, a well-karstified aquifer is characterized by high drainage potential, high transmissivity, and turbulent type of flow within conduits. Groundwater response at all the studied sites shows a lag time of 1-2 months. From this it may be concluded that the studied karst systems are intermediate class between high and low karstification, according to Obarti's

**Table 6. Time lag response of groundwater level and spring discharge to rainfall based on cross-spectrum analysis.**

| well or spring | greatest coherency, $Ch_{xy}(f)_{max}$ | Frequency, $f$ (cycles/month) | Period $1/f$ (month) | Phase, $\theta$ (radian) | lag (month) |
|---|---|---|---|---|---|
| E-8 | 0.94 | 0.083 | 12 | 0.94 | 1.8 |
| E-10 | 0.94 | 0.083 | 12 | 0.84 | 1.6 |
| E-14 | 0.95 | 0.083 | 12 | 0.84 | 1.6 |
| E-17 | 0.89 | 0.083 | 12 | 1.09 | 2.1 |
| P-2 | 0.94 | 0.083 | 12 | 1.09 | 2.1 |
| P-6 | 0.94 | 0.083 | 12 | 1.09 | 2.1 |
| P-23 | 0.96 | 0.083 | 12 | 0.94 | 1.8 |
| S-4 | 0.93 | 0.083 | 12 | 0.48 | 0.9 |
| S-7 | 0.95 | 0.083 | 12 | 0.60 | 1.1 |

classification. Higher frequency data (i.e. weekly or daily) are needed for the identification of highly karstified systems with conduit flow. But for the case of our karst system, based on weekly data, Samani and Ebrahimi (1996) analyzed the recession curves of the spring hydrographs. They reported that the discharge of both Pirbanow and Pol-Brengi springs consists of 90% diffuse and 10% conduit flow.

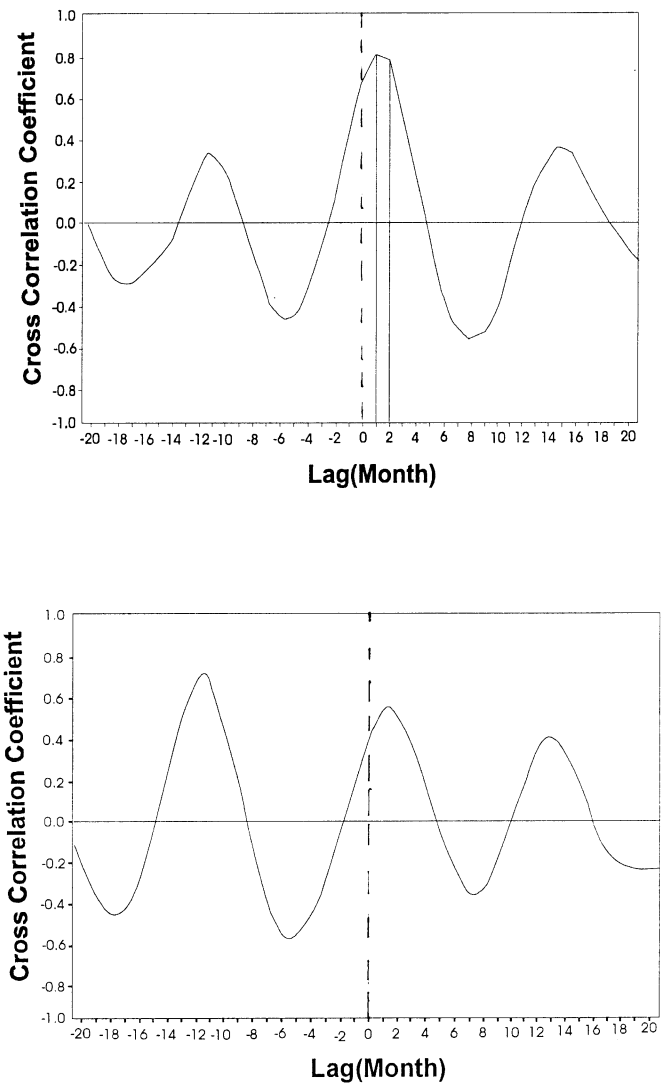


**Figure 6. Cross correlograms: a- (E-17 and S-4), and b- (E-17 and S-7).**

On the basis of statistical parameters of the physical characteristics of the two springs (Tables 1 & 2), and with reference to Jacobson and Langmuir (1974), the flow regime in the karst system feeding Pirbanow spring is of diffuse type. Similarly, and with the exception of high values of EC (more than 600 $\mu S/cm$, i.e., the upper limit given by Jacobson and Langmuir, 1974), the flow regime in the system feeding Pol-Brengi spring is also of diffuse type. Both springs emerge from the Sabzposhan anticline and the lag-time responses (residence times of the infiltrated rainfall in the karst system) of both springs are close to each other, therefore the flow regime of their respective karst system is diffuse. It is logical to consider Sabzposhan aquifer as a single hydrogeological unit. However, the high value of EC for Pol-Brengi spring (1190-1693 $\mu S/cm$) refutes this conclusion. To substantiate this the cross correlation coefficient between the springs and water levels at exploration well E17 were computed. A lag time of 1-2 month exists between Pirbanow spring discharge and the groundwater level at exploration well E-17 (Fig. 6a), but Pol-Brengi discharge is totally independent of groundwater level variations at exploration well E17 (Fig. 6b). In other words there is no connection between Pol-Brengi spring and exploration well E-17, and they are not fed by the same aquifer. This, together with the high value of EC and the fact that Pol-Brengi spring is 2 km further away from E-17 compared to Pirbanow spring, imply that Sabzposhan aquifer consists of two hydrogeological units, the North Sabzposhan unit drained by Pirbanow and the South Sabzposhan unit drained by Pol-Brengi spring. It seems that the Ghasrodasht fault is the cause of this separation that brings lower shaly and gypsiferous marly Pabdeh-Gurpi Formation in contact with karst water and, hence, increases EC value of Pol-Brengi and creates a groundwater barrier between two units (see Fig. 2).

In order to interpret different lags of water level-rainfall in different wells, well logs were examined and depth to water table or the water percolation path from ground surface to the water table for each well was estimated. Table 3 summarizes the mean elevation and depth of groundwater level in all the wells.

Groundwater level variations at wells P-2, P-23, and E-8 penetrating into the Kaftarak aquifer show the same patterns (see Fig. 1). Visual inspection of their logs indicates similar lithology and structural features, in terms of porosity and fractures density (Sahraie 1995). The mean depth of groundwater level at P-2, P-23 and E-8 is 72.72 m, 34.08 m and 30.70 m, respectively (Table 3). The time lag response of E-8 and P-23 with respect to rainfall is 1.8 month and that of P-2 is, however, somewhat longer, i.e. (2.1 months) (Table 6). From this comparison it seems logical to assume the longer time lag response of P-2 to rainfall is a result of a deeper groundwater level.

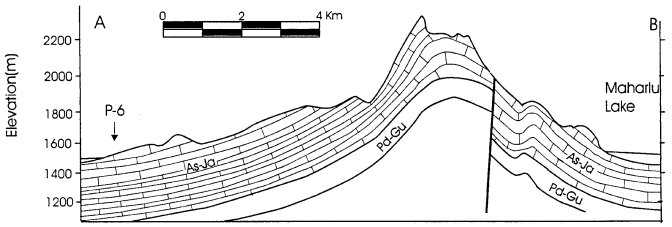


**Figure 7. Geological cross section of the Gharah Anticline.**

In spite of the fact that exploration wells E-10 and E-14 and piezometer P-6 penetrate into the Gharah aquifer, and the water level at P-6 is at a considerably shallower depth (7.61 m), the time lag response of P-6 is longer. Therefore, in contrast to the Kaftarak aquifer, the mean depth of water level does not control the time lag. Inspection of well logs shows no major contrast (in terms of porosity and fractures density) between them (Sahraei 1995) that would cause faster flow towards E-10 and E-14 or that would slow down flow toward P-6. Piezometer P-6 is located at the foot of the southwestern flank of the Gharah anticline and exploration wells E-10 and E-14 on the northeastern flank. Examination of the geological map and cross-section of the anticline (Figs. 2 & 7), shows that the SW flank of the anticline covers a more extensive surface area than the NE flank and the slope of the NE flank is very much steeper than that of the SW flank. From these observations it may be concluded that the mean groundwater flow path toward P-6 is longer, causing a longer time-lag response to rainfall.

## CONCLUSIONS

A combination of statistical methods, physical characteristics of springs, and geologic evidence was used to study the interrelationship of groundwater level and spring discharge to rainfall and evaporation in the Maharlu karst basin. The available groundwater data were the result of several years of monitoring natural level variation at various boreholes (extending through three karst aquifer systems) and of the natural variation of discharge of two springs. Rainfall and evaporation data were taken from two meteorological stations in the basin. The combination of statistical analysis, physical properties of springs, and geologic evidence proved to be complementary in providing useful information about the hydrogeology of the study area. Groundwater levels in all the boreholes respond to rainfall but are independent of evaporation. Different lags between rainfall and water level in different boreholes are probably due to different path lengths of percolating water from sinking points to the water table. The Sabzposhan aquifer was previously believed to be a single hydrogeologic unit, but seems to consist of two separate units. The Ghasrodasht fault is the possible cause of this separation. The impermeable shaly Pabdeh-Gurpi Formation may be an impediment to groundwater flow. This type of study has several advantages: 1) lack of disturbance to the groundwater system; 2) relative simplicity in terms of the statistical method; 3) low cost associated with analysis of data from existing wells and springs.

## ACKNOWLEDGMENT

This research was supported by the Iranian National Center for Scientific Research. Useful comments and suggestions given by the Associate Editor and the two anonymous reviewers are appreciated.

## REFERENCES

Chatfield, C., 1982, The analysis of time series: Theory and practice: London, Chapman and Hall.

Chow, V.T., 1978, Stochastic modeling of watershed systems, Advances in Hydroscience: New York., Academic Press.

Granger, C.W.J. & Hatanaka, M., 1964, Spectral Analysis of Economic Time Series: Princeton, New Jersey, Princeton University Press.

Jacobson, R.L. & Langmuir, D., 1974, Controls on the quality variation of some carbonate spring waters: Journal of Hydrology, v. 23, p. 247-265.

James, G.A. & Wynd, J.G., 1965, Stratigraphic nomenclature of Iranian Oil Consortium Agreement Area: Bulletin of the American Association of Petroleum Geologists, v. 49, no. 12, p. 2182-2245.

Jenkins, G.M. & Watts, D.G., 1968, Spectral Analysis and its Application: San Francisco, Holden-Day Inc.

Obarti, F.J., Garay, P. & Morell, I., 1988, An attempt to karst classification in Spain based on system analysis, *in* IAH 21st Congress, Karst hydrogeology and karst environment protection, Guilin, China, p. 328-336.

Padilla, A., Pulido, A. & Mangin, A., 1994, Relative importance of baseflow and quickflow from hydrographs of karst spring: Ground Water, v. 32, no. 2, p. 267-277.

Sahraei, H., 1995, Response of karstic aquifer to hydrological factors [MS thesis]: Shiraz University, 181 p.

Salas, J.D. *et al*., 1988, Applied modeling of hydrological time series, Water Resources Publication: Fort Collins, Colorado.

Samani, N. & Ebrahimi, B., 1996, Analysis of spring hydrographs for hydrogeological evaluation of karst aquifer system: Journal of Theoretical and Applied Karstology, v. 8, p. 97-112.

Tamab, 1993, Comprehensive study and research in water resources of Maharlu karst basin (Fars): Final report, v. 1, Hydrogeology of the Basin, 284 p.

Todd, D.K., 1980, Groundwater Hydrology: New York, John Wiley and Sons, Inc.

Yevjevich, V., 1982, Stochastic processes in hydrology: Water Resources Publication, Fort Collins, Colorado.

Ivo Karmann, Luis Enrique Sánchez and Thomas Rich Fairchild - Caverna Dos Ecos (Central Brazil): Genesis and geomorphologic context of a cave developed in schist, quartzite, and marble. *Journal of Cave and Karst Studies 63*(1): 41-47.

# CAVERNA DOS ECOS (CENTRAL BRAZIL): GENESIS AND GEOMORPHOLOGIC CONTEXT OF A CAVE DEVELOPED IN SCHIST, QUARTZITE, AND MARBLE

IVO KARMANN
*Department of Sedimentary and Environmental Geology, Geoscience Institute, University of São Paulo, Rua do Lago 562, 05508-900 São Paulo, BRAZIL Ikarmann@usp.br*
LUIS ENRIQUE SÁNCHEZ
*Escola Politécnica, University of São Paulo, Av. Prof. Mello Moraes, 2373, 05508-900 São Paulo, BRAZIL lsanchez@usp.br*
THOMAS RICH FAIRCHILD
*Department of Sedimentary and Environmental Geology, Geoscience Institute, University of São Paulo, Rua do Lago 562, 05508-900 São Paulo, BRAZIL trfairch@usp.br*

*Caverna dos Ecos (Echoes Cave) occurs in low-grade metamorphic rocks of the Mesoproterozoic Canastra Group, 60 km west of Brasília, and exhibits a total linear development of 1600 m and a depth of 140 m, with halls up to 100 m across and 35 m high, a gallery 350 m long and 70 m wide, and at its lowest point, a lake 280 m long and 10 m deep. What makes this cave so unusual is that ~70% of its large volume is presently developed within schist and quartzite. Detailed structural study, together with speleomorphologic analysis, revealed two phases of speleogenesis: the first, typical of carbonate rocks, created phreatic tubes along the intersections of fractures and bedding planes, whereas the second involved breakdown processes that opened up large vadose cavities in the overlying schist and quartzite but without producing any indication of karstic relief in the overlying topography.*

Caverna dos Ecos (Echoes Cave; Sociedade Brasileira de Espeleologia register number GO-18) occurs at 15º40´S, 48º15´W, and 1050 m altitude in the Municipality of Cocalzinho, State of Goiás (GO), about 60 km west of Brasília, central Brazil (Fig. 1). Contrary to typical regions of carbonate caves, there is no evidence whatsoever of karstic relief, either at the local scale or on aerial photographs, that might suggest the presence of this or any other cave in this area. This paper describes the morphology and geology of the cave and proposes a model for its formation based on a detailed study of geologic structures in the cave. Exploration and mapping of Caverna dos Ecos was first carried out by the Espeleo Grupo de Brasília in the 1970s. Remapping by the Grupo de Espeleologia da Geologia of the University of Brasília between 1990 and 1996 increased its known dimensions.

Despite its relatively small proportion of carbonate rocks and isolated nature, Caverna dos Ecos is a remarkable subterranean karstic feature held in special esteem by Brazilian speleologists as no other Brazilian cave of comparable size is known from similar lithologies (mica schist, quartzite, and marble), with ~70% of its volume developed within schists and quartzite. The cave also represents a potential geotechnical hazard, as a road, albeit a secondary dirt track, passes directly over the unsuspected and surficially undetectable, voluminous 35-m high Hall of Clouds.

## REGIONAL CONTEXT OF THE CAVE

The cave is on the Central Goiano Plateau in the highest part of central Brazil that divides the Paraná and Amazon River Basins. It lies specifically within the Verde River Basin, a


**Figure 1. Location of Caverna dos Ecos in central Brazil. GO, Goias; DF, Distrito Federal; MG, Minas Gerais.**

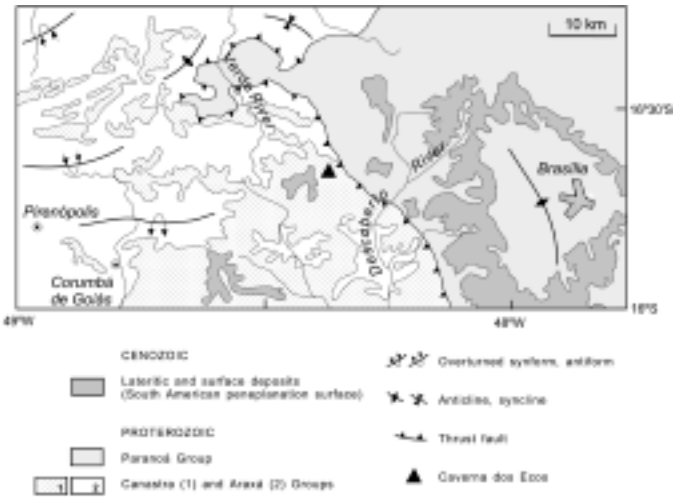


**Figure 2. Geologic setting of Caverna dos Ecos.**

southern tributary of the Maranhão River, which itself comprises part of the headwaters of the Tocantins River (Fig. 1). The region is hilly, between 450 and 1200 m in altitude, with very broad, flat divides and symmetrical valleys predominantly with convex slopes.

A geomorphologic feature typical of the region (and of great importance for understanding the timing of speleogenesis) is the lateritic crust that developed during the Sul-Americano erosional cycle (King 1956; Braun 1971) and gave rise to vast planar surfaces, dissected and incised by Holocene and earlier erosional processes to produce tabular relief.

The Caverna dos Ecos lies within the Cerrado Morphoclimatic Dominion (Saber 1977), typified by open scrub and savanna with two distinct seasons, one cool and dry from May to September, and the other warmer with irregular rain between October and April. Annual rainfall is ~1500 mm and mean annual temperatures are between 19º-22ºC.

The cave developed within metasediments of the Mesoproterozoic Canastra Group (Fig. 2), regionally made up of muscovite schist, muscovite-chlorite schist, calcschist, quartz schist, and garnet-biotite schist, with subordinate lenses of calcitic and dolomitic marble (Schobbenhaus *et al*. 1975; Marini *et al.* 1984). Dardenne (2000) estimates the age of sedimentation between 1200 and 900 Ma and regional metamorphism between 800 and 630 Ma for the Araxá and Canastra Groups in this region.

The schistosity of the metasediments in the area is associated with low-angle reverse faults, as well as with recumbent folds whose axial planes dip SW from 20º-30º with NE-directed tectonic transport. Farther to the east, the Canastra and Araxá Groups override the slate, metasiltstone, and metalimestone of the Paranoá Group (Fig. 2).

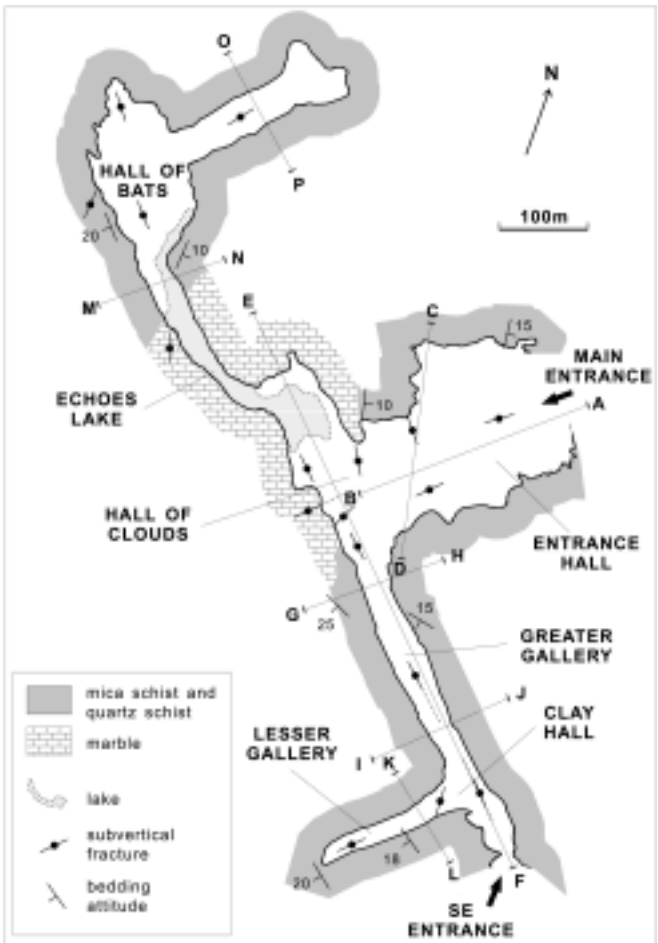


**Figure 3. Geospeleologic map of Caverna dos Ecos.**

## CAVE MORPHOLOGY

Caverna dos Ecos exhibits a total linear length of 1600 m and a depth of 140 m. There are two entrances, the main one to the NE and the other to the SE (Fig. 3 & 4). In plan view the cave exhibits an orthogonal rectilinear pattern of conduits following two main directions. In cross section the ceilings are domed, typical of breakdown profiles (Fig. 4). Except in the area of the lake and in some parts of the large conduits, the primary morphology of solutional enlargement has been completely modified by collapse processes.

The cave floor is dominated by 1-m or even 10-m blocks of mica schist and quartz schist that have fallen from the ceiling. Lower in the cave, close to the lake, great fallen blocks of carbonate occur. Fine-grained detritus, partly external in origin, partially covers blocks and the lateral portions of the lowest parts of the galleries and halls. Such sediments totally cover blocks in Clay Hall.

The roof and floor of the cave are generally parallel. Lengthwise in the Entrance Hall and in the southeast entrance to the cave, the roof roughly follows the slope of the pile of fallen blocks. In the Greater and Lesser Galleries, roof and floor are approximately horizontal, as can be seen in the map

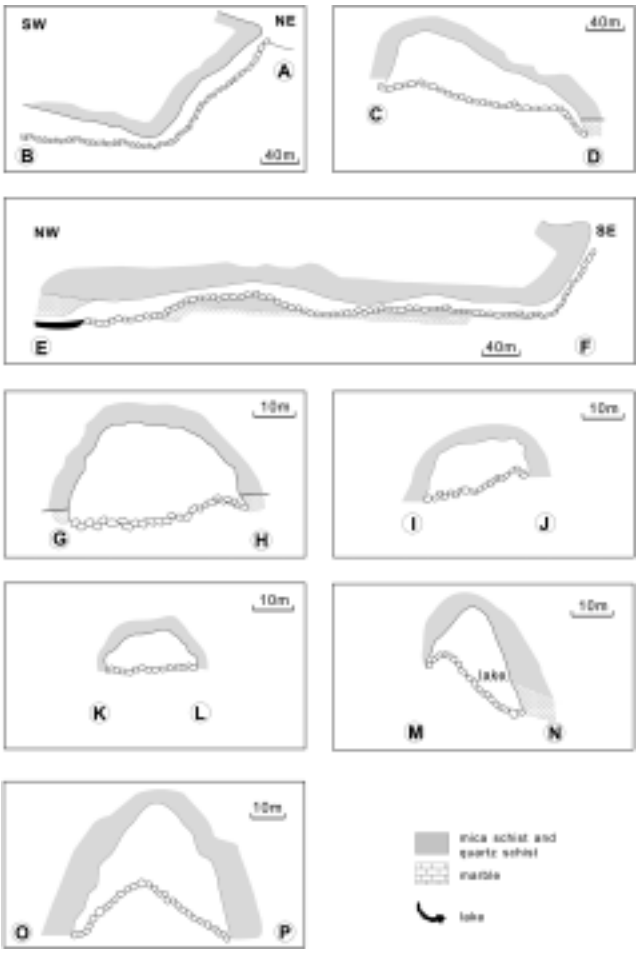


**Figure 4. Cross-sections of the cave. See figure 3 for location of sections.**

and cross sections in figures 3 and 4.

A subterranean lake, 280 m long, 2-50 m wide, and 10 m deep in July 1980, stretches between the Hall of Clouds and Hall of Bats (Fig. 5). Water depth varies, as the lake is known not only to have dried up but also to have completely filled its gallery, cutting off access to the northwest portion of the cave. An annual variation of 2 m has been observed. The bottom of the lake consists of limestone blocks covered by fine, white calcite and quartz sand. The water is crystal clear, and currents are not evident.

## GEOLOGY OF THE CAVERNA DOS ECOS

### LITHOLOGY AND STRUCTURE

The geologic section in figure 6 schematically shows the lithologies observed along the walls of the galleries and halls of the cave. Two distinct units are apparent: upper metapelites and metapsammites and lower metacarbonates. Chlorite schist, predominant in the upper unit, is made up of chlorite, muscovite, biotite, and quartz, with such accessory minerals as tourmaline, epidote, pyrite, albite, and calcite. Intercalated

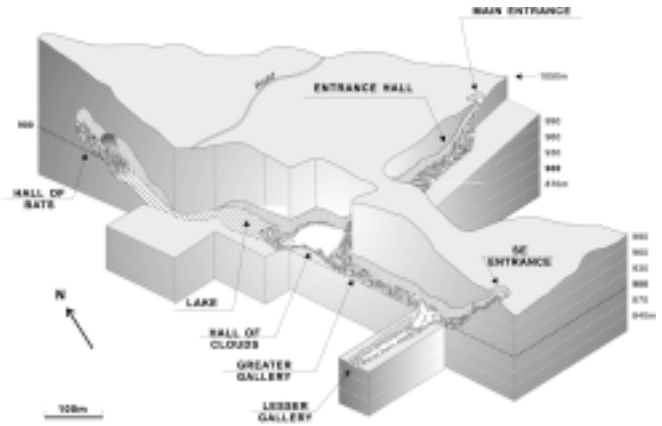


**Figure 5. Block diagram of Caverna dos Ecos. Altitude in meters indicated along right side of diagram. Vertical lines represent walls of the cave.**

subordinate quartz-chlorite schist and muscovite quartzite within the predominantly pelitic succession provide evidence of original bedding. Contacts between these strata are gradational. The quartz-chlorite schist contains rotated porphyroblasts of chlorite with quartz at their centers, representing garnets altered by retrograde metamorphism. Quartz-bearing marble and muscovite-bearing marble comprising the lower unit are made up of carbonate (calcite and dolomite), muscovite, and quartz. Two distinct beds of fine-grained black marble rich in organic matter and tiny pyrite crystals stand out in this part of the section.

Schistosity is concordant with bedding in both the schists and the marbles with the principal foliation (bedding and schistosity) striking approximately N60º-70ºW and dipping 15º-20ºSW. In the marbles, foliation is expressed by the flattening and recrystallization of carbonate grains. Common tight to isoclinal folds have axial planes parallel to bedding, attesting to a phase of transposition and shearing during generation of the schistosity. Fold axes associated with transposition have horizontal attitudes near N80ºE. Later deformation produced crenulation cleavage expressed locally as undulations on the principal foliation surface.

### FRACTURE SYSTEMS

Various sets of fractures (Fig. 7 & 8) are recognizable along the walls of the cave. A set with steep NW and SE dipping beds that strike N30º-50ºE, almost perpendicular to the principal axis of the cave, is prominent in both the metapelites and the carbonates. Fractures of this set are closely spaced (from 0.1m to several meters apart), commonly filled by quartz, and evident for lengths of 1-10 m in the marbles, principally near the lake (Fig. 3 & 8).

Sets oriented N30º-40ºW and N70º-80ºW are represented by unfilled subvertical fractures that are few in number but rather extensive within the cave. These sets are continuously evident for the entire extent of the roof of the Greater Gallery

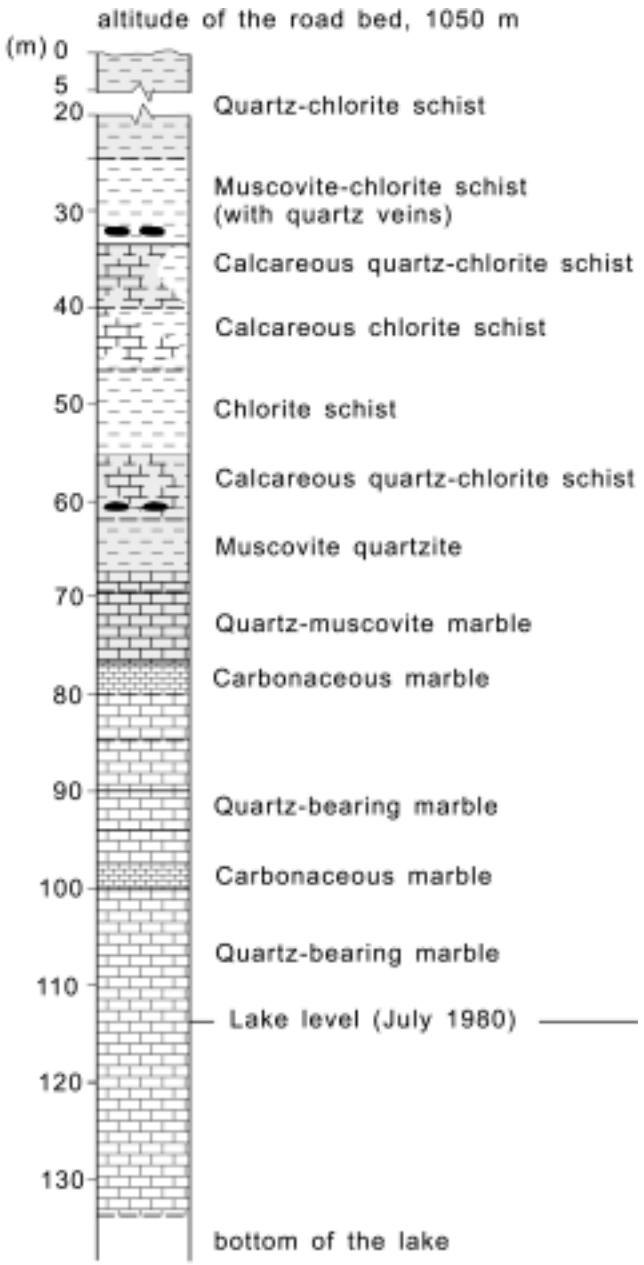


**Figure 6. Lithologic columnar section for the cave.**

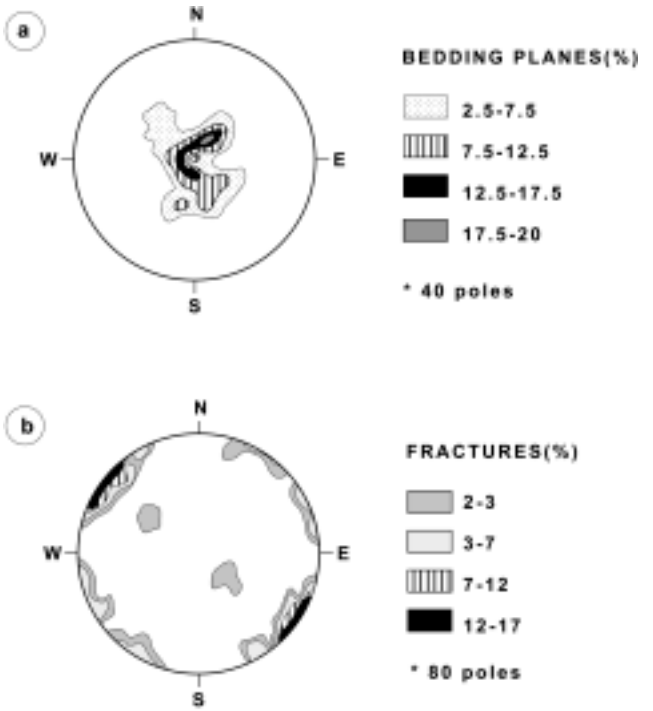


**Figure 7. Wulff net stereographic projections for: (a) bedding planes and foliation and (b) fractures in as measured within the cave.**

(Fig. 3). Quartz-filled fractures of the N70º-80ºW set, oblique to the cave walls, stand out in relief due to carbonate dissolution, whereas fractures of the N30º-40ºW set, paralleling the principal direction of cave development, although visible on the roof, cannot be observed along the walls. Despite the greater abundance of structural data for the N30º-50ºE fractures oblique to the main direction of cave development (Fig. 8), aerial photographs of the area of the cave at a scale of 1:60,000 reveal the regional importance of linear topographic features (Fig. 9; interpreted as disruptive subvertical planar structures) exactly paralleling the primary direction of development (N30º-40ºW), with a secondary direction oriented N40º-50ºE, parallel to the secondary direction of development.

## SPELEOGENESIS

The genesis of Caverna dos Ecos can be differentiated into two principal phases according to the traditional model (Bögli 1969). The first phase (phreatic initiation and development) took place under phreatic conditions and resulted in the opening of conduits along discontinuities in the carbonates. In the second phase (vadose development), collapse occurred under vadose conditions while phreatic dissolution processes continued deeper within the carbonates. The change from one phase to the other was related to regional epeirogenic uplift.

The first phase is evidenced by phreatic dissolution features, such as tubular "wall pocket" cavities (Bretz 1942), observed principally along the walls of the Greater Gallery and along the margins of the lake, where phreatic dissolution is still active. There, "boxwork" structures (Bretz 1942) appear as the carbonate dissolves away, revealing intersecting platy, microcrystalline quartz-filled fractures in relief.

Given that phreatic dissolution of carbonate occurs along the paths of greatest groundwater flux (Bögli 1978; Ford & Ewers 1978), the opening of phreatic conduits in Caverna dos Ecos most likely began along the lines of intersection between bedding planes (and foliation) in the marble and the two principal sets of fractures described above. Their intersection produces N35ºW lineations plunging gently SE and N40ºE lin-

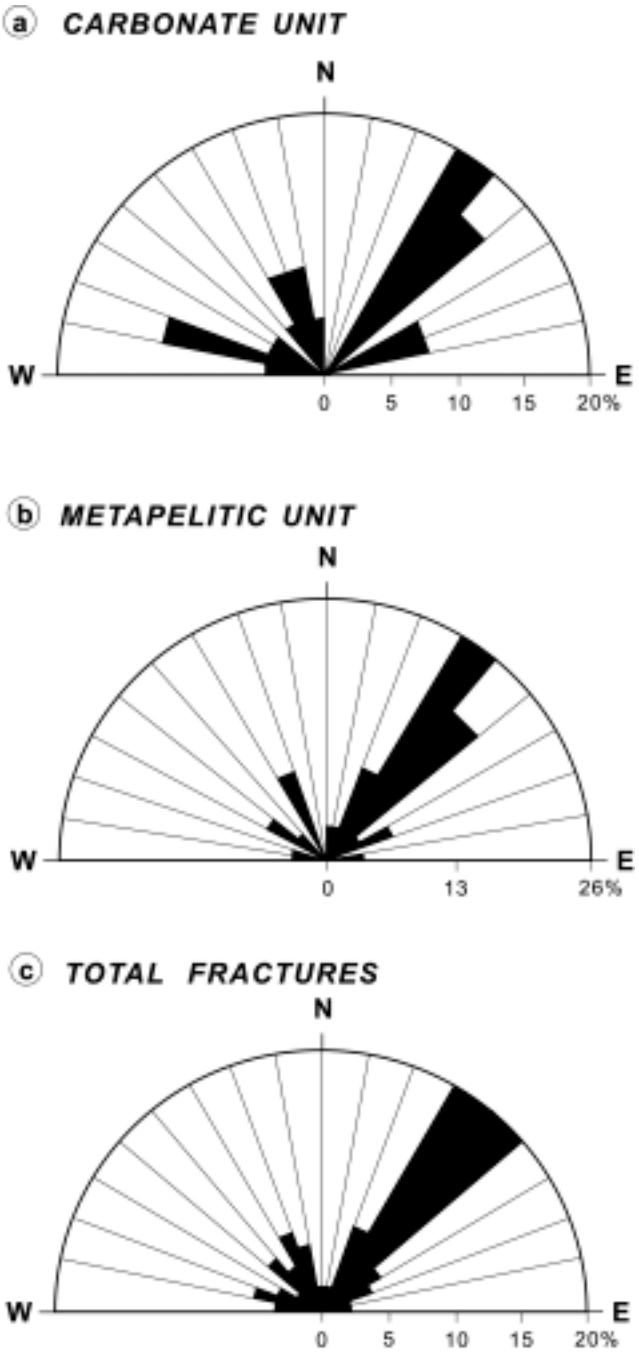


**Figure 8. Rose diagram of vertical to subvertical fractures observed in Caverna dos Ecos.**

eations plunging S10º-20ºW (Fig. 10), that are exactly collinear with the major and minor axes of cave development, respectively. This is strong evidence that the opening of protocaves began along these lines of intersection. As these conduits enlarged by dissolution, and water flux gradually increased, the principal fracture and bedding planes in the carbonate layers themselves began to open up, thereby giving rise to ever larger phreatic conduits.

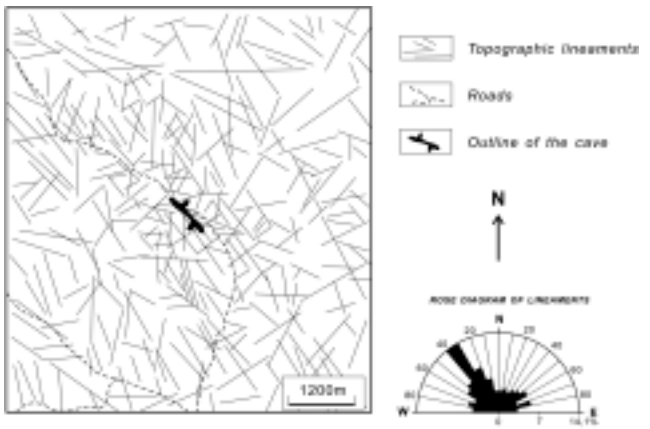


**Figure 9. Topographic lineaments traced from aerial photographs of the study area (1:60,000 scale, USAF 1964).**

The second phase began when the original phreatic cavities started to drain, withdrawing considerable support (potentially up to 42% according to Warwick 1976) from the roof. This led to physical accommodation through the process of breakdown, in which roof blocks delimited by the fracture system and bedding planes collapsed to the floor. Phreatic cavities began to drain when local valleys deepened due to regional epeirogenic uplift and surficial erosional processes intercepted the phreatic level of the cave. As local base level changed, phreatic dissolution continued ever deeper within the carbonates below the water table. These processes correspond to typical covered-karst speleogenesis.

## GEOMORPHOLOGIC CONTEXT OF CAVE DEVELOPMENT

The geomorphologic history of central Brazil during the final part of the Mesozoic and the Cenozoic was one of slow uplift of the South American Platform, as deduced from the relatively low elevations of this region and partially quantified by recent fission-track analysis in apatite (Amaral *et al*. 1997). Superimposed upon this general tendency for uplift were two periods of peneplanation, first recognized by King (1956) on the basis of comparison and correlation of the topographic relief of southern Africa and eastern Brazil.

The older period was responsible for the development of the most extensive and most nearly horizontal planation surface in Brazil, known as the Sul-Americano Surface. The duration of Sul-Americano erosion is not well defined. Nevertheless, by identifying sedimentary deposits correlative with erosion and on the basis of correlation with southern Africa, Braun (1971) attributed the peneplanation phase of the Sul-Americano cycle to sometime between the Eocene and Pliocene, ending with deposition of the extensive Barreiras Group along the coast in the Tertiary (Neogene).

Peneplanation and aggradation of the Sul-Americano Surface were interrupted by an uplift event resulting in the Velhas cycle of King (1956), evidenced by the dissection of

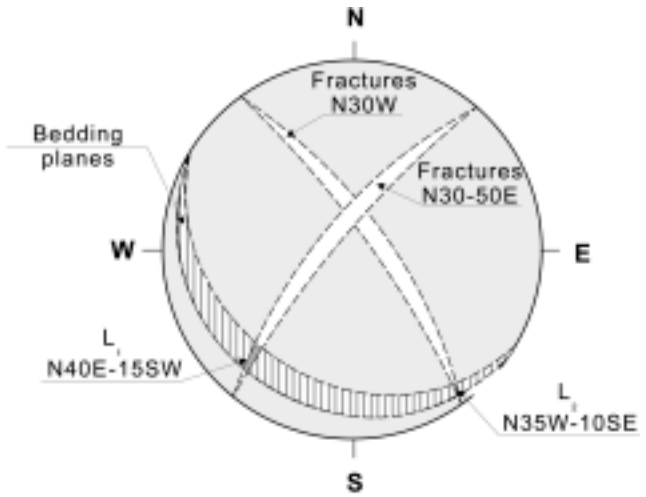


**Figure 10. Wulff net stereographic representation of the intersection between main fracture sets and bedding planes showing the collinear relationship between the lines of intersection (L1 and L2) and the main axes of cave development.**

both the Barreiras sediments along the coast and the detrital-lateritic cover in central Brazil. This cycle gave rise to the main drainage pattern presently observed in central Brazil and continues to this day. Based on geochronology of the Barreiras Group along the coast (Braun 1971), but without equivalent data available for the interior of Brazil, the beginning of this cycle is placed somewhere within the Pliocene or Pleistocene. There are suggestions that this cycle may have begun first along the coast, perhaps in the Miocene (Valadão & Dominguez 1999), subsequently extending further into the country.

In previous studies, Karmann (1994) has shown that large phreatic volumes in other caves in the state of Goiás are related to slow cratonic uplift in the same manner as the Sul-Americano surface. We interpret the large phreatic volumes of Caverna dos Ecos in a similar manner. Thus, we correlate initiation and development of phreatic cavities, the first phase of speleogenesis of Caverna dos Ecos, with peneplanation and aggradation of the Sul-Americano Surface, sometime between the Eocene and Pliocene, following King's (1956) suggestion for the initiation of calcareous caves of the State of Minas Gerais. Later generalized uplift associated with the Velhas cycle (beginning in the Pliocene or Pleistocene) led to the installation of the present-day drainage pattern, gradually lowering the water table and draining the phreatic conduits within the carbonates, subjecting them to vadose conditions. This initiated the second phase of speleogenesis, marked by the instability of the open spaces and modification of the conduits by breakdown. Upward propagation of open spaces through a series of roof collapses eventually breached the surface, allowing access to the present-day Caverna dos Ecos.

## CONCLUSION

Caverna dos Ecos represents an isolated feature of covered karst that developed within mica schist, micaceous quartzite, and marble of the Proterozoic Canastra Group. An initial phreatic phase of cave formation opened up conduits along the intersection of bedding planes with two sets of subvertical fracture planes, one oriented N30º-40ºW and the other N40º-50ºE. A second phase greatly enlarged cavities under vadose conditions as a result of the collapse of phreatic conduits due to the mechanical instability of the rock mass as a result of the lowering of the water table. The first phase may be correlated with the formation of the Sul-Americano Surface sometime between the Eocene and Pliocene, the second phase began with the Velhas cycle in the Pliocene or Pleistocene and continues to the present.

Besides being one of the largest Brazilian caves developed in areas without karst topography, the Caverna dos Ecos is also important as a reminder of the potential problems and danger of carrying out large construction projects above undetected caves in non-karstic terrains. Hence, thorough investigation of the subsoil is necessary in order to detect large subterranean cavities prior to initiating major civil engineering projects in terrains occupied by the extensive Canastra Group in central Brazil. It is, thus, significant that other smaller caves have been reported in the same geological context from areas under consideration for power plant construction in this region (Augusto Auler, pers. comm., December 2000).

## ACKNOWLEDGEMENTS

This paper resulted as a part of an undergraduate research project (Grant No. 80/796-4 to I. Karmann, L.E. Sanchez, A.A. Montanheiro, and P.E. Milko) and financial aid (Proc. No. 80/794 to T.R. Fairchild) sponsored by the São Paulo Foundation for Scientific Research (FAPESP). Volkswagen do Brasil S/A graciously loaned a vehicle for field work. We would also like to thank the Espeleo-Grupo de Brasília, represented by Mr. Fernando Quadrado Leite, whose support during the work in Caverna dos Ecos was fundamental for the success of the project, as well as the GREGEO-UnB for cartographic data. To Thelma Samara we are grateful for the drawings. The reviewers, George W. Moore and Augusto Auler, kindly provided constructive criticism.

## REFERENCES


Amaral, G., Born, H., Hadler, J.C., Iunes, P.J., Kawashita, K., Machado, D.L., Oliveira, E.P., Paulo, S.R. & Tellos, C.A., 1997, Fission-track analysis of apatites from São Francisco Craton and Mesozoic alkaline-carbonatite complexes from central and south-eastern Brazil: Journal of South American Earth Sciences, v. 10, no. 3-4, p. 285-294.

Bögli, A., 1969, Neue Anschauungen über die Rolle von Schichtfugen und Kluften in der karsthydrographischen Entwicklung: Geologische Rundschau, v. 58, p. 395-408.

Bögli, A., 1978, Karsthydrographie und physische Speläologie: Heidelberg, Springer Verlag, 292 p.

Braun, O.P.G., 1971, Contribuição à geomorfologia do Brasil Central: Revista Brasileira de Geografia, v. 3, no. 32, p. 3-36.

Bretz, J H., 1942, Vadose and phreatic features of limestone caverns: Journal of Geology, v. 50, p. 675-811.

Dardenne, M.A., 2000, The Brasília Fold Belt, *in* Cordani, U.G., Milani, E.J., Thomaz-Filho, A., Campos, D.A., eds., Tectonic Evolution of South America, 31st International Geological Congress: Rio de Janeiro, p. 231-263.

Ford, D.C. & Ewers, R., 1978, The development of limestone cave systems in the dimensions of length and depth: Canadian Journal of Earth Sciences, v. 15, no. 11, p. 1783-1798.

Karmann, I., 1994, Evolução e dinâmica atual do sistema carstico do Alto Ribeira, São Paulo, Brasil [PhD thesis]: Universidade de São Paulo, 210 p.

King, L.C., 1956, A geomorfologia do Brasil Oriental: Revista Brasileira de Geografia, v. Ano XVIII, no. 2, p. 147-265.

Marini, O.J., Fuck, R.A., Danni, J.C.M., Dardenne, M.A., Loguercio, S.O.C. & Ramalho, R., 1984, As Faixas de Dobramentos Brasília, Uruaçu e Paraguai-Araguaia e o Maciço Mediano de Goiás, *in* Schobbenhaus, C., et al. (coordenadores), ed., Geologia do Brasil, Texto Explicativo do Mapa Geológico do Brasil, escala 1:2,500,000: Brasília, Departamento Nacional da Produção Mineral (DNPM-DGM), p. 251-303.

Saber, A.N., 1977, Os domínios morfoclimáticos da América do Sul, primeira aproximação: Geomorfologia, Instituto de Geografia - USP, v. 52, p. 1-21.

Schobbenhaus, C., Ribeiro, C.L., Oliva, L.A., Takanohashi, J.C., Lindenmayer, Z.G., Vasconcelos, J.B., & Orlandi, V., 1975, Carta geológica do Brasil ao Milionésimo, Folha GOIÁS (SD-22): Departamento Nacional da Produção Mineral (DNPM-DGM).

Valadão, R.C. & Dominguez, J.M.L., 1999, Soerguimento, flexura e nucleação de grabens na área continental adjacente ao litoral oriental brasileiro no Neocenozóico, VII Congresso da ABEQUA, Porto Seguro.

Warwick, G.T., 1976, Geomorphology and caves, *in* Ford, T.D., Cullingford, C.H.D., ed., The Science of Speleology: London, Academic Press, p. 61-125.

# DISCUSSION: "EXTRAORDINARY FEATURES OF LECHUGUILLA CAVE, GUADALUPE MOUNTAINS, NEW MEXICO"

DALE J. GREEN
*4230 Sovereign Way, Salt Lake City, UT 84124 USA, dajgreen@burgoyne.com*

I would like to address some matters of basic physics and morphology concerning Davis's explanation of rimmed vent formation. He states: "The mechanism of rim formation is not well understood, but they are believed to develop via simultaneous condensation and evaporation across a wall projection. The encrusted sides normally face the surface or the entrance (i.e., a source of cooler, drier air), while the corroded sides face the warmer, moister cave interior. The moisture condensing on the corroded side is assumed to dissolve the substrate there, then move by wicking action to the other side, where evaporation redeposits the material as a rim. In some places, aragonite rims form along walls and ceiling while gypsum rims grow on the floor at the same site, suggesting that slightly drier and therefore denser air tends to follow the floor. (Davis 2000, p.149.)"

Heat flux can only move from a higher temperature to a lower temperature. As Davis observes, this makes the interior, lower areas of a cave warmer than the outer, higher areas. All condensation is the result of decreasing temperature. If warm vapor rising from the cave's interior is in contact long enough with a cold surface for the vapor to be cooled below its dew point, then condensation results. Upon condensing, the vapor transfers the latent heat of condensation, equal to ~600 cal/gm, to the cooling surface, thereby warming the surface unless a heat sink is provided. In the case of a cave roof, the latent heat is probably dispersed throughout the limestone. If this condensation is wicked to a cooler area, then evaporation is impossible. Evaporation requires the addition of 600 cal/gm of water, the latent heat of vaporization, before vapor will enter the air. No source of heat to cause evaporation is available since the rim area (vent exit) is cooler than the vent entrance where condensation occurred, given the direction of heat flow. Dry, or "drier air" may allow evaporation to occur if its vapor pressure is below the vapor pressure of the condensate, but heat is still required.

Physics aside, the morphology of vents and associated rims cannot be explained by a process of condensation, wicking and evaporation, in my opinion. The inside surface of rims appears to be dissolving from the inside out and is always concordant with the bedrock surface of the vent. A physical force, like moving air or water through the vent, must be involved. If air, several obstacles are presented. To overcome surface tension, a velocity of over 40 km/hr is required to drag condensate along the surface. At the same time, for condensation to form, the air must be in contact with a cool surface long enough to reduce its temperature below the dew point, which would not happen unless the velocity was considerably less than 40 km/hr. Consider also, that at these velocities, evaporation is greatly increased, even in 99% RH. How does condensate get blown along a wall for several meters from an entrance to vent without evaporating? Further, the turbulence within the calcite-laden moisture being dragged by air currents would surely cause the loss of $CO_2$, resulting in deposition long before reaching the vent exit.

Vents, rims, and a wide variety of associated forms appear in all stages of development in caves of the Basin and Range, where I have studied them. Many of these occurrences are in physical situations where only the force of moving water would be considered as the likely cause of rims and vents, not condensation corrosion (Green 1997a).

It was a study of vents and rims that led me to the formulation of a totally different theory for deposition of folia than that presented by Davis. He believes them to "…represent a water-table equivalent of shelfstone. Shelfstone maintains a distinct horizontal level controlled by a fixed, perched overflow point. Folia shelves are sloping and overlapping because the calcite accretion attempts to follow the irregular fluctuations of a calcite-saturated water table" (Davis 2000, p.152).

In Goshute Cave, Nevada, two side-by-side passages are at the same elevation. In the west passage, a thick mammillary coating of calcite is mostly dissolved away, exposing bedrock. A rimmed vent connects from the west passage to the east passage, where the mammillary coating is undisturbed and is coated with folia. The lowest folia occurrence is coincident with the lowest part of the vent. If folia are deposited at a fluctuating water table, then why are there no folia in the west passage? My interpretation is that the west-side dissolution, vent scouring, rim and folia deposition, were all occurring at the same time. As the dissolving waters in the west passage emerged from the vent, an out-gassing of $CO_2$ occurred, depositing the rim and creating calcite nuclei, which then form crystallites. It is beyond the scope of this discussion to explain how these crystallites attach to the downward-facing surfaces (folia are only found on downward-facing surfaces), form small ribs, then through accretion, create upside-down cups capable of trapping gas. When studied in detail, folia exhibit very complex forms that, in my opinion, cannot be explained with the fluctuating water table theory but are completely plausible with a subaqueous origin. A more complete discussion of this theory of folia genesis is described in Green (1997b).

Additionally, it is stated in Davis's article that Utah has caves with folia. I believe this is an error.

REFERENCES

Davis, D.G., 2000, Extraordinary features of Lechuguilla Cave, Guadalupe Mountains, New Mexico. Journal of Cave and Karst Studies, v. 62, no. 2, p. 147-157.

Green, D.J., 1997a,. Is it condensation corrosion or something else? Journal of Cave and Karst Studies, v. 59, no. 1, p. 60.

Green, D.J., 1997b, The origin of folia. Technical Notes 96 of the Salt Lake Grotto, N.S.S., November 1997. (Reproduced in the 1997 SpeleoDigest, p. 421-429.)

# REPLY: "EXTRAORDINARY FEATURES OF LECHUGUILLA CAVE, GUADALUPE MOUNTAINS, NEW MEXICO"

DONALD G. DAVIS
*441 S. Kearney St., Denver, CO 80224-1237 USA, dgdavis@nyx.net*

Condensation-corrosion/evaporation cycles have been shown to be capable of significant influence on cave morphology (Sarbu & Lascu 1997). I know of no quantitative studies specifically on rimmed vents, but my speculative rim model does not violate the physics of evaporation. External warming is not needed to evaporate condensed moisture that has seeped to a cooler, drier spot. If atmospheric humidity is low enough that the condensate's vapor pressure is not in equilibrium with it, evaporation will take place. The air, water, and, to a lesser extent, the substrate will cool further to satisfy the energy budget.

Green devises an alternative subaerial mechanism postulating strong wind blasting the condensate film along the wall, then dismisses it, for good reasons. Having rejected both my idea and his, he concludes, in effect, that a subaerial mechanism for rimmed vents is theoretically impossible, so they must be subaqueous. This reminds me of proverbial theoretical claims that bumblebees can't fly. There is overwhelming evidence, in composition, morphology, and context, that the hundreds of rims in Lechuguilla Cave originated subaerially. Those composed of carbonates are mostly acicular aragonite in the form of frostwork. Frostwork grows in air, typically under evaporative conditions; I am aware of no example of demonstrated subaqueous growth. The many non-carbonate rims in Lechuguilla are gypsum. I know of no plausible mechanism to deposit and preserve gypsum preferentially around underwater orifices; $CO_2$ degassing is irrelevant. Nor do these rims ever show any genetic association with demonstrably subaqueous features.

My suggested model for rimmed vent development may or may not be correct, but the correct one (at least for Lechuguilla Cave) must certainly be subaerial. The process is apparently very slow and subtle, and may have started almost as soon as the water table dropped below the levels where the rims occur, taking up to several million years to translocate a few centimeters of wall rock from one side of a projection to the other. The physical gradients involved may be extremely small.

Green has never been to Lechuguilla Cave, but extrapolates from observations in Great Basin caves. In Goshute Cave, Nevada, he proposes that wall dissolution, creation of a rimmed vent, and folia deposition via $CO_2$ degassing in the next chamber outflow, were simultaneous and subaqueous. I have also visited Goshute Cave, and saw no proof of this assertion. The denuded chamber and rimmed vent appeared consistent with condensation-corrosion. Goshute Cave, like Lechuguilla, is an old cave of hypogenic origin—quite possibly hydrothermal—and could have had a sufficient temperature gradient to drive a corrosion/evaporation cycle before it was entirely drained. If folia had existed in the corroded chamber, they would have been the first layer removed. If they never grew there, it may be because this chamber was closed to air circulation by a sump at the connecting orifice, so $CO_2$ degassing and evaporation could take place only on the outer side of the constriction.

In Green's model, as exemplified by Goshute Cave, the relationship between rimmed vents and folia deposition predicts that folia should occur in the outflow direction from vents. In Lechuguilla Cave, the converse is true. Vents and rims are predominantly in the middle to upper levels, whereas folia are limited to the lower levels, in the inflow direction (assuming rising water) from any scoured and rimmed vents. The Lechuguilla folia are well developed only in two laterally separated areas within ~40 m vertically above the present water table. In all other caves where I have observed folia, they are even more restricted to a narrow vertical range, being limited in the most extreme case to a few-centimeter-high "bathtub ring" in Groaning Cave, Colorado. This seems to me consistent only with a fluctuating-water-level interpretation, not with a fully subaqueous one. The invariable association of calcite rafts with calcite folia also strongly suggests water-level con-

trol. Deposits of unquestionably subaqueous origin, such as mammillary crusts, may be associated with rafts but often are not.

Green has made a valuable observation in pointing out that folia can trap gas when they *are* submerged. This is no doubt important in development of folia morphology (restricting most accretion to the top and edge of each inverted cup). This gas may be degassing $CO_2$, or it may be no more than cave atmosphere trapped when water level rises periodically. $CO_2$ degassing, though clearly favorable to carbonate folia growth, is not essential to folia accretion, as the existence of mud folia (Davis 1984) and sulfur folia (Hose *et al*. 2000) shows. Probably the critical requirement is simply a variable water level with a surface scum and/or subsurface suspension of fine particles capable of adhering to growing folia.

I have read Green's prior publications on these matters, but remain unconvinced that rimmed vents develop underwater (though subaqueous features of similar appearance—variants on "geysermites"?—may be possible), or that folia are more than intermittently subaqueous. Continued controversy, however, shows that these phenomena are not understood well enough to remove all doubt. I hope that this will provoke others to contribute new thoughts and observations.

Finally, Green is probably correct in questioning my inclusion of Utah among states known to have folia. I may have been thinking of Indian Burial Cave, which is just inside Nevada.

ACKNOWLEDGMENTS

This reply benefited from discussions of atmospheric physics with Rane Curl, Harvey DuChene, Larry Fish, Paolo Forti, Carol Hill, Stuart Marlatt, and Art Palmer.

REFERENCES

Davis, D.G., 1984, Mysteries in mud: Ancient frost crystal impressions and other curiosities in Cave of the Winds. Rocky Mountain Caving, v. 1, no. 3, p. 26-29.

Hose, L.D., Palmer, A.N., Palmer, M.V., Northup, D.E., Boston, P.J., & DuChene, H.R., 2000, Microbiology and geochemistry in a hydrogen-sulphide-rich karst environment. Chemical Geology, v. 169, p. 399-423.

Sarbu, S.M. & Lascu, C., 1997, Condensation corrosion in Movile Cave, Romania. Journal of Cave and Karst Studies, v. 59, no. 3, p. 99-102.

**SPELEOGENESIS:**
**EVOLUTION OF KARST AQUIFERS**

Alexander B. Klimchouk, Derek C. Ford, Arthur N. Palmer, and Wolfgang Dreybrodt (editors) with members of the Commission on Karst Hydrogeology and Speleogenesis, International Union of Speleology. January 2000 Edition. National Speleological Society, Huntsville, Alabama 527 p., ISBN 1-879961-09-1. $60.00US. Order on line at http://www.caves.org/service/bookstore.

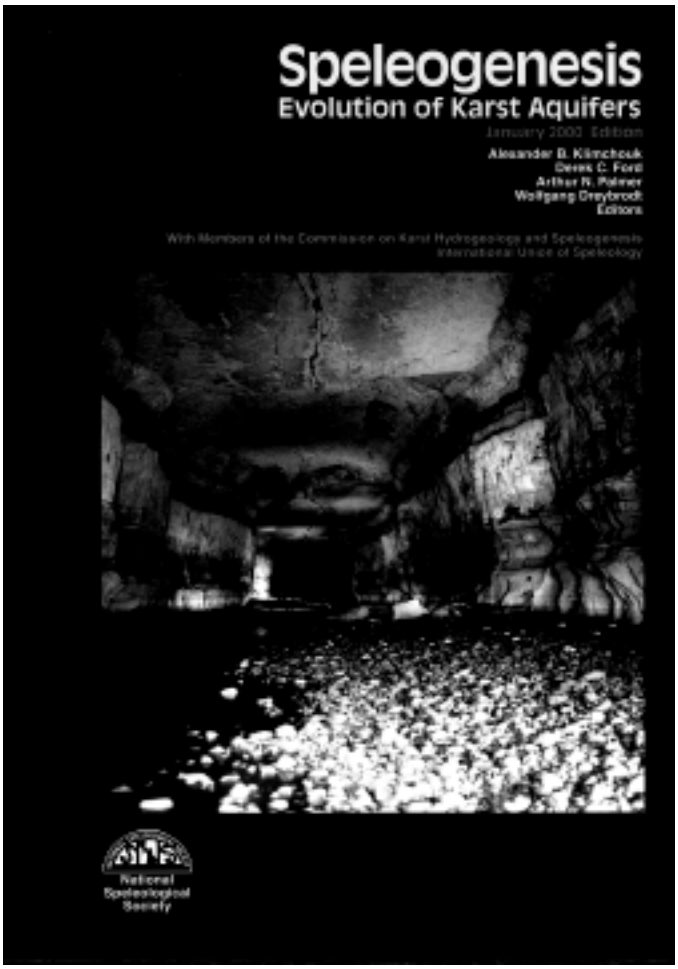


*Speleogenesis*, published by the National Speleological Society in 2000, is a monumental book, long in the making and eagerly awaited by speleologists and cavers worldwide. Without doubt, it is the most inclusive compilation of English-language papers yet published in a single volume on the origin of caves and the hydrogeomorphic evolution of karst groundwater systems. It is a veritable textbook on the subject of karst processes.

The concept of a comprehensive reference book on the physical and chemical processes that form caves and karst had been discussed and formulated for many years. In fact, several notable textbooks in English have been published within the last three decades, including those of Sweeting (1973), Jakucs, (1977), Bogli (1980), Jennings (1985), Trudgill (1985), Dreybrodt (1988), White (1988), Ford and Williams (1989), and Gillieson (1996). Most of these works are an assimilation of knowledge compiled by one or two internationally recognized authors.

*Speleogenesis*, as stated in the preface and introduction, is "a pioneer attempt by an international group of cave scientists to summarize modern knowledge about the origin of caves in various settings, to examine the variety of approaches that have been adopted, and to outline the role of speleogenesis in the evolution of karst aquifers." Concepts presented in this compilation are largely based on advances in cave and karst science made during the last few decades.

The book consists of 61 selected contributions from 44 authors and co-authors representing 15 countries. The papers were prepared during the years 1994 to 1998 and edited by four internationally noted speleologists: Alexander B. Klimchouk (Ukraine), Derek C. Ford (Canada), Arthur N. Palmer (USA), and Wolfgang Dreybrodt (Germany). Some of the papers are upgrades, revisions, or summaries of previously published findings of the individual authors, many of which have appeared in refereed journals, proceedings of symposia, or elsewhere in the technical literature. The astute reader will recognize many of the contributions as modified benchmark papers. However, many of the articles in this book are original contributions. In all cases, *Speleogenesis* includes the most recent findings, interpretations and principles as described by those who have developed them. The most important aspect of the volume is that it represents the state of the art in modern speleology, as presented by the leading researchers, all in one readily accessible resource. Not only is the book encyclopedic in covering virtually all aspects of speleogenesis and karst processes, but each paper is supported with ample references to the extant literature of interest. This fact alone is of prime consideration, as anyone wishing to access current research in speleology need only refer to this book, rather than track down dozens if not hundreds of references in a widely scattered literature. There is a large bibliography (28 pages) on caves and karst at the back of the book, as well as detailed indices to authors and subjects covered in the text.

Some comments on the contents, layout, and organization of the book are in order. The magnitude and scope of the emerging book dictated that it would have to be produced as a volume of large format (22 cm x 29 cm) and length (527 pages), which makes it similar in size to a standard desktop dictionary. Pages are laid out in three columns, 6 cm wide and the type is a small (~8) font. Despite this compact style, the text is clear; although prolonged reading may lead to eyestrain. The staff responsible for design, layout, style and production (in particular, David McClurg, Margaret Palmer, and George Moore) is to be commended for maximizing the content while keeping the cost of this encyclopedic tome at a minimum. In comparison to other geologic advanced textbooks and specialized reference books produced by major publishers, *Speleogenesis* is a bargain, well within the budget of any seri-

ous speleologist or caver.

The articles range in length from 2-14 pages, with most around 6-8 pages. This is comparable to the length of papers in professional journals. The figures, photographs and line drawings have been reduced to efficiently fit 1, 2, or 3 columns or, in places, half the width of a page. Many of the figures are quite detailed; however, clarity has been maintained despite reduction. All photographs are black-and-white and are reasonably clear. The line drawings are crisp and very readable.

As expected, each paper is technical in nature, comparable in scientific detail and vocabulary to articles in refereed technical journals. Geologists, especially geomorphologists and hydrogeologists specializing in karst, will find the writings and expositions to be consistent with the geotechnical literature and should have little difficulty following the text. Cavers who are not professional earth scientists, for example most of the rank-and-file members of the National Speleological Society, may find the material somewhat challenging to read. However, a great many cavers have been exposed to cave science in the course of exploring, mapping, and communicating about caves and, in general, have assimilated considerable knowledge about geologic processes in the development of caves and karst. By and large, long-term active cavers should benefit greatly from this book. As a whole, *Speleogenesis* integrates the complexities implicit in the hydrogeomorphology of karst into a coherent whole.

Papers are grouped into seven major parts within the book. The first two are an introduction (1 paper) and a historical overview of cave science (3 papers) consisting of abbreviated versions of more extensive discourses by Shaw (1992), Lowe (1992a,b) and Watson and White (1985), respectively. Parts 3 and 4 include geologic and hydrogeologic controls on the development of caves and karst (7 papers) and theoretical fundamentals of speleogenetic processes (15 papers). Part 5 includes 27 papers related to cave development in various geologic and hydrologic settings. Speleogenesis of many of the largest cave systems in the world is included in this part. Part 6 (2 papers) considers the origin of small and mid-scale features in caves (dissolutional features and breakdown). Part 7 (4 papers) considers speleogenesis in non-carbonate rocks. Finally, Part 8 (3 papers) is a brief introduction to applied speleology. The major emphasis of *Speleogenesis* (and the most comprehensive coverage) lies in the papers in Parts 3, 4, and 5.

Who should own this book? The answer is unequivocal. Anyone who has a need or desire to understand how speleogenetic processes work, including research scientists, cavers, college students, and those working in applied karst projects such as geotechnical consultants, environmental geologists and hydrologists and appropriate personnel of governmental agencies. This book should be on the shelf of anyone involved in the study and understanding of karst systems.

## REFERENCES

Bögli, A., 1980, Karst Hydrology and Physical Speleology (translated from the German by June C. Schmid): Springer-Verlag, New York, 284 p.

Dreybrodt, W., 1988, Processes in Karst Systems Physics, Chemistry and Geology: (Springer Series in Physical Environment 4): Springer-Verlag, New York, 288 p.

Ford, D.C. and Williams, P., 1989, Karst Geomorphology and Hydrology: Unwin Hyman, Winchester, Massachusetts, 320 p.

Gillieson, D.S., 1996, Caves: Processes, Development, Management: Blackwell Publishers, Oxford, England and Malden, Massachusetts, 324 p.

Jakucs, L., 1977, Morphogenetics of Karst Regions: Variants of Karst Evolution (translated from the Hungarian): Halstead Press, John Wiley and Sons, New York, 284 p.

Jennings, J.N., 1985, Karst Geomorphology (revised and expanded edition of Jennings, 1971): Basil Blackwell, Oxford and New York, 293 p.

Lowe, D.J., 1992a, The origin of limestone caverns: An inception horizon hypothesis: Ph.D. dissertation (unpublished), Manchester Metropolitan University, Manchester, Great Britain, 512 p.

Lowe, D.J., 1992b, A historical review of concepts of speleogenesis: Cave Science, v. 19, no. 3, p. 63-90.

Shaw, T.R., 1992, History of Cave Science: The Exploration and Study of Limestone Caves, to 1900 (second edition): Sydney Speleological Society, Sydney, Australia, 338 p.

Sweeting, M.M., 1973, Karst Landforms: Columbia University Press, New York, 362 p.

Trudgill, S., 1985, Limestone Geomorphology (Geomorphology Texts, No. 8): Longman, London and New York, 196 p.

Watson, R.A. and White, W.B., 1985, The history of American theories of cave origin: Geological Society of America, Centennial Special Volume 1, p. 109-123.

White, W.B., 1988, Geomorphology and Hydrology of Karst Terrains: Oxford University Press, New York, 464 p.

Book reviewed by Ernst H. Kastning, Ph.D., Department of Geology, Box 6939, Radford University, Radford, Virginia 24142 (ehkastni@radford.edu) November 2000.

# CAVE SCIENCE NEWS

**ESRI Offers Web Site for Cave and Karst GIS**

Leading Geographic Information Systems (GIS) software developer ESRI, based in Redlands, California, offers a Web site for those using ESRI GIS software for cave and karst applications. GIS is used by various government agencies and an increasing number of private organizations and individuals to store, map, manage, and analyze cave and karst data, and is an important tool in the management and conservation of cave and karst resources.

The site offers a variety of resources, including a discussion forum, examples of utilizing GIS in cave and karst applications, an electronic newsletter, white papers, technical documents, and news and contributions from various users. The site also includes links to the ESRI Cave and Karst Conservation Program, offering grants and other assistance in software acquisition for those involved in cave and karst conservation and management activities.

For more information contact NSS member Bernie Szukalski, ESRI Cave and Karst Program Manager (volunteer), at bszukalski@esri.com, or visit the ESRI Cave and Karst Web site at:

http://www.esri.com/industries/cavekarst/index.html

**Deadline for Abstract Submission for Geology and Geography Section at 2001 NSS Convention Announced**

The NSS Section of Cave Geology and Geography is accepting abstracts of papers for presentation at the Geology and Geography Session of the 2001 NSS Convention, to be held in Mt. Vernon, Kentucky, from 23-27 July 2001. Abstracts should be no more than 250 words in length (this limit must be strictly met). In addition to the text, the abstracts should contain the title of the paper, and the name(s) and address(es) of the author(s). The abstracts should be informative summaries that include the conclusions, and not lists of topics that "...will be discussed." Bibliographies and references should not be given in the abstracts. Papers may be submitted for either oral presentation or as a poster.

Send any questions and your abstracts by mail, e-mail, disk, or fax to: George Veni, 11304 Candle Park, San Antonio, Texas 78249-4421 210-558-4403 413-383-2276 (fax) gveni@flash.net

The deadline for abstracts is 1 May 2001. Early submissions are encouraged. Confirmation notes will be sent to everyone sending an abstract. Details on presentations times, dates, and other information will be sent to all confirmed participants after the deadline. For online details about the convention, visit: http://www.nss2001.com/.

**Position Available - Chairperson of the NSS Research and Advisory Committee**

The Research and Advisory Committee is in the office of the Executive Vice President. The duties include coordinating the research grants given by the Society, offering candidates for the annual Ralph W. Stone Research Award, administering the NSS Young Investigator Award program, designating official NSS research projects, collecting annual project summaries for NSS Projects and Study Groups, providing advice to members concerning scientific efforts, answering speleological inquiries from others, and reviewing research proposals and award grants. Members interested in this position should contact the NSS Executive Vice President, Ray Keeler, via email <rkeeler@pcslink.com> or call h/602-561-2917, w/602-822-3954.

**Obituary**

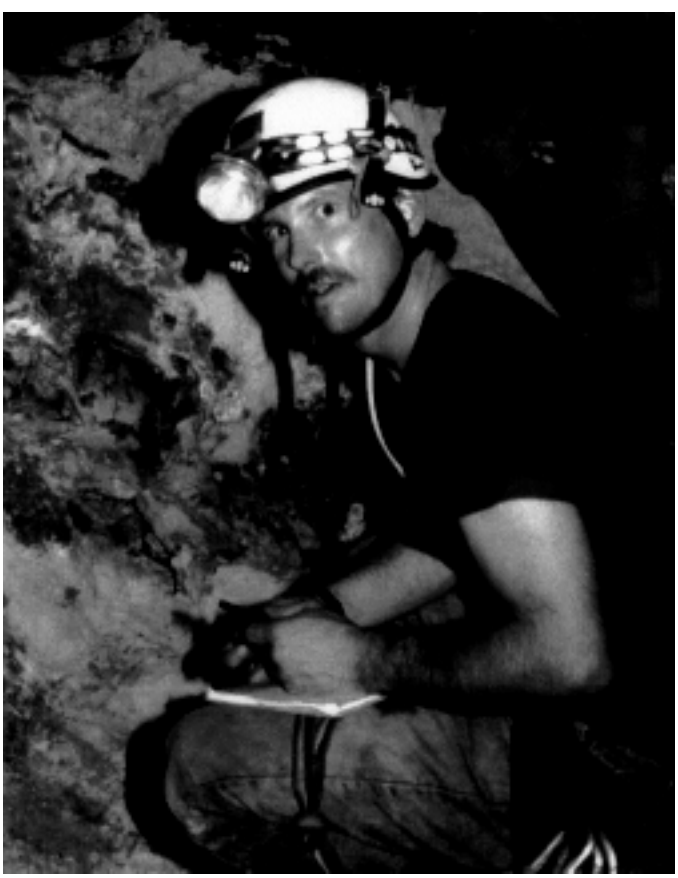

**Kim Cunningham**
**NSS 22063**

Kimberley (Kim) I. Cunningham (NSS 22063) died from heart complications at his home outside Boulder, Colorado, on

December 20, 2000. Born March 11, 1954 in Austin, Texas, he grew up in Northern Virginia and began caving in West Virginia. Sites Cave with its 190-foot entrance pit was his first in 1977. Other trips quickly followed to Windy-Cassell and Cass in West Virginia, and many of the vertical caves of Skydusky Hollow, Virginia. Kim completed his undergraduate Geology degree at the State University of New York - Stony Brook. His senior research project involved measuring amino acids contained in calcite at Cass Cave.

He moved to Colorado in 1979 to work for the United States Geological Survey and was well respected for his pioneering work in developing exploration technologies for oil and gas. This extended to his recent employment with Geo-Microbial Technologies, Inc. Kim enjoyed many of the caves in the Guadalupe Mountains of New Mexico and co-authored a research paper on Wind Cave, South Dakota, helictite bushes. He traveled to Ukraine and collaborated with the Ukrainian Speleological Association on studies of aerosol speleothems in the large gypsum caves of the Western Ukraine.

Kim was perhaps best known in caving for his scientific research in Lechuguilla Cave, New Mexico. These activities included coordinating extensive climate/ radon survey expeditions and initially recognizing the diverse microbiology of the cave (*i.e*. corrosion residues are from rock-eating bacteria) and its possible analog to Martian ecosystems. He also served on a Bureau of Land Management task force to prevent oil and gas drilling from impacting Guadalupe caves (including the helium expedition using the "cylinders from hell"). He gave many presentations promoting science in Lechuguilla Cave, including appearing in the National Geographic Society TV production "Mysteries Underground".

Kim's enthusiasm for the potential role of microbes in geological processes seen in Lechuguilla Cave successfully "infected" a number of microbiologists who are actively working on these issues. The study of microorganisms in the corrosion residue of Lechuguilla and Spider Caves is currently supported by a Life in Extreme Environments Grant from the National Science Foundation, and the role of caves in future extraterrestrial missions is currently supported by a NASA Institute for Advanced Concepts Grant. These are important parts of Kim's legacy.

Kim's wife Holly, son Kyle, daughter Shannon and family in Virginia survive him. His family and many caving friends across the US and around the world will miss him. Members of the Ukrainian Speleological Association pushing toward the world depth record in West Caucasus will name a new pit below the -1410 meter (4625 foot) depth after Kim. The Imax film "Journey into Amazing Caves" will include a memorial credit for Kim's cave research. He was a true advocate for caves and cave science throughout his professional and personal life. His work is published in many USGS reports and other professional journals including the old *NSS Bulletin*. Kim's latest research concerns a sulfide source for Guadalupe speleogenesis from breached backreef hydrocarbon deposits and will be submitted to this publication in the future.

A fund is being created to provide grants to individuals doing their own in-cave research. Contributions can be made to: The Kim Cunningham Cave Research Fund, National Speleological Society, First National Bank of Colorado c/o Maureen Mac Mackin, PO Box 9032, Boulder, CO 80301-9683.

*Ed LaRock and Penny Boston*

## ERRATUM

In Figure 1 of Davis's "Extraordinary Features of Lechuguilla Cave, New Mexico" (*Journal of Cave and Karst Studies 62*(2): 147), the map location numbers starting with 19 in the caption are out of phase with the numbers in the image. To find the correct locations, add 2 to each caption number above 18.

## EDITOR'S NOTE

The authors of "Eyed cave fish in a karst window" in the December 2000 issue of *Journal of Cave and Karst Studies* (p. 180-183) have asked us to note that correspondence should be directed to R. Borowsky.

## OMISSION

The following abstract was inadvertently omitted from the publication of *Selected Abstracts from the 2000 National Speleological Society Convention in Elkins, West Virginia – Survey & Cartography*

### HOW ACCURATE ARE OUR CAVE SURVEYS?

*Robert Thrun, 204 Blair Rd. No. 204, Indian Head, MD. 20640*

In one of the earliest papers on cave survey errors, Denis Warburton compared the actual loop misclosures in cave surveys with theoretical expected errors. Following this lead, the CMAP survey data reduction program does a similar comparison. For this study, the BCRA Grade 5 error specification was used instead of the CMAP defaults. The BCRA grade is the only standard that has a widespread acceptance, at least in some countries. The most informative plot seems to be error ratio *vs.* traverse length on a log-log plot. The plots consist of a cloud of points that can be used to judge a survey's accuracy, or at least its internal consistency. Many cave surveys of different types were studied. No survey met the expectations of the BCRA specification, though a few were close. A typical survey might have 2-4 times the Grade 5 errors. Poor surveys have 5-7 times the BCRA errors. The dispersion of the clouds was always wider than would be obtained from a single random error distribution. It may be possible to characterize the accuracy of a survey from the shape and size of the point clouds. The amount of adjustment and the percentage adjustment are possible alternatives to error ratio for characterizing survey accuracy.

# GUIDE TO AUTHORS

The *Journal of Cave and Karst Studies* is a multidisciplinary journal devoted to cave and karst research. The *Journal* is seeking original, unpublished manuscripts concerning the scientific study of caves or other karst features. Authors do not need to be members of the National Speleological Society but preference is given to manuscripts of importance to North American speleology.

LANGUAGES: Manuscripts must be in English with an abstract, conclusions, and references. An additional abstract in another language may be accepted. Authors are encouraged to write for our combined professsional and amateur readership

CONTENT: Each paper will contain a title with the authors' names and addresses, an abstract, and the text of the paper. Acknowledgments and references follow the text.

ABSTRACTS: An abstract stating the essential points and results must accompany all articles. An abstract is a summary, not a promise of what topics are covered in the paper.

REFERENCES: In the text, references to previously published work should be followed by the relevant author's name and date (and page number, when appropriate) in brackets. All cited references are alphabetical at the end of the manuscript with senior author's last name first, followed by date of publication, title, publisher, volume, and page numbers. Geological Society of America format should be used. Please do not abbreviate periodical titles.

SUBMISSION: Authors should submit three copies of their manuscript (include only copies of the illustrations) to the appropriate specialty editor or the senior editor. Manuscript must be typed, double spaced, and single-sided. Electronic mail submissions require prior permission of the Associate Editor, and is only encouraged from countries where timely transmission of air mail is a problem. Authors submitting manuscripts longer than 15 typed pages may be asked to shorten them. Authors will be requested to submit an electronic copy of the text, a photograph, and brief biography upon acceptance of the paper.

DISCUSSIONS: Critical discussions of papers previously published in the *Journal* are welcome. Authors will be given an opportunity to reply. Discussions and replies must be limited to a maximum of 1000 words and discussions will be subject to review before publication. Discussions must be within 45 days after the original article appears.

MEASUREMENTS: All measurements will be in *Systeme Internationale* (metric) except when quoting historical references. Other units will be allowed where necessary if placed in parentheses and following the *SI* units.

FIGURES: Figures and lettering must be neat and legible. Figure captions should be on a separate sheet of paper and not within the figure. Figures should be numbered in sequence and referred to in the text by inserting (Fig. x). Most figures will be reduced, hence the lettering should be large. Once the paper has been accepted for publication, the original drawing (with corrections where necessary) must be submitted to the editor. Photographs must be sharp and high contrast. Color will be printed at author's expense only.

COPYRIGHT AND AUTHOR'S RESPONSIBILITIES: It is the author's responsibility to clear any copyright or acknowledgement matters concerning text, tables, or figures used. Authors should also ensure adequate attention to sensitive issues such as land owner and land manager concerns.

PROCESS: All submitted manuscripts are sent out to at least two experts in the field. Reviewed manuscripts are then returned to the author for consideration of the referees' remarks and revision, where appropriate. Revised manuscripts are returned to the appropriate associate editor who then recommends acceptance or rejection. The Senior Editor makes final decisions regarding publication. Upon acceptance, the author should submit all photographs, original drawings, and an electronic copy of the text to the editor. The senior author will be sent one set of proofs for review. Examine the current issue for more information of the format used.

ELECTRONIC FILES: The J*ournal's* final layout is done using Quark Xpress. Microsoft Word is used in word processing and all figures and photographs should be submitted in either EPS or TIF format. The *Journal* is printed at 305 dpi. Thus illustrations that are to be printed at 3.5 inches wide require at least 1068 pixels.

---

National Speleological Society
2813 Cave Avenue
Huntsville, Alabama 35810-4431